

**AES/PE/13-14 Downhole depth estimation for
automated subsurface navigation**

July 8, 2013 Praveen Jain



Shell Global solutions International B.V., Rijswijk

Title : Downhole depth estimation for automated subsurface navigation

Author(s) : Praveen Jain

Date : July 8, 2013

Professor(s) : Prof. Jan dirk Jansen

Supervisor(s) : Dr. Eduard Hoogenboom
Dr. Patricia Astrid

TA Report number : AES/PE/13-14

Postal Address : Section for Petroleum Engineering
Department of Geoscience & Engineering
Delft University of Technology
P.O. Box 5028
The Netherlands

Telephone : (31) 15 2781328 (secretary)

Telefax : (31) 15 2781189

Copyright ©2013 Section for Petroleum Engineering

*All rights reserved.
No parts of this publication may be reproduced,
Stored in a retrieval system, or transmitted,
In any form or by any means, electronic,
Mechanical, photocopying, recording, or otherwise,
Without the prior written permission of the
Section for Petroleum Engineering*

Executive summary

This thesis proposes and evaluates a concept for downhole depth estimation by matching subsurface measurements from two sensors in a bottom hole assembly. The application of a downhole depth estimate in automated subsurface navigation has also been demonstrated.

One of the key hurdles in achieving real time subsurface navigation lies in communication bottom neck between surface and downhole. Modern measurement while drilling and logging while drilling tools measure all vital information downhole except depth. Real time availability of depth estimate in the downhole can open new doors for real time automated bit steering and optimization in well drilling operations.

The downhole depth estimation concept introduced in this thesis is based on correlation of gamma ray responses from two sensors to estimate average rate of penetration at the bit. This average rate of penetration of the bit is used to estimate distance travelled by the bit. An algorithm is proposed for correlation of gamma ray sensor response. Various parameters in the algorithm are investigated and discussed in detail for optimized performance. The error in the estimation is a result of difference between average and instantaneous rate of penetration as well as wrong correlation. Synthetic sensor response is created from a gamma ray data set to evaluate the algorithm for different noise levels and count rates. The error in estimated depth due to difference between average and instantaneous rate of penetration is approximately 2.2%. The total error is observed to be less than 4% for lower statistical noise levels. To reduce the error associated with proposed system, a nuclear marker - detector system is proposed and evaluated using Monte Carlo based nuclear simulations. In the last section the application of downhole depth for automated well-plan execution through a rotary steerable system is realised.

Acknowledgement

I offer my sincerest gratitude to my thesis supervisor Prof. Jan Dirk Jansen for his constant and invaluable guidance. I have been indebted in the preparation of this thesis to Dr. Patricia Astrid and Paul McClure, who have supported me throughout my thesis with their patience and knowledge whilst allowing me the room to work in my own way.

I am very much grateful to Dr. Jan Eduard Hoogenboom for his guidance and generous help in performing nuclear simulations. I would like to thank Dr. Jan Jette Blangé for introducing me to such an interesting topic and providing me an opportunity to work at Shell Global Solutions International BV, Rijswijk.

I also express my thankfulness to Dr. Mirano Spalburg, Dr. Dan Minette, John Runia, Colin Haslett, Duncan McDonald, Sander de Vries, Piet van den Heuvel and Scott Goligher, for their valuable inputs throughout this thesis.

In addition, I am grateful to member of my thesis committee Dr. Auke Barnhoorn for spending his time on careful reading of my thesis as well as for his valuable comments.

List of abbreviations

BHA	Bottom hole assembly
GR	Gamma ray
LWD	Logging while drilling
MWD	Measurement while drilling
MSE	Mechanical specific energy
NMR	Nuclear magnetic resonance
NPS	Number of source particles
PDC	Polycrystalline diamond compact (Drill bit)
PNG	Pulsed neutron generator
ROP	Rate of penetration
API	American petroleum institute
VSP	Vertical seismic profile
RSS	Rotary steerable system
SD	Standard deviation
MD	Measured depth
TVD	True vertical depth
RPM	Rotations per minute
DLS	Dogleg severity
TD	Total depth
MCNP	A General Monte Carlo N-Particle Transport Code

List of symbols

a	Constant
D	Depth
F_p	RSS pad force
L	Length
W	Weight of BHA
X	Dataset
Y	Dataset
x	Data point
y	Data point
Rp	Rate of penetration
t	Time
$T_{1/2}$	Half life
α	Inclination
β	Angle build-up rate
σ	Standard deviation
γ	Gamma ray data
λ	Activity constant
ε	Gaussian noise
Ω	Offset
η	Detector counting efficiency
τ	Tolerance

Table of contents

Executive summary	II
Acknowledgement	III
List of abbreviations	IV
List of symbols	V
1. Introduction	1
1.1. Project objectives	2
2. Downhole depth estimation	3
2.1. Literature survey	3
2.2. Depth estimation by correlation of geological markers	3
2.3. Pattern search algorithms	6
2.3.1. <i>Normalised Cross-correlation algorithm</i>	7
2.3.2. <i>Hybrid matching algorithm</i>	8
2.4. Evaluation of algorithms	9
2.4.1. <i>Synthetic sensor responses</i>	10
2.4.2. <i>Sensor distance</i>	11
2.4.3. <i>Matching tolerance and fit</i>	12
2.4.4. <i>Size of set</i>	13
2.4.5. <i>Size of pattern</i>	13
2.5. Results	14
2.6. Other possible measurements for pattern matching	17
3. Calculated depth correction	19
3.1. Correction with help of pipe tally data	19
3.2. Correction by man-made marker tracking	20
3.2.1. <i>Subsurface element to be activated</i>	21
3.2.2. <i>Marker-detector separation</i>	21
3.2.3. <i>Nuclear simulation using MCNP</i>	22
4. Application of downhole depth estimation for automated subsurface navigation	28
4.1. System for automated subsurface navigation	28
4.2. Rotary steerable system (RSS) performance model	29
4.3. Automated well-plan execution	31
4.4. Simulation results	32
5. Conclusions and recommendations	34
References	35
Appendix 1. Directional drilling and Geosteering	38
A1.1. Directional drilling and Geosteering	38
A1.2. Current state of the art in geosteering	38
A1.3. Rotary steerable system	39
A1.4. Wellbore depth measurement system	39
Appendix 2. Downhole depth measurement concepts	41
A2.1. Concepts of downhole depth measurement	41

<i>A2.1.1. Correlation of subsurface markers:</i>	41
<i>A2.1.2. Use of accelerometers:</i>	42
<i>A2.1.3. Use of pipe tally:</i>	42
<i>A2.1.4. Use of pressure or gravity measurements</i>	42
<i>A2.1.5. Use of manmade markers</i>	42
<i>A2.1.6. By means of positive contact with borehole wall</i>	43
<i>A2.1.7. Use of acoustic waves in the drill string</i>	43
<i>A2.1.8. Use of pressure pulse in mud</i>	43
<i>A2.1.9. By means of electromagnetic signals</i>	44
A2.2. Acoustic waves in drill-string	44
<i>A2.2.1. Drill-string channel characteristics</i>	44
<i>A2.2.2. Wave velocity</i>	45
<i>A2.2.3. Signal attenuation</i>	45
<i>A2.2.4. Noise</i>	46
A2.3. Mud pulse telemetry	46
<i>A2.3.1. Signal attenuation</i>	46
<i>A2.3.2. Wave velocities:</i>	47
A2.4. Synchronised time measurement	47
A2.5. Concept selection for downhole depth measurement system	48
Appendix 3. Pattern matching and gamma measurement	50
A3.1. String matching	50
A3.2. Approximate string search	51
A3.3. Minimum squared distance method for pattern recognition	51
A3.4. Gamma ray measurement for identifying geological markers	51
Appendix 4. MCNP and Nuclear simulation input	53
A4.1. Introduction to MCNP and the Monte-Carlo method	53
A4.2. Neutron Generator	53
A4.3. Gamma ray detector	54
<i>A4.3.1. Detector counting efficiency</i>	55
A4.4. Subsurface elements	55
<i>A4.4.1. Chlorine-37</i>	55
<i>A4.4.2. Sodium-23</i>	55
<i>A4.4.3. Silicon-30</i>	56
A4.5. Creation of photon source for the second simulation	56
5.1.1. Location of activated nuclei	56
5.1.2. Energy of gamma ray	56
5.1.3. Time of decay	57
5.1.4. Initial direction	57
A4.6. MCNP input files	58
<i>A4.6.1. Neutron simulation</i>	58
<i>A4.6.2. Photon simulation</i>	59

Appendix 5.	MATLAB codes	61
A5.1.	MATLAB code for Cross-correlation with surface correction	61
A5.2.	MATLAB code for Hybrid pattern matching with RSS integration	63

List of figures

Figure 1:	Current (Left) and proposed (right) system for bit steering	1
Figure 2:	Correlation of subsurface markers with two sensors separated by distance L	4
Figure 3:	Sensor arrangement and datasets for correlation algorithm	5
Figure 4:	Algorithm for depth calculation with correlation of geological markers	5
Figure 5:	Hybrid algorithm for pattern matching	8
Figure 6:	Well trajectory	9
Figure 7:	ROP variation with time	10
Figure 8:	Effect of distance between the sensors on calculated depth	11
Figure 9:	% Error in calculated depth with change in sensor distance	11
Figure 10:	Original and averaged ROP for a sensor separation of 2.5 m	12
Figure 11:	Linear relationship with slope of unity between responses from two sensors	13
Figure 12:	Error in calculated depth with original GAPI dataset without any offset	14
Figure 13:	Error in calculated depth with original GAPI dataset and an offset of 5	15
Figure 14:	Error in calculated depth with dataset scaled by a factor of 2, No offset	15
Figure 15:	Error in calculated depth with dataset scaled by a factor of 2 and an offset of 10	16
Figure 16:	Error in calculated depth with dataset scaled by a factor of 3, No offset	16
Figure 17:	Error in calculated depth with dataset scaled by a factor of 3 and an offset of 15	17
Figure 18:	Depth calculation results with gamma ray and density measurement	17
Figure 19:	Original and repeat sections for density and gamma ray measurements	18
Figure 20:	Correction in downhole depth with help of pipe tally	19
Figure 21:	Error with correction from surface every 40 m	20
Figure 22:	Nuclear source based marker-detector system	20
Figure 23:	Model dimensions and location of source and detectors in the borehole	22
Figure 24:	Crystal geometry and location of detectors	23
Figure 25:	Statistical variation in results for different number of source particles with 95% confidence	24
Figure 26:	Spread of activated nuclei in subsurface	24
Figure 27:	Decay profile of activated nuclei	25
Figure 28:	Flux variation in moving detector with space and time	25
Figure 29:	Change in photon flux in detectors with time and distance from source	26
Figure 30:	Percentage change in signal strength per 100 sec. at detector locations	26
Figure 31:	Energy distribution of photons in the detectors	27
Figure 32:	Absorption efficiency of NaI crystals of different thickness	27

Figure 33:	Subsurface navigation flow chart	28
Figure 34:	Simplified BHA schematic	29
Figure 35:	Anticipated BUR at various deflection settings and well bore inclinations	30
Figure 36:	Approximated BUR at various deflection settings and hole inclinations	31
Figure 37:	Flow chart for evaluating real time automated well-plan execution	32
Figure 38:	Results of automated well-plan execution from the surface and in downhole	33
Figure 39:	Deviation from well plan in east, north and vertical direction along depth	33
Figure 40:	Detector schematic	54

List of tables

Table 1:	Strengths and weaknesses of downhole depth measurement concepts	48
----------	---	----

1. Introduction

One of the emerging areas of interest in hydrocarbon industry is development of thin and tight reservoirs. These developments require greater reservoir contact area which establishes the need of long horizontal and multilateral drilling. Most of these modern day drilling applications uses real time formation evaluation techniques and sophisticated downhole tools to find the geological target zone and maintain contact with the reservoir for several kilometres while drilling ahead. The act of changing well bore trajectory while drilling to achieve greater contact with geological target or to avoid risk zones is called geosteering and result in a complex three dimensional wellbore geometry.

Modern day geosteering systems constitute of complex electro-mechanical systems which are quite expensive to build and maintain. This cost factor limits their use in economically marginal projects. One other limitation of current geosteering technology is its dependency on human expertise in interpretation of subsurface data and drilling parameters for real time decision making. Constant reliance on human judgement leaves a room for error and inconsistency and increases risk exposure. An improvement over current system can be achieved in simpler tool construction and automation of the process for lower cost and consistent performance.

To realise the concept of automated subsurface navigation, one of the primary decision is to fix the location of the 'Brain' of the system which will take input from all possible measurements and process it with acquired intelligence for real time decision making. If the 'Brain' of the system is situated on the surface it will need all the downhole measurements to be sent on the surface and decision in terms of tool settings, to be sent downhole.

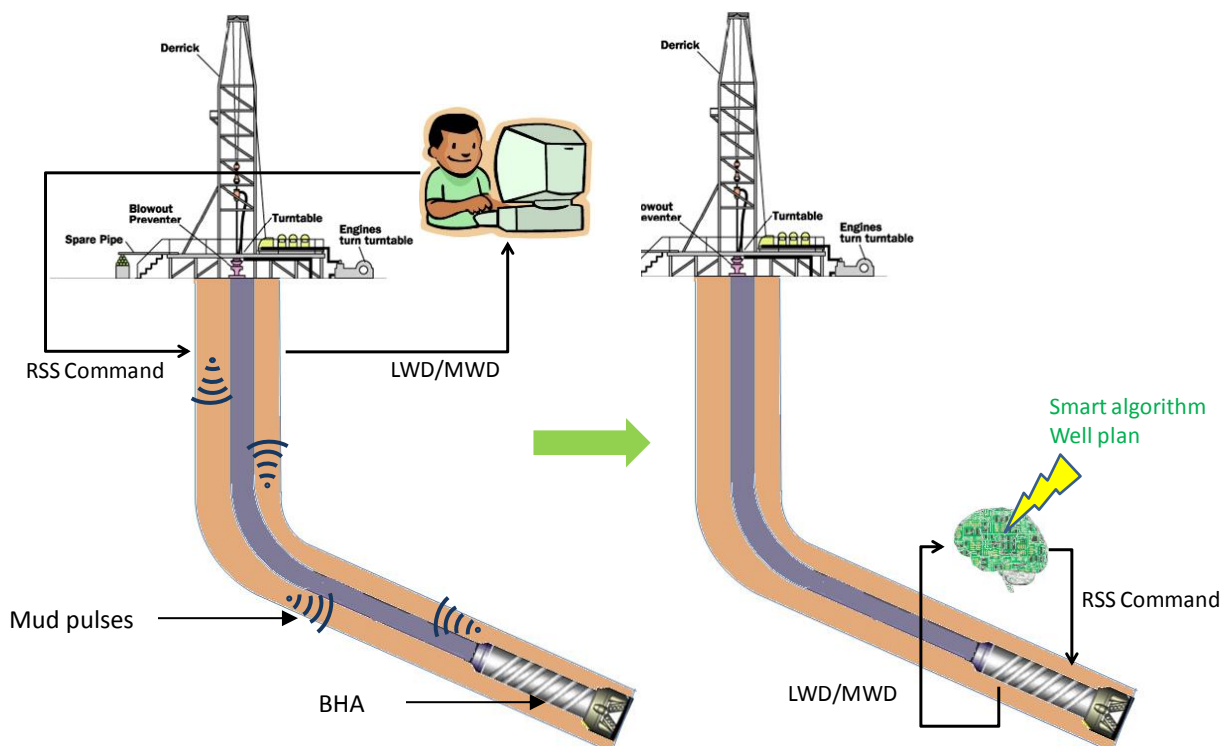


Figure 1: Current (Left) and proposed (right) system for bit steering

One of the key challenges in the development of surface based automation lies in the capacity bottle neck of current communication systems. Current state of the art technology for

communication between bottom hole and surface is mud-pulse telemetry which suffers from decrease in data carrying capacity with increase in the depth of the hole due to higher attenuation of high frequency signals. Commercial systems claim data rates of 40 bit/s for shallow wells which decreases down to 3 bit/s for extended reach wells [43] with an additional overhead of disruption in operations for down-linking. There is also a time lag between subsurface measurement and surface reproduction of information which along with limited data transfer rates severely limit system's capability to achieve real time closed loop control on the bit and reap full benefits of high frequency, high resolution data acquisition downhole.

The other possibility is to bring the 'Brain' closer to the bit where all measurements related to formation evaluation (Gamma ray, resistivity, density, sonic velocity, etc.) are taken and based on which geosteering decisions are made. This system will greatly reduce the data transmission requirements to and from the surface utilizing high resolution dataset in real time eliminating time lag issues and data compression requirements, which can further enhance decision quality. It is possible to acquire all the vital drilling parameters such as weight on bit, bit RPM, mud flow rate, temperature, pressure, etc. with current measurement while drilling systems in downhole conditions enabling better monitoring and optimization. But not all the measurements are made subsurface yet. The depth of drill bit in current arrangement on rigs is still made on the surface and will need to be communicated downhole for the realisation of such a system. Downhole measurement of depth can eliminate this need of depth data transmission from surface to the BHA and enhance the real time capabilities of an automated subsurface navigation system.

1.1. Project objectives

As the subsurface depth measurement came out as major limitation in achieving real time, closed loop automation. The main objectives of the project are chosen in line with this challenge and are summarised below.

1. Investigate the feasibility of downhole depth measurement.
2. Evaluate various concepts for downhole depth measurement on their strengths and weaknesses.
3. Select most promising concepts and design in detail.
4. Test the concept
5. Establish applicability of the concept

A detailed survey of possible concepts for downhole depth determination was carried out. The concepts generated based on survey outcome were compared against each other on their strengths and weaknesses to choose the most promising concept. A summary of the survey along with the comparison is given in **Appendix 2**. Based on the comparison correlation of geological markers was chosen as the best method for downhole depth estimation and is explained in **Chapter 2**.

2. Downhole depth estimation

2.1. Literature survey

Though downhole depth estimation has been researched in the past for its potential to eliminate errors of surface based depth measurement, yet no commercial system exists till date. Many ideas have been proposed in various patents and publications using mechanical wheel [15], pipe tally [11] [6], magnetic marker-detector system [15], correlation of geological markers [5] [44], etc. Out of these use of pipe tally is less complicated to implement, but it gives no better estimate than the surface based measurement. The depth points available from the system are relatively coarse (spaced by pipe joint length) and unsuitable for a real time automation application. System proposals based on pressure or gravity measurements [12] [13] can only give estimate of vertical depth and need robust gravity or pressure models as well as highly accurate measurements in downhole environment. Few authors have proposed use of accelerometer [6] [8] [9] [10] similar to inertial navigation systems for rockets and aeroplanes. However, these systems suffer from integration drift and need a secondary system to correct their estimation.

A new family of concepts can be proposed using wave velocities and wave travel time between a source and receiver located at the ends of a drill string. These concepts draw their cue from vertical seismic profile measurements while drilling. The waves for application can be acoustic waves in drill string, pressure waves in mud column or electromagnetic waves in subsurface. The biggest challenges in materialising these concepts are creating an accurate velocity model and drift in clocks. State of the art quartz based downhole clocks have measurement accuracy in milliseconds which will limit the accuracy of estimated depth to few meters.

There are inherent advantages in using correlation of geological markers for downhole depth estimation as it can be built on current logging while drilling systems and does not require new development in measurement technology. On the other hand, the correlation part can be built upon pattern recognition methods from image analysis or cross-correlation from signal processing domains which further reduce total development effort. It is also a superior choice over other systems as its usability can be tested with available log data for use in any geological setting and system can easily be tuned to the specific requirements.

2.2. Depth estimation by correlation of geological markers

The concept involves making continuous measurements along the borehole with two or more sensors separated by a known distance in the BHA and calculates the time difference between appearances of the same log signature on those measurements. With the measured time difference and known separation between the sensors, the average rate of penetration can be calculated and the same can be integrated to calculate along hole depth. A schematic of the arrangement is shown in Figure 2, where *S1* and *S2* are identical sensors located in a bottom hole assembly.

In Figure 2, a high GR signature at location *g1* passes the first sensor at time t_1 and then the same high GR signature passes the second sensor at t_2 and the sensors are L meters apart along the drillstring. It can now be determined that the drill string has progressed a distance of L m along the hole in time difference $(t_2 - t_1)$.

Hence average rate of penetration (ROP) is

$$R_p = \frac{L}{t_2 - t_1} \quad \{1\}$$

By integrating this ROP, incremental change in depth ΔD can be calculated.

$$\Delta D = R_p \Delta t \quad \{2\}$$

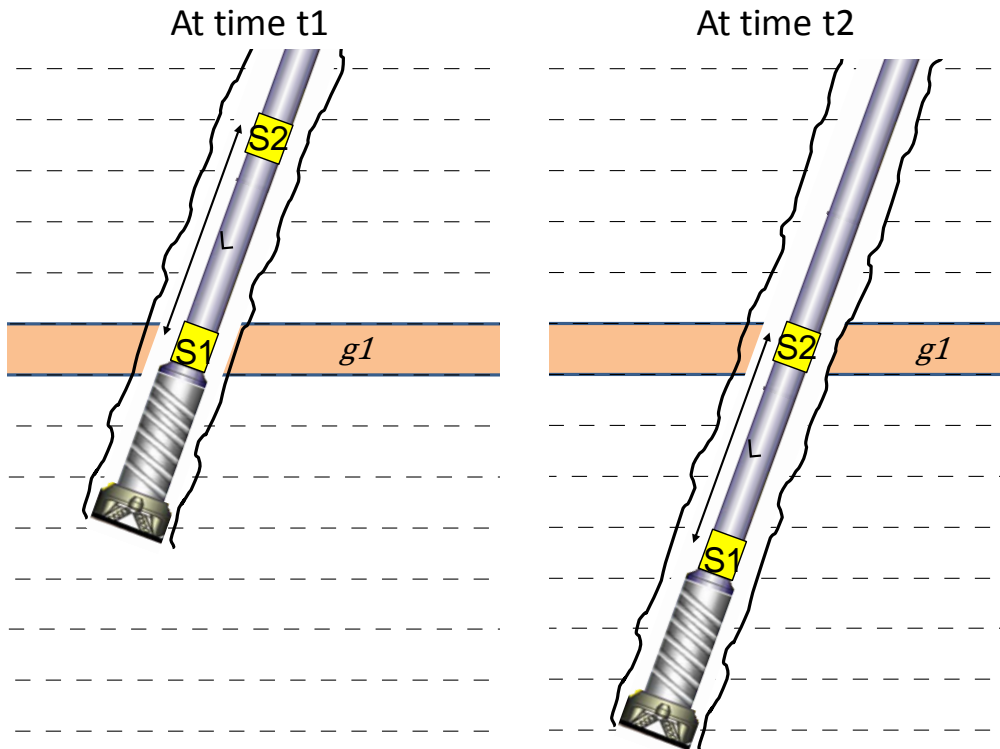


Figure 2: Correlation of subsurface markers with two sensors separated by distance L

One of the core elements of this concept is correlation of multiple logs to identify the appearance of every unique point in subsurface on all these logs.

In correlation of subsurface measurements, there exist three challenges

- (1) Some times downhole measurements can have erroneous values which need to be filtered out from the datasets to be correlated.
- (2) The down hole measurement at the same point in subsurface may not repeat exactly in value on multiple sensors, which requires to introduce a tolerance band to account for measurement precision of different tools.
- (3) Within the same formation, variation in measured values of any rock property along the hole may be very small. Thus the rock property selected for correlation should have associated measurement precision less than the minimum anticipated variation. This may require use of different types of measurements in different formations or different sensor designs.

In order to cope up with above mentioned challenges, an algorithm for such a correlation exercise needs to be flexible to adapt to subsurface chemistry and rock properties. In general any suitable logging suit or group of suits can be used for making correlation as far as rock properties vary sufficiently along the borehole depth. The system is insensitive to the location of the sensors on the BHA and they can be near or far from the bit. Also azimuthal measurements can be made for correlation of more than one data points at any subsurface location.

A simple arrangement for the concept is shown below in Figure 3. Here the sensor1 shown as $S1$ is the leading measurement instrument in the borehole and sensor2 shown as $S2$ is the trailing measurement instrument. The dataset N is sufficiently large to include all possible matches corresponding to dataset M .

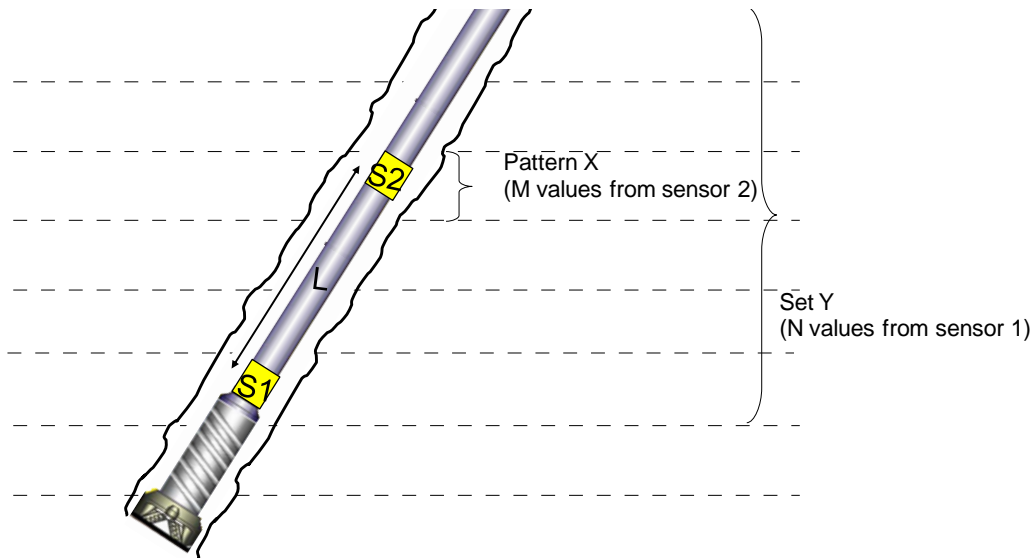


Figure 3: Sensor arrangement and datasets for correlation algorithm

An algorithm for depth calculation with two sensor arrangement is shown in Figure 4 to explain the concept. This algorithm can be further expanded for more than one rock properties or sensors.

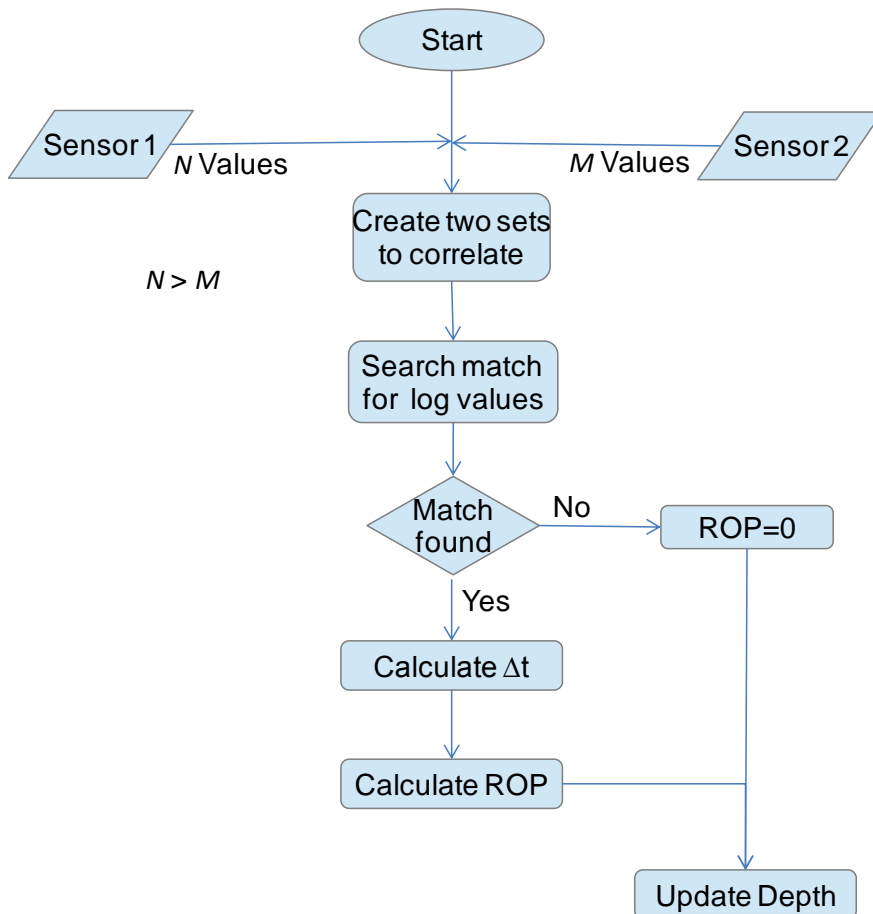


Figure 4: Algorithm for depth calculation with correlation of geological markers

The main steps in algorithm are as follows

1. The datasets of N and M data points are taken from measurements made by leading sensor1 and trailing sensor2, respectively. These sets will be dynamically updated with time by addition of the latest acquired data points and removal of the oldest data point. The value of M and N need to be determined for each specific situation and configuration.

Let the dataset from the trailing sensor be \mathbf{X} and from leading sensor be \mathbf{Y} such that at any time t_s

$$\mathbf{X}(t_s) \in \mathbb{R}, \quad \mathbf{X}(t_s) = \{x(t_2^j)\}_{j=1}^M$$

$$\mathbf{Y}(t_s) \in \mathbb{R}, \quad \mathbf{Y}(t_s) = \{y(t_1^k)\}_{k=1}^N$$

2. Any correlation algorithm will be used to identify an acceptable match for pattern \mathbf{X} constituting M data points from sensor 2 in the set \mathbf{Y} constituting N data points from sensor 1 such that

$$\mathbf{X}(t_s) \approx \tilde{\mathbf{Y}}(t_s)$$

Where $\tilde{\mathbf{Y}}(t_s) \subset \mathbf{Y}(t_s)$

$$\tilde{\mathbf{Y}}(t_s) \in \mathbb{R}, \quad \tilde{\mathbf{Y}}(t_s) = \{y(t_1^k)\}_{k=a}^{a+M-1}$$

3. If an acceptable match is found the time difference between measurements from sensor 1 and sensor 2 will be calculated and with help of the time difference, the rate of penetration (R_p) will be calculated. If the separation between the sensors is L

$$\Delta t = t_2^M - t_1^{a+M-1} \quad \{3\}$$

$$R_p(t_s) = \frac{L}{\Delta t} \quad \{4\}$$

If an acceptable match could not be found, the rate of penetration will be equated to zero.

4. For a non-zero rate of penetration, the depth (D) will be calculated by multiplying it with the time difference between current and last calculated non-zero rate of penetration.

$$dt = t_s - t_{s-1}$$

$$D(t_s) = D(t_{s-1}) + R_p(t_s)dt \quad \{5\}$$

For zero rate of penetration (ROP), the depth will be updated with the previous depth. Alternatively the depth can also be updated with last non-zero ROP considering the change in ROP to be very small in successive calculations.

2.3. Pattern search algorithms

One of the key components in correlation of geological markers is matching of responses from multiple sensors. In order to find the most effective pattern search algorithm for the purpose, different domains such as string matching in text editors, signal processing and image processing were explored for different possibilities. A summary of literature survey is given in **Appendix 3**. Each of the methods presented in **Appendix 3** have their own advantages in different situations but most of them are either inefficient or unemployable for the current problem. The selection of

a potential method for correlation should be made based in the specific needs and properties of datasets detailed below.

1. All data are numeric, which allow us to use numerical operations for comparing possible matches.
2. Due to the known size of pattern \mathbf{X} and set \mathbf{Y} , the upper limit on number of measurements outside the tolerance band resulting in mismatch can be quantified and chosen as per need to ease complexities.
3. The mismatch is only limited to having a different value in the set \mathbf{Y} corresponding to the value in pattern \mathbf{X} and does not include cases of missing values in pattern \mathbf{X} or set \mathbf{Y} .
4. Two values within a given tolerance should be considered a match.
5. Even if we don't find a suitable match once in a while, we can simply ignore that data point from ROP calculation and can use previous ROP for the calculation of depth as ROP will not change drastically with in successive measurements.
6. Size of pattern \mathbf{X} and set \mathbf{Y} should be relatively small compared to text search problems in editors and should not cause any computational capacity related issues even with the use of brute force algorithms.

Based on the unique needs and simplicity of the problem, two possible solutions for pattern matching are considered and explained in next sub-sections.

2.3.1. Normalised Cross-correlation algorithm

Cross correlation is one of the common methods used in signal processing to recognise time-lag between two signals. The same has been used in determining average rate of penetration at the end of drilling, after receiving the logs on the surface [44]. The cross correlation method calculates correlation coefficient for all possible matches, and the highest value of correlation coefficient identifies most probable match. The size of the pattern still remains a variable of choice and can be optimised. This method is computationally more expensive as all possible matches need to be investigated and more complex calculations are involved.

If a set of N data points and pattern of M data points are taken from measurements made by leading sensor $S1$ and tailing sensor $S2$ respectively such that

$$\begin{aligned} \mathbf{X}(t_s) \in \mathbb{R}, \quad \mathbf{X}(t_s) &= \{x(t_2^j)\}_{j=1}^M \\ \mathbf{Y}(t_s) \in \mathbb{R}, \quad \mathbf{Y}(t_s) &= \{y(t_1^k)\}_{k=1}^N \end{aligned}$$

Then the correlation coefficient for any subset $\tilde{\mathbf{Y}}(t_s) \subset \mathbf{Y}(t_s)$

$$\text{Such that } \tilde{\mathbf{Y}}(t_s) \in \mathbb{R}, \quad \tilde{\mathbf{Y}}(t_s) = \{y(t_1^k)\}_{k=a}^{a+M-1}$$

is given by

$$r_i = \left\{ \frac{\sum_{l=i}^{i+M-1} (x_l - \bar{X})(y_l - \bar{Y})}{\sqrt{\sum_{l=i}^{i+M-1} (x_l - \bar{X})^2} \sqrt{\sum_{l=i}^{i+M-1} (y_l - \bar{Y})^2}} \right\}_{i=1}^{N-M+1} \quad \{6\}$$

The denominator in the expression above serves to normalise the correlation coefficients such that $-1 \leq r_i \leq 1$, where the bounds indicate maximum correlation and '0' indicate no

correlation. A high negative correlation indicates a high correlation but of the inverse of one of the series.

One of the key advantages of cross correlation is its ability to handle any drift in sensors. Any offset caused by sensor drift will not affect the cross-correlation coefficient as the offset will also reflect in the mean which is subtracted from both the set and pattern in numerator and denominator leaving cross correlation coefficient unchanged

2.3.2. Hybrid matching algorithm

The pattern matching algorithm for the application of log correlation is a combination of brute force method and square distance method. Algorithm first finds out possible match on fit and tolerance criteria by brute force method and if more than one match qualifies, match with minimum squared distance is chosen. This algorithm is flexible in using different size of pattern (M) and set (N) for matching depending upon the change in formation properties and drilling parameters. The values of tolerance and fit requirements can be decided based on the type of measurement. Here the algorithm is explained for gamma ray measurements which govern the choice of fit and tolerance on statistical basis. The flow chart of the algorithm is explained in Figure 5.

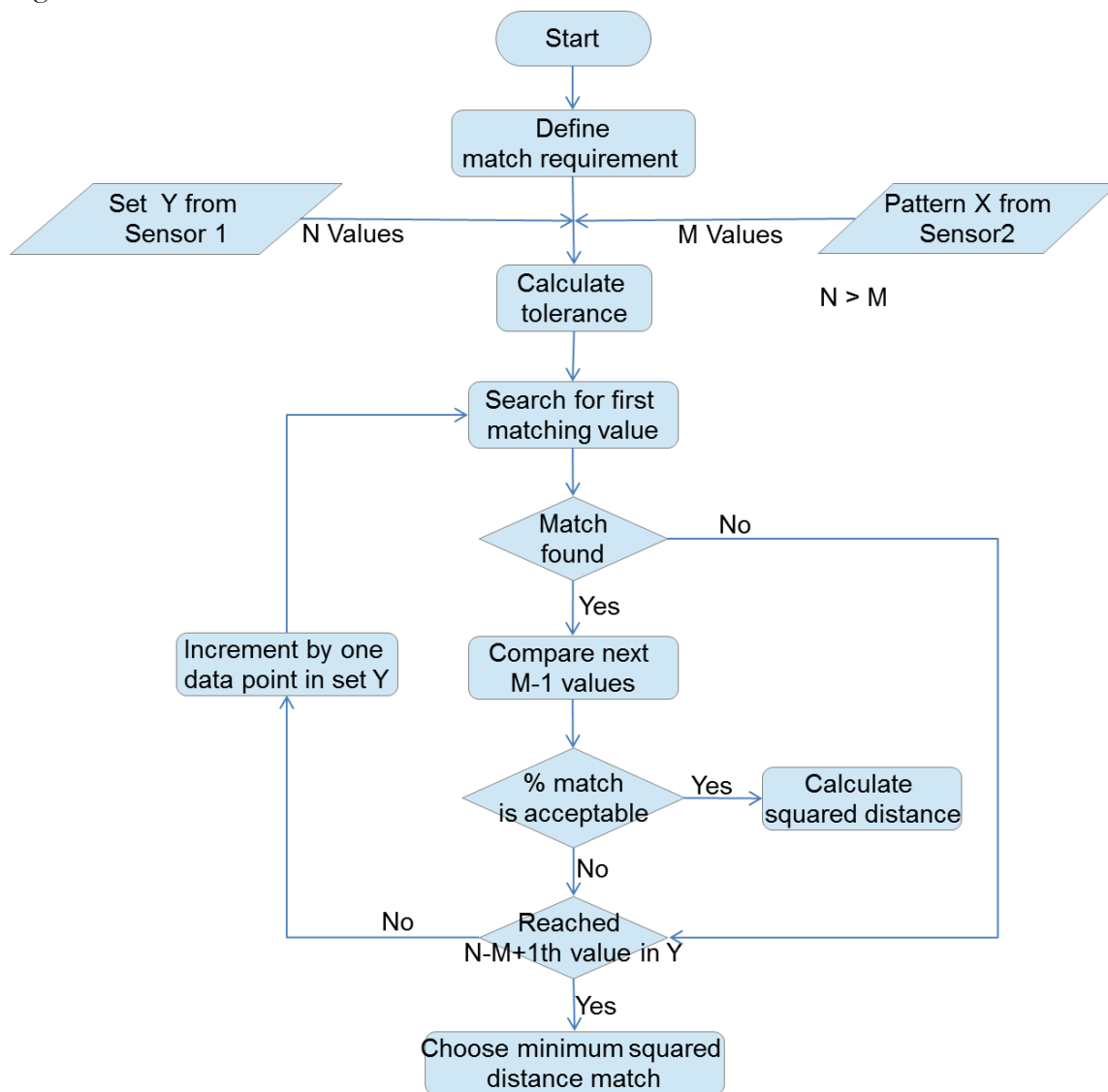


Figure 5: Hybrid algorithm for pattern matching

The algorithm works in the following steps

1. Initialize : % match requirement (μ),
2. Calculate tolerance : $\tau = \tau_i \quad \forall i = [1, M]$
 - for* $i = 1, 2 \dots N-M+1$ *do*
 - if* $|x_1 - y_i| \leq \tau_1$ Compare first value of pattern
 - $count=1$
 - for* $j = 1, 2 \dots M$ *do*
 - if* $|x_j - y_{i+j-1}| \leq \tau_j$
 - then* $count = count + 1$
 - end for*
 - if* $count \geq \mu$ Accept if match requirement is fulfilled
 - then* $d_i = \sum_{l=1}^M (x_l - y_l)^2$ Calculate squared distance
 - end for*
3. Choose index of minimum squared distance for declaring match

2.4. Evaluation of algorithms

Two algorithms namely cross-correlation (section 2.3.1) and hybrid pattern matching (section 2.3.2) were evaluated. Synthetic sensor responses were created from the log data of a well in Dutch subsurface. The well geometry is shown in Figure 6. The data is available in the depth domain only at every 0.1 m distance so the time domain data is created with the help of given ROP shown in Figure 7. The given well trajectory is inclined in the section of 483m-963m along hole depth and horizontal in the section of 963m-1450m along hole depth.

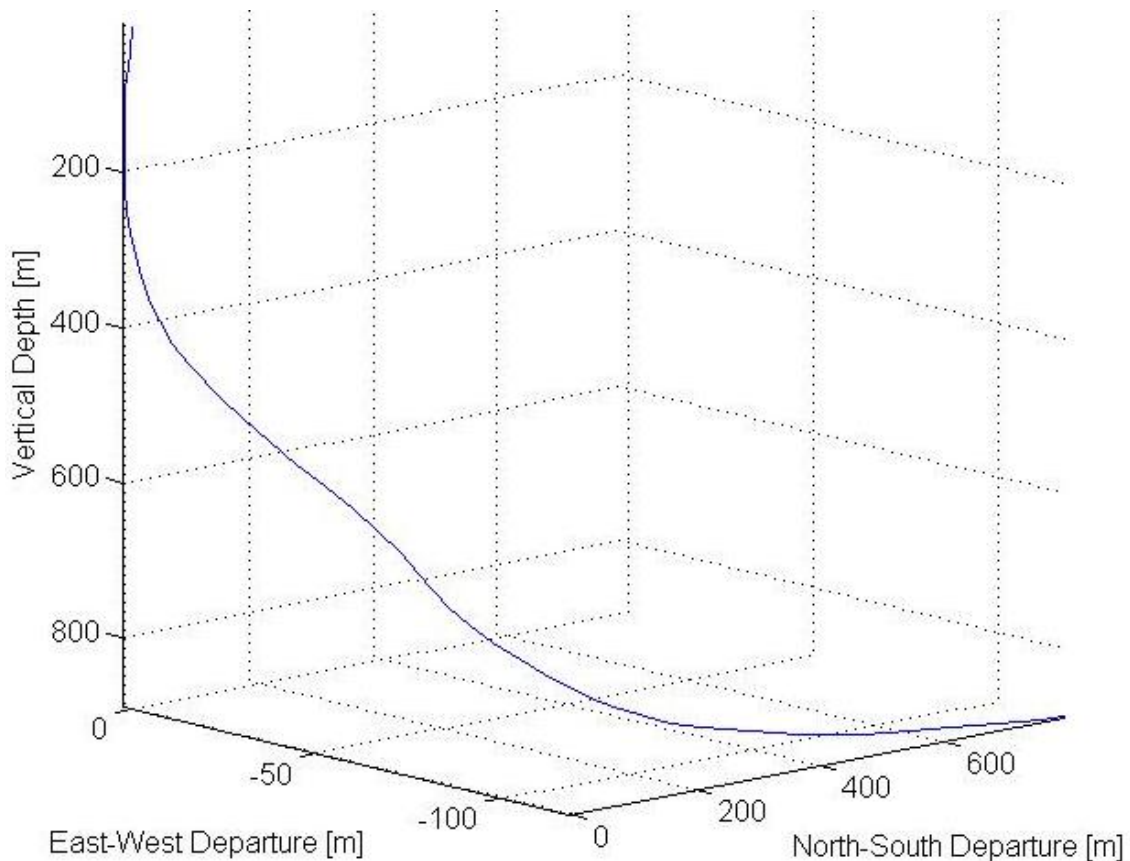


Figure 6: Well trajectory

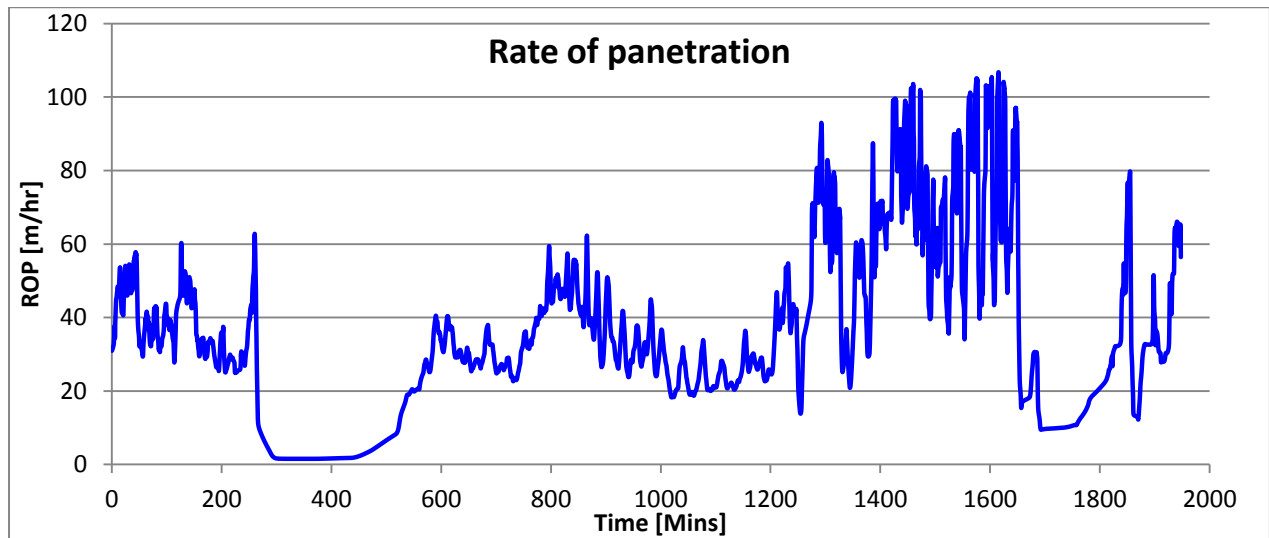


Figure 7: ROP variation with time

2.4.1. Synthetic sensor responses

Gamma ray measurements from LWD in API units are used for the correlation, treating them as absolute counts. As mentioned in **Appendix A3.4**, the total count rate in case of gamma ray measurements can be increased by

1. Changing in sensor design i.e. Increasing crystal size
2. Increasing the radiation collection time window for each data point

Also, the higher the count rate, the lower is the relative standard deviation. To see the effect of increase in count rate on the results, two additional datasets are created by scaling the log data by a factor of 2 and 3. These three datasets are used to evaluate the algorithms for effect of noise level and sensor drift separately.

In usual LWD tool strings from major suppliers, no two gamma sensors of the same design can be run in the same BHA. So in order to create response from two sensors of the same design $X(t_p)$ and $Y(t_p)$ Gaussian noise (ϵ) is added to the original and scaled up datasets. The difference between measured values from closely separated two sensors depends on a number of factors such as ROP fluctuation, change in borehole environment, statistical variation, etc. Out of these factors, effect of statistical variation can be easily quantified. Radiation measurements follow a Gaussian distribution [34] and statistical variation in the measurement results has a standard deviation equal to square root of total count [35].

To account for statistical variation, Gaussian noise with standard deviation equal to the square root of the total count was added in the original gamma ray data to formulate the response from two sensors. In order to include the effect from other possible factors as well, another dataset is created by adding Gaussian noise with standard deviation equal to twice of the square root of the total count. If the total count is γ then $\sigma_1 = \sqrt{\gamma}$ and $\sigma_2 = 2\sqrt{\gamma}$.

Other than random noise there can be drift between the two sensors. To simulate the drift, along with Gaussian noise a constant offset (Ω) of 5, 10 and 15 counts is added on second sensor response created from original and scaled datasets respectively. Mathematically response from both the sensors can be summarised in the equations below.

$$X(t_p) = a \cdot \gamma(t_p) + \epsilon_1(\sigma)$$

$$Y(t_q) = a \cdot \gamma(t_q) + \epsilon_2(\sigma) + \Omega$$

where,

$$\sigma_1 = \sqrt{a\gamma} ; \sigma_2 = 2\sqrt{a\gamma} \quad \forall a = 1, 2, 3$$

$$\Omega = 5a \quad \forall a = 1, 2, 3;$$

2.4.2. Sensor distance

The distance between the two sensors measuring identical formation properties can have a big impact on the associated error with calculated depth. This effect is due to the fact that the calculated ROP at any time is the average of ROP values over the time interval elapsed between both the sensors passing through same subsurface location. Original surface recorded ROP and average ROP for sensor separation of 2.5 m is shown in Figure 10.

To isolate the effect of sensor distance itself, both the datasets were identical and no noise was added in order to get a perfect match to eliminate the effect of mismatch or incorrect match on the calculated depth. Intuitively we can say that the smaller the time interval the smaller will be the ROP variation and thus the smaller will be the effect of averaging. The same trend can be seen in the simulation results as well. The results of simulations are shown in Figure 8.

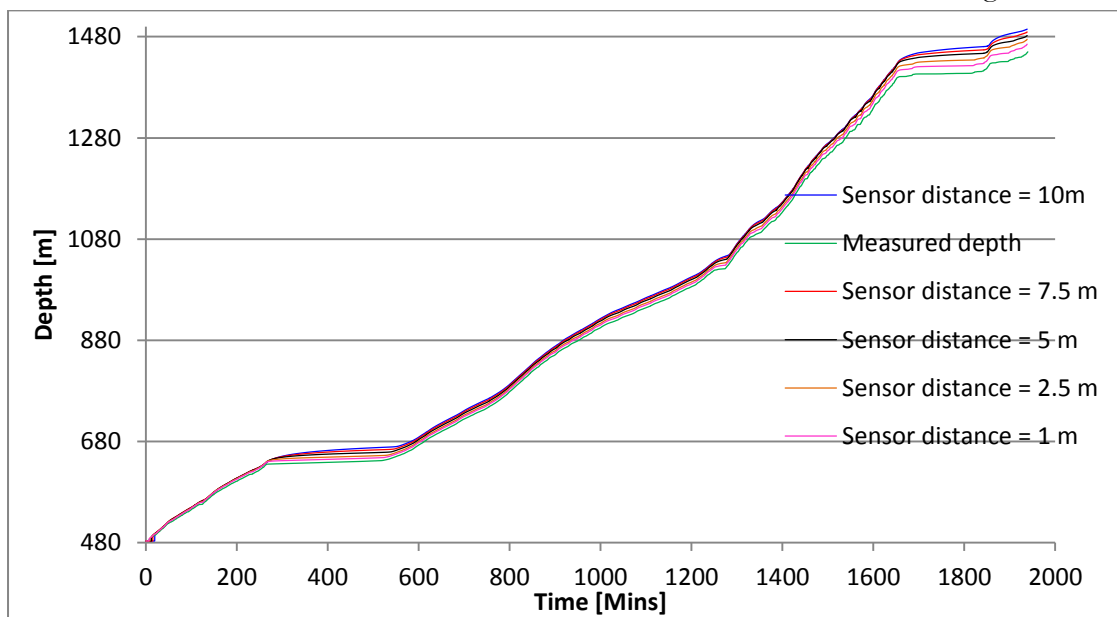


Figure 8: Effect of distance between the sensors on calculated depth

The calculated values are always found higher than the actual measured values of depth and the error increases almost linearly from 1.16 % for sensor distance of 1m to 3.21% for the sensor distance of 10m shown in Figure 9.

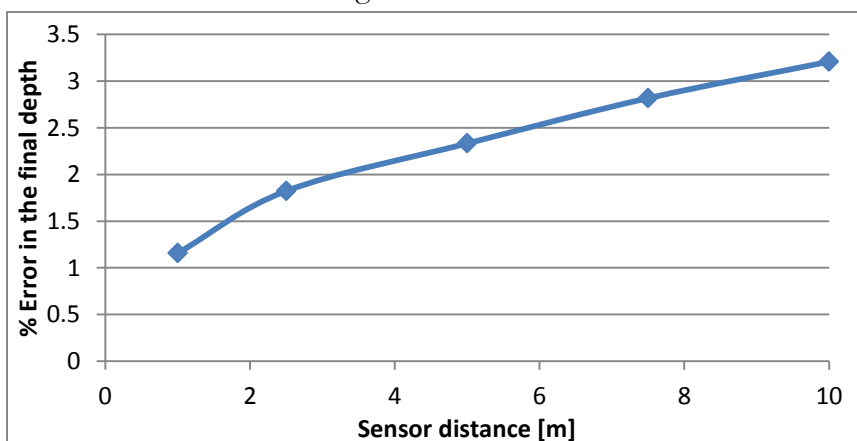


Figure 9: % Error in calculated depth with change in sensor distance

It is also important to note that the more is the fluctuation in ROP; the more will be the effect of averaging and associated error. If the fluctuation in ROP can be eliminated, the error associated with ROP averaging can be avoided, and theoretically zero error is achievable.

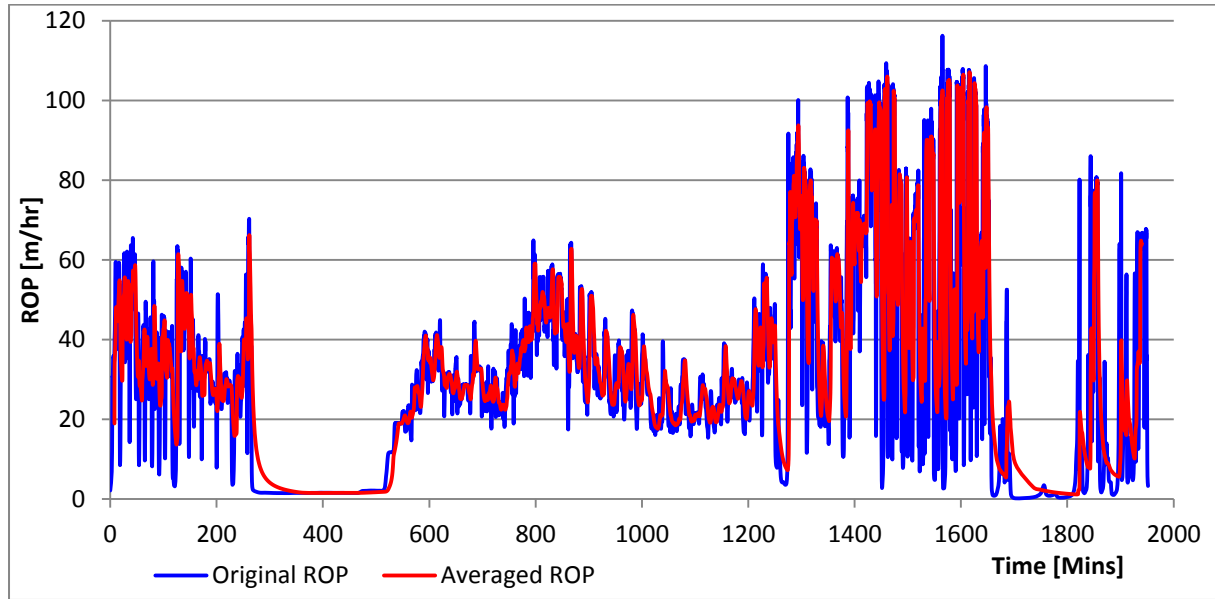


Figure 10: Original and averaged ROP for a sensor separation of 2.5 m

2.4.3. Matching tolerance and fit

These values are only relevant to hybrid matching algorithm. As gamma ray measurements can be approximated by a Gaussian distribution, statistically 68% of measurements at any location should produce a count within one standard deviation ($\pm\sigma$) and for Gaussian distribution the standard deviation can be approximated by the square root of the total count. Using rules of propagation of error, total standard deviation (σ_t) between the two datasets from different sensors of same design can be given by

$$\sigma_t = \sqrt{\sigma_x^2 + \sigma_y^2} \quad \{7\}$$

Where σ_x and σ_y are the standard deviation of measured counts at the same location

$$\sigma_t = \sqrt{x(t_p) + y(t_p)} \quad \{8\}$$

This total standard deviation can be used as a tolerance (τ) window to find an acceptable match and statistically 68% of the times values from both sensors corresponding to same location should lie in the tolerance band of $\pm\sigma_t$ which gives us the fit requirement of 68% for the tolerance of $\pm\sigma_t$.

As the $y(t_p)$ is unknown and need to be found, the total standard deviation can be approximated as

$$\tau(t_p) = \sqrt{2 * x(t_p)} \quad \{9\}$$

In the case of drift the value of tolerance calculated above does not remain valid and an additional term to account for the drift need to be added and updated with time if drift grows with time. This offset due to drift can be approximated by the difference between the mean of the pattern and a potential match such that

$$\Omega = \bar{X}(t_s) - \bar{Y}(t_s) \quad \{10\}$$

and new tolerance can be given by

$$\tau(t_p) = \sqrt{2x(t_p)} + \Omega \quad \{11\}$$

2.4.4. Size of set

The size of the set in which a match for the pattern will be searched should be long enough to contain the pattern in all scenarios. The upper limit on the set size comes from the need to minimise any possibility of finding a faulty match which will increase with increase in size of the set. To minimize occurrences of faulty match the set size should be kept to a minimum. With help of calculated average ROP and known sensor separation an approximate time band can be defined in which trailing sensor should pass through the location of leading sensor.

Suppose the average ROP = R_p and the sensor distance is L . let us assume the uncertainty in the ROP is given by ρ then the time window for search of pattern can be given by

$$T = \frac{L}{R_p - \rho} - \frac{L}{R_p + \rho} \quad \{12\}$$

If the time window for making each measurement is given by ω the length of set is given by

$$N = \frac{T}{\omega} \quad \{13\}$$

2.4.5. Size of pattern

The size of the pattern remains an important parameter to optimise, as the pattern should be long enough to capture enough variation helping to find a unique corresponding match in the set yet the upper limit on pattern size comes from the computational time considerations. The pattern size can be chosen as constant for a particular formation or can be iteratively optimised with another algorithm.

With help of linear regression analysis of the response from two sensors the optimum pattern size can be estimated. As the difference between measurements from two sensors is of Gaussian noise, for the minimum representative pattern size both datasets should be linearly related to each other with a slope of unity (Figure 11).

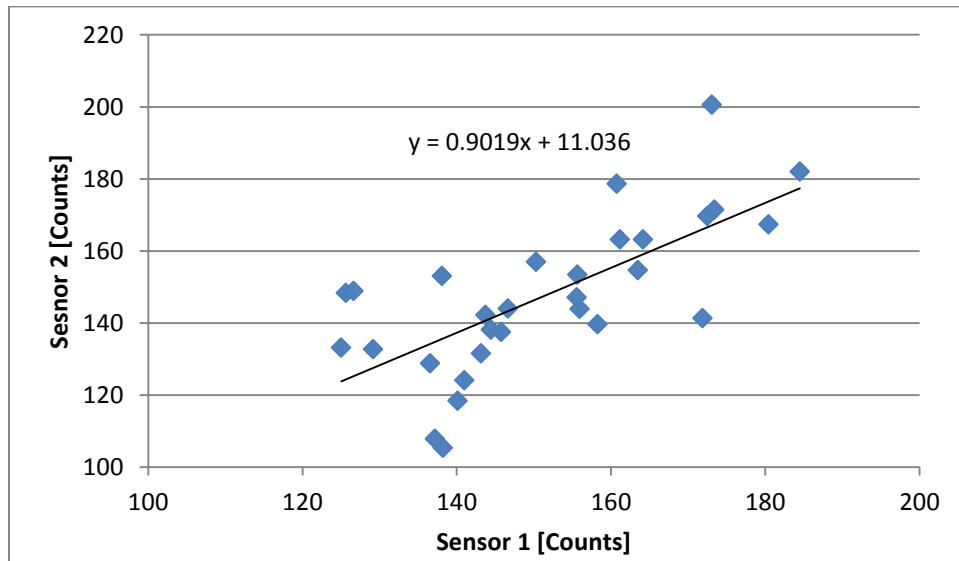


Figure 11: Linear relationship with slope of unity between responses from two sensors

Once linear relationship with slope of unity is met, adding more data point will not add value to the pattern.

2.5. Results

In order to assess the effect of the noise level, sensor drift and total count on the depth calculated by hybrid matching and cross correlation based algorithms, various simulations are run and absolute error with time is captured for each case. A pattern size of 25 data points and a set size of 100 data points are chosen and kept constant for all simulations. To avoid unrealistically high ROP resulting from a mismatch, an upper limit of 150 m/hr. is kept in both the algorithms.

The results from the simulations are shown in Figure 12 to Figure 17, where each figure contains the absolute error with time, calculated with both algorithms for two levels of noise (amplitude of square root of counts and double of square root of counts). The results with an offset in sensor response are shown in figure 13, 15, 17. In legends PM refers to the Hybrid pattern matching algorithm and CC refers to the cross correlation algorithm along with SD and 2xSD being amplitudes of Gaussian noise. In order to compare the error due to other factors with the error due to averaging of ROP, the error due to ROP averaging has also been given in each curve.

The key findings from all these simulations are

1. Cross correlation remains unaffected by the offset and produces identical results.
2. With increase in total count the maximum error reduces
3. In general error increases with increase in noise level
4. The error due to averaging of ROP itself is almost 22m.
5. Error increases more rapidly in the later part of section which can be accounted to the fact that the well becomes horizontal after 1400 minutes time. In this horizontal section the variation in gamma ray readings is subtle which might result in wrong matches being considered for the depth calculation.

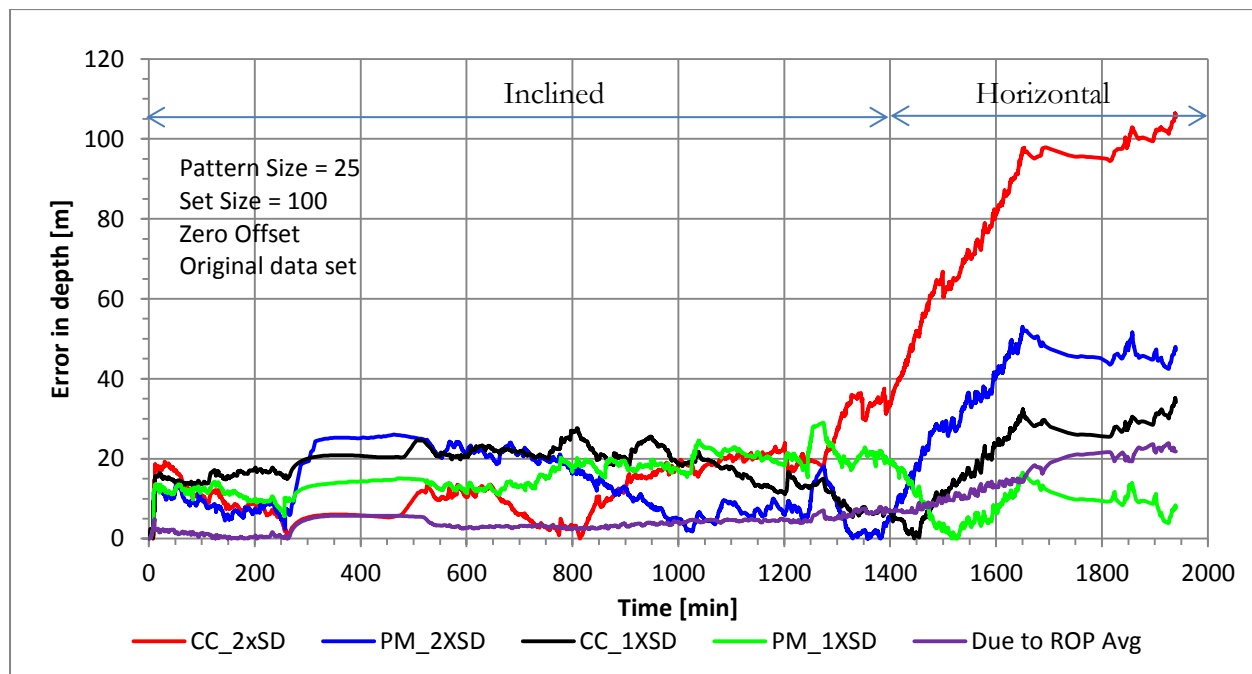


Figure 12: Error in calculated depth with original GAPI dataset without any offset

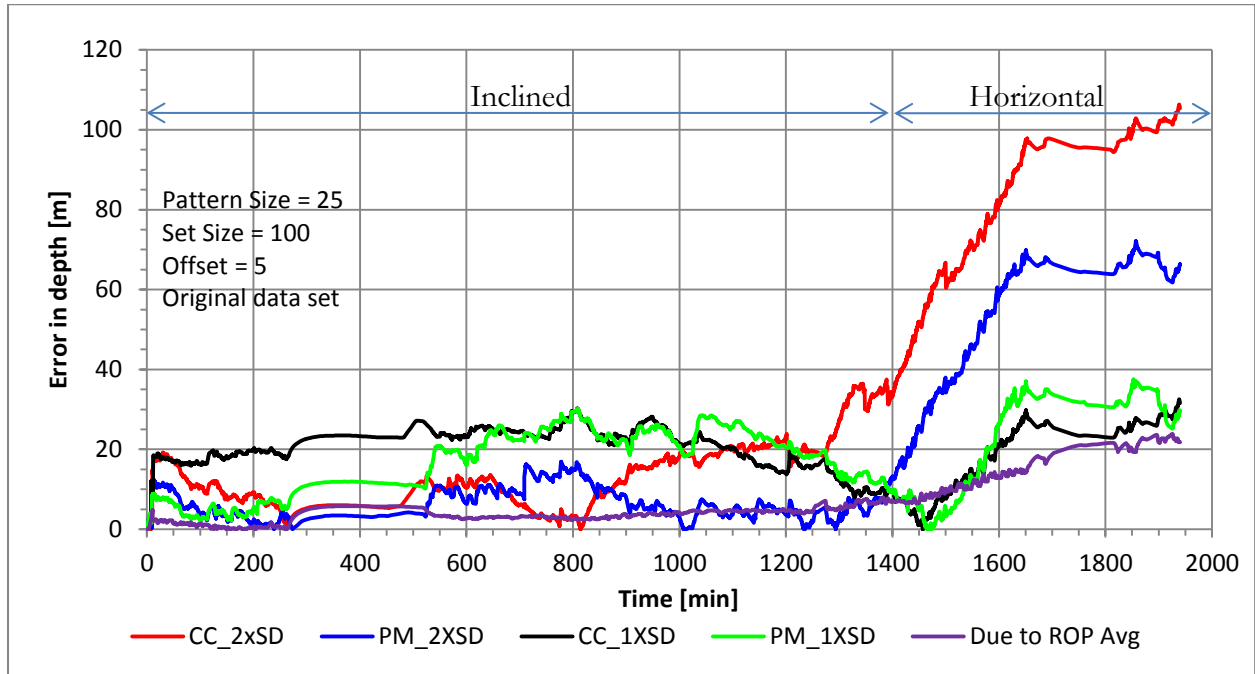


Figure 13: Error in calculated depth with original GAPI dataset and an offset of 5

In all these results, there is a very sharp increase in error at the beginning. This effect is due to the fact that the algorithm does not work till it gathers enough data for creating a pattern from sensor1 and a set from sensor2. During that period the depth does not update. Once the algorithm starts working after gathering enough data points, first calculated value of ROP is considered as the average ROP from the beginning and a high value of calculated ROP results in high initial error. In practice this effect will not be very significant as original time based data will have higher frequency than the current data.

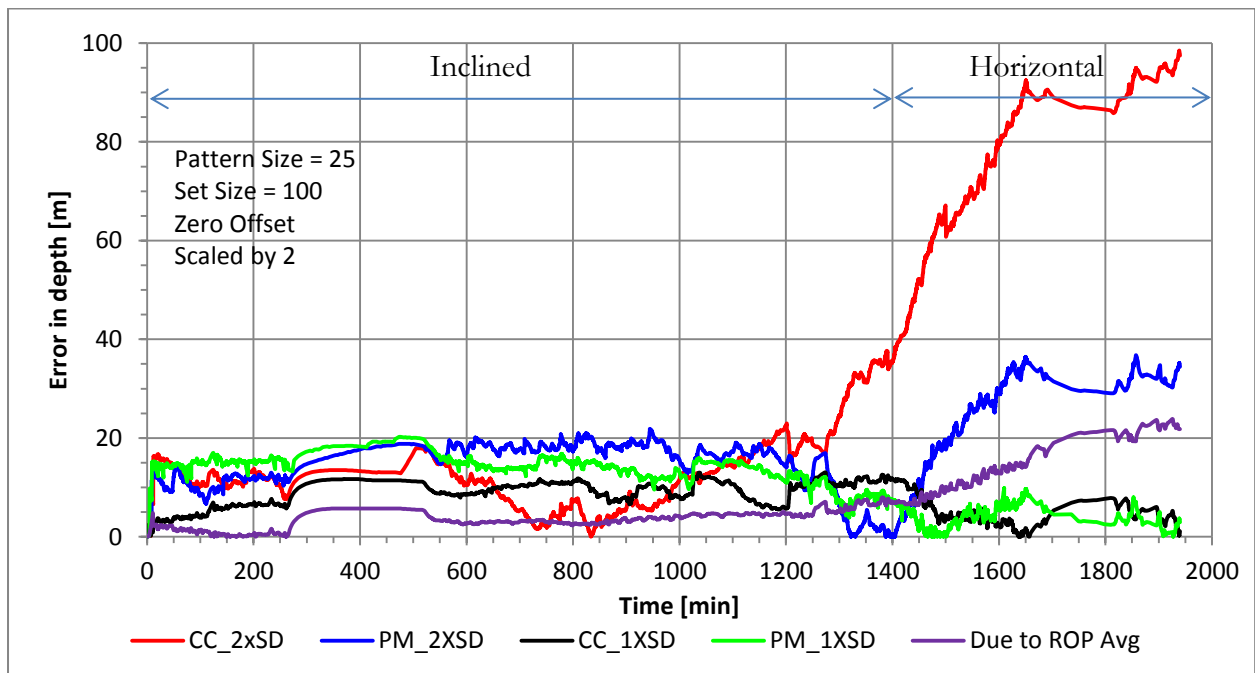


Figure 14: Error in calculated depth with dataset scaled by a factor of 2, No offset

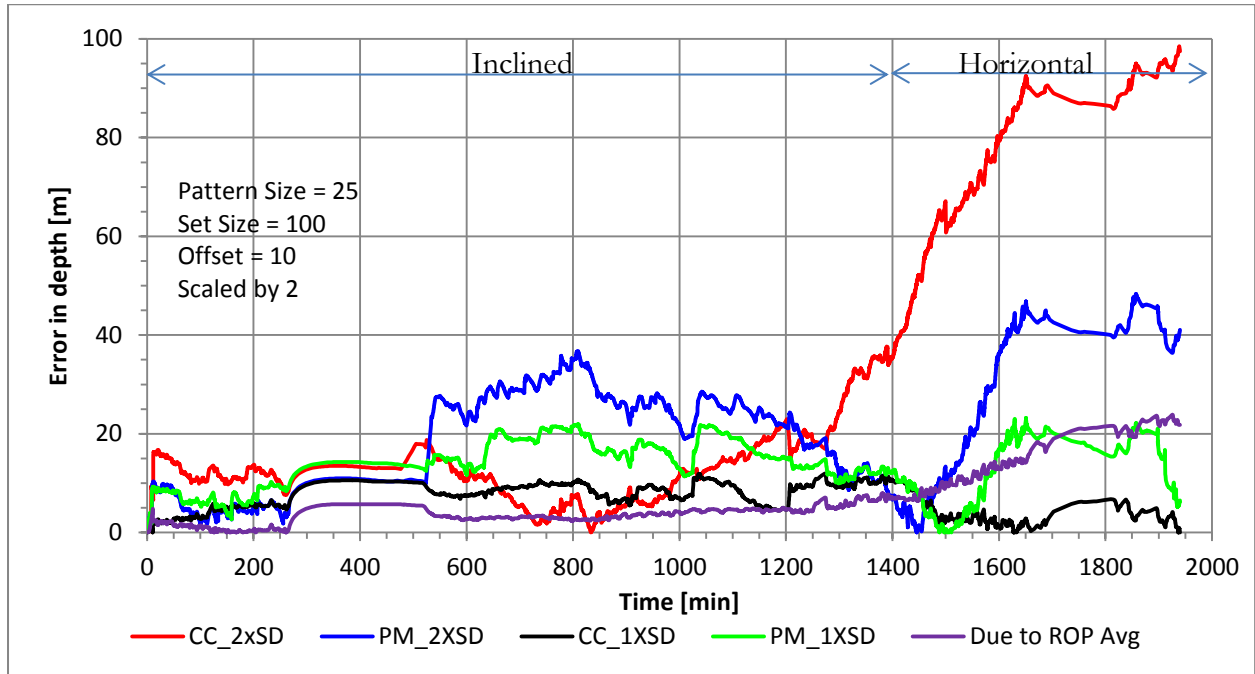


Figure 15: Error in calculated depth with dataset scaled by a factor of 2 and an offset of 10

From Figure 15, it can be seen that offset affects pattern matching adversely and error increases even more with higher noise level. It suggests that the 25 data points of pattern may not truly represent the Gaussian distribution and difference in mean of pattern and potential match does not reflect the offset.

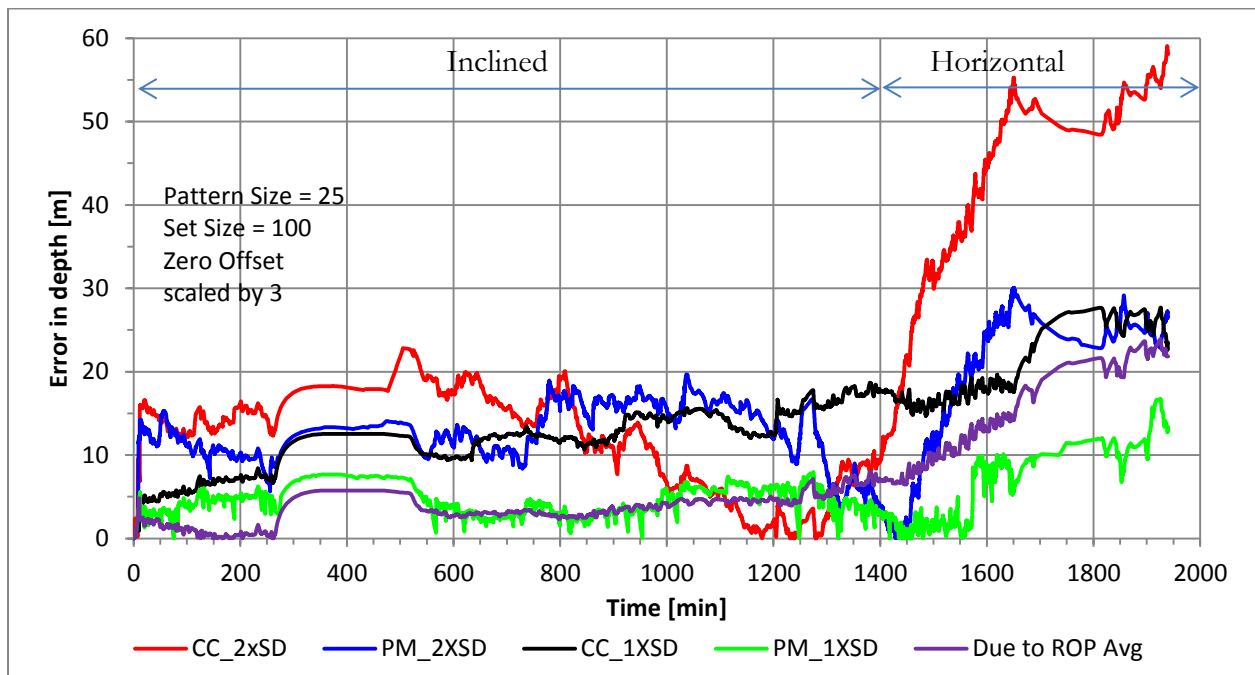


Figure 16: Error in calculated depth with dataset scaled by a factor of 3, No offset

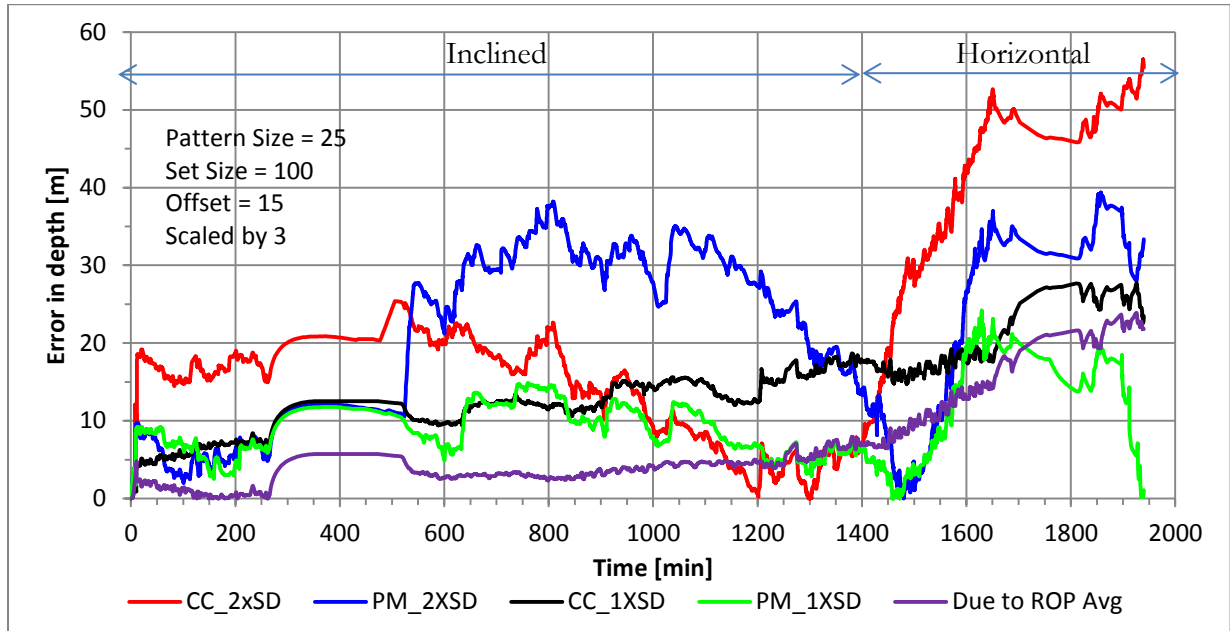


Figure 17: Error in calculated depth with dataset scaled by a factor of 3 and an offset of 15

2.6. Other possible measurements for pattern matching

So far gamma ray measurement is considered as a potential measurement for the pattern matching exercise but other than that density measurements can also be considered for the purpose. Figure 19 shows the original measurements and repeat section values of gamma ray and density measurements for the horizontal section of some well. The equi-spaced peaks in the gamma ray values should be neglected as measurement error. It is quite evident that both gamma and density measurement shows very good repeatability. It proves the potential of density measurements correlation based depth estimation.

In Figure 18, results of depth calculation for both the measurements with help of both algorithms are shown. In general, estimated depth results for density data are in better agreement (Maximum deviation 10.6 m at 1035 min) with surface measured depth compared to gamma ray results (Maximum deviation 17.6 m at 969 min). In practice density measurement requires an active neutron source and is more expensive compared to gamma ray measurements. However, efforts are being made to use a pulsed neutron generator for the density measurements which can reduce the associated risk and can improve its applicability for the purpose.

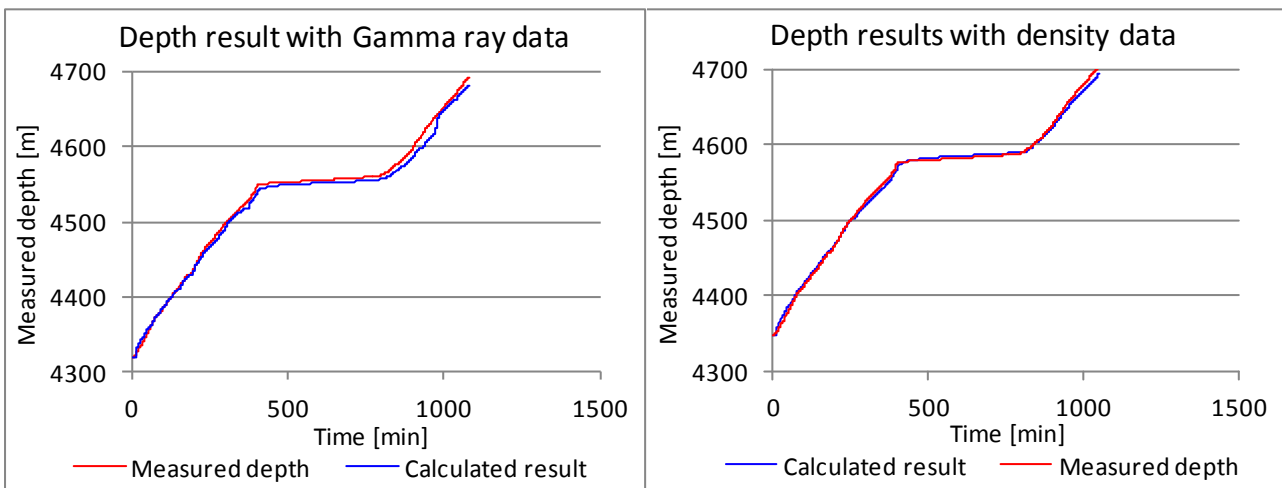


Figure 18: Depth calculation results with gamma ray and density measurement

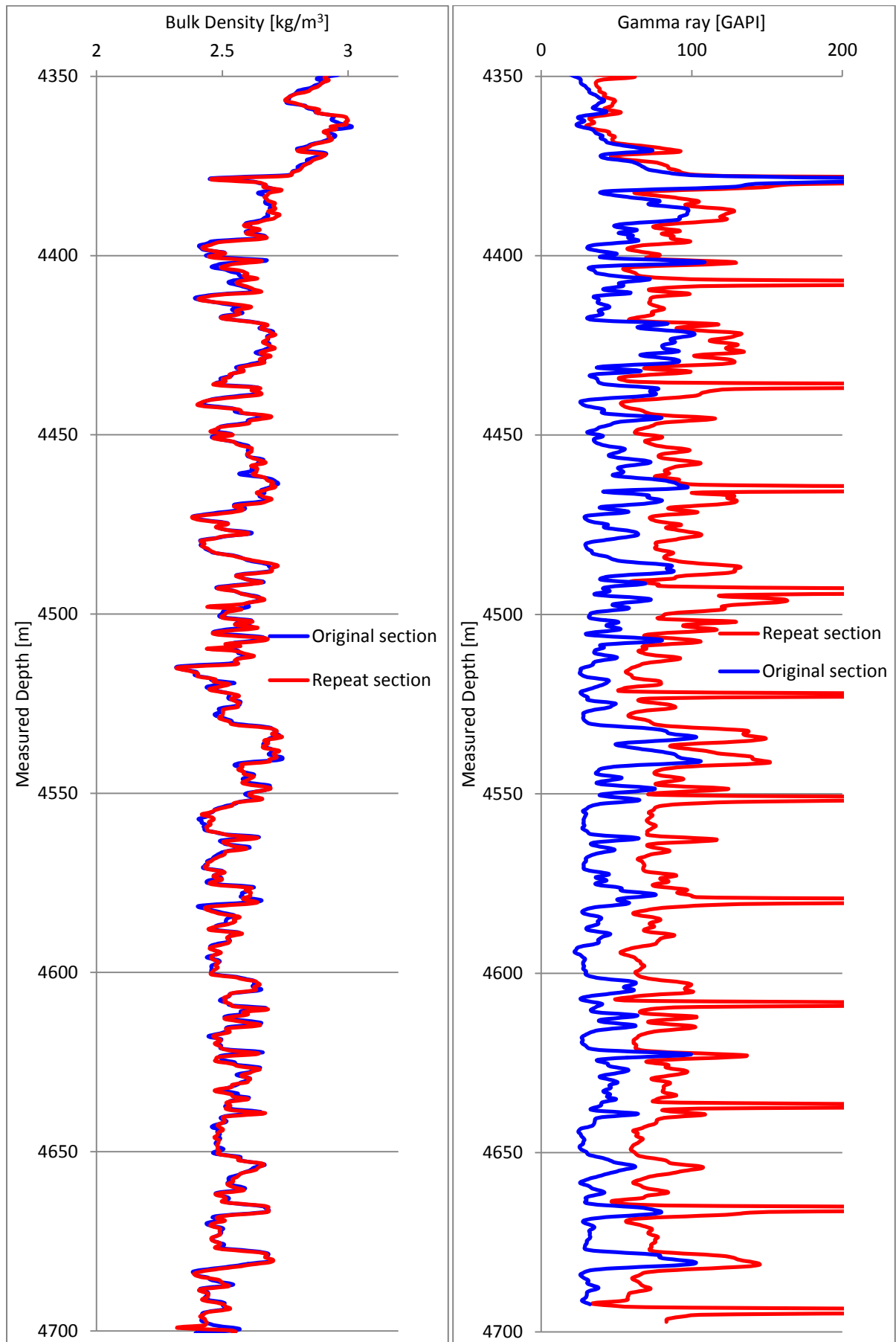


Figure 19: Original and repeat sections for density and gamma ray measurements

3. Calculated depth correction

There are two sources of error in depth calculated with correlation of logs

1. Wrongly identified match
2. ROP averaging.

Due to this inherent limitation of depth calculation concept by correlation of subsurface measurements, to minimise the overall error in the measured depth a secondary system should be used in parallel to the proposed system. Required measurement frequency of the secondary system depends on the error in the primary system and the limiting value of the acceptable error. Two possible methods for such a secondary system are explained in next sub-sections which in parallel to the proposed system can improve overall quality of the depth estimation.

3.1. Correction with help of pipe tally data

One of the easiest solutions to introduce a correction in the estimated depth is by down-linking from the surface. The length of tubular is available on the surface in the form of pipe tally and the same can be stored in a downhole system. A signal can be triggered with the making of each pipe joint, which can be transmitted downhole through the mud column. On receiving the signal the downhole system can identify addition of another pipe joint in the drill string and search for the length of added pipe in stored tally. On adding length of each tubular incrementally the total length of tubular in the well and hence depth of the bit can be calculated. An algorithm for such a system is explained in Figure 20.

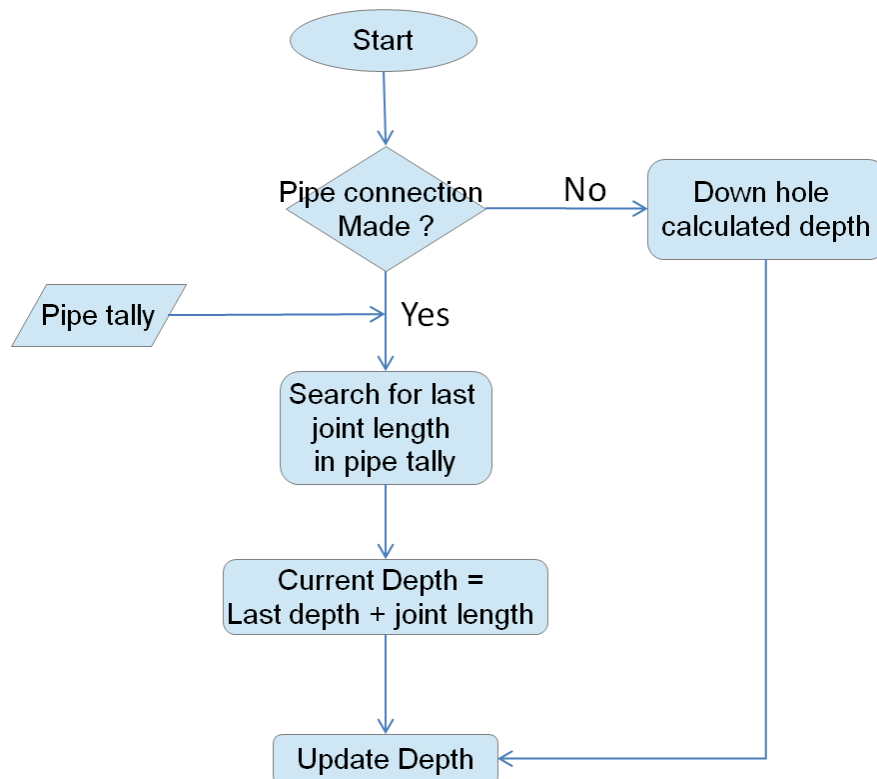


Figure 20: Correction in downhole depth with help of pipe tally

Though this system utilizes mudpulse telemetry for the purpose, due to infrequent transfers (depending upon joint length) over all load on the system will be limited. However, the errors of surface based measurements also penetrate the downhole measurement system and no absolute correction can be made without incorporating any mathematical model for estimating the error associated with surface based measurements.

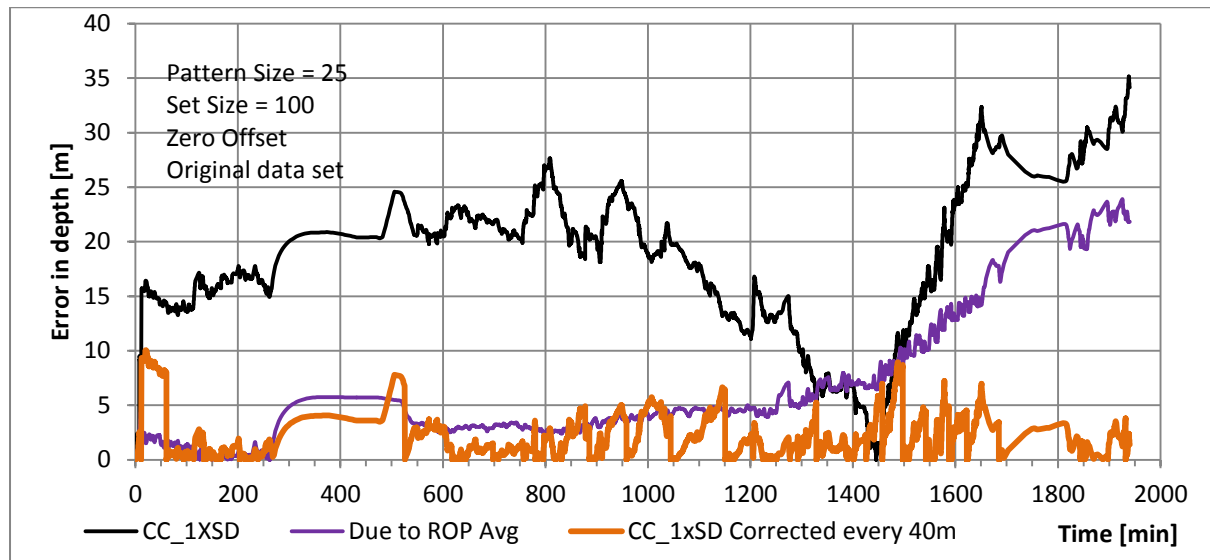


Figure 21: Error with correction from surface every 40 m

Figure 21 above shows the reduction in error if correction in depth is made every 40 m. The simulation was run with cross-correlation algorithm for original dataset. Here the maximum error is limited to 10m.

3.2. Correction by man-made marker tracking

Building on the concept of correlation of geological markers, another concept for estimation of downhole depth is based on creating a mark in the subsurface by a leading marker and then detecting it by a trailing detector fixed in a BHA. When the detector detects the mark, it infers that the drill string has advanced by a distance equal to separation between marker and detector. With every detected mark if a new mark is made in subsurface, downhole depth can be calculated in the multiples of marker-detector separation. By measuring the time difference between the creation of a mark and its detection the average ROP can also be calculated.

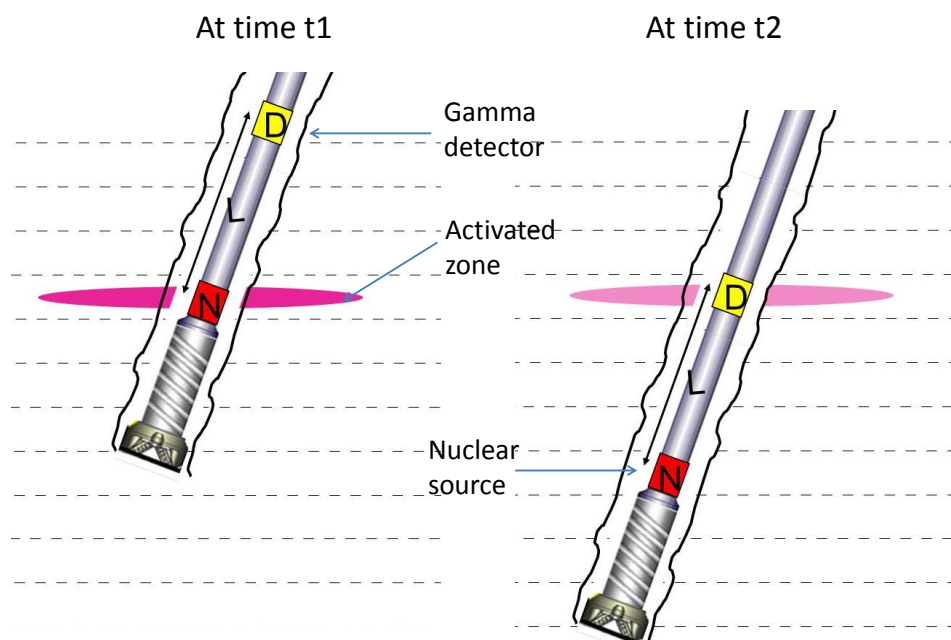


Figure 22: Nuclear source based marker-detector system

Radioactive nuclide such as Californium-252 or accelerator based systems are used as nuclear sources for measuring subsurface properties such as bulk density and porosity. On bombarding subsurface elements with neutrons, they can be activated to unstable nuclides which on deactivation yield radiation of specific characteristics. A specific section of the borehole can be activated with the help of a switchable neutron source such as commercially available pulsed neutron generators. By identifying the characteristic emissions from decay of unstable nuclides, location of such activation can be identified. This gives a concept for a subsurface marker-detector system using an accelerator based neutron generator as a marker and a gamma ray scintillator based detector shown in Figure 22.

To investigate the workability of this concept a detailed study is carried out and is summarised in next subsections.

3.2.1. Subsurface element to be activated

Subsurface contains enormous variety of elements in the compounds of rock formation and associated fluids. However, not all subsurface elements are suitable for the marker-detector system. The suitability of the elements depend on three major factors

1. Neutron capture cross-section: This signifies the probability of activation of any nuclide for a given neutron energy at a temperature.
2. Abundance in the subsurface: The higher the concentration the higher will be the yield of activated atoms and the more will be the characteristic radiation from deactivation.
3. Decay constant: The half-life of the radioactive nuclide created from the neutron capture signifies the number of decaying atoms at any given time. Nuclides which are highly unstable decay in very short time which might not be enough for the detector to reach the activated location and capture decay photons. On the other hand nuclides which are almost stable will not decay in high enough number to give a detectable signal.

On considering half-life of most common elements in subsurface the most favourable elements are chlorine isotope Cl-37, Silicon isotope Si-30 and naturally occurring sodium Na-23. Both Chlorine and sodium atoms are present as ions in saline formation water and silicon is present as silicate minerals in sandy and shaly formations. Even though chlorine and silicon are abundant in nature, usually Cl-37 and Si-30 isotopes occur in lower concentrations (24% and 3%, respectively) and have lower neutron capture cross-section (0.433 and 0.11 barn, respectively). Hence, detailed calculations are required to evaluate the number of activated atoms and resulting photons.

3.2.2. Marker-detector separation

For any activated element, at any given point in time the amount of decay depends upon the concentration of radioactive nuclides. With increasing time the concentration of activated nuclide decreases exponentially and also decrease the radiation from the decay. Hence for the maximum signal the separation between detector and source should be small. But the neutrons from the source travel in all possible directions and are not restricted to the formation just in front of the source. Due to larger region of activation with smaller marker-detector separation it will be very difficult to precisely locate the source position corresponding to activation. Hence the distance between source and detector need to be decided such that the concentration of activated nuclei remains high enough yet the locations remain distinguishable. For validation of concept the axial spread of activated zone and signal strength in a detector need to be computed.

3.2.3. Nuclear simulation using MCNP

To investigate the feasibility of the concept and resulting signal from activated nuclei in subsurface, nuclear simulations are carried out to simulate the neutron and photon transport in the subsurface. These simulations are carried out with MCNP. It is a Monte Carlo based general purpose nuclear transport code capable of simulating time based transport of nuclear particles such as neutron, photon and electron through generalised geometries. Monte Carlo based calculations involve the behaviour simulation of each particle with the help of statistical sampling using random numbers from their probability distributions. It consists of actually following each particle from its source throughout its life to its death in some terminal category (absorption, escape, etc.) Probability distributions are randomly sampled using transport data to determine the outcome at each step of its life.[36]

The concept validation requires simulation of two problems

1. Activation of suitable isotopes
2. Detection of photons generated from deactivation

Both these problems require separate simulations in the MCNP code. In the first simulation transport of neutrons from the neutron generator till their capture in the formation is carried out. Output of the first problem gives the location of activated isotopes resulting from the neutron capture. This output is used to create the input for the second problem. As the location of the start of photons is the location of the activated nuclide and is known, to complete the input for second problem a statistical sampling of decay time with the help of random numbers and the decay constant of the nuclide is used to associate the time of decay with each nuclide. This space and time domain photon source is used in a second simulation to simulate transport of photons in the subsurface to count the number of photons which can reach the detector. These photons quantify the strength of signal in the detector and its number should be big enough to be detected and to be distinguished from background noise for this concept to work. The details of simulation are given in Appendix-4

3.2.3.1. Model description

For the simulations a simplified model of subsurface is created as shown in Figure 23. A sandstone reservoir with 30 percentage porosity and salinity of 30,000 ppm is modelled.

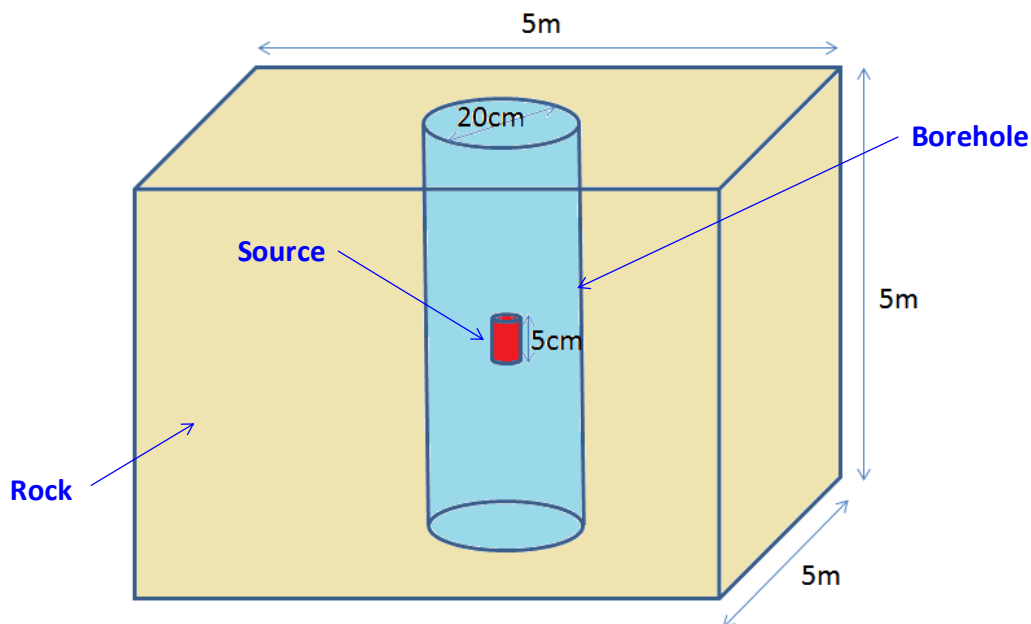


Figure 23: Model dimensions and location of source and detectors in the borehole

It is assumed that salinity is due to sodium chloride with 25% of chlorine atoms being Cl-37 isotopes as occur naturally. The borehole of diameter 20cm is modelled filled with water to simulate the drilling scenario. The neutron source and detector should be part of BHA and hence are considered at the axis of borehole for respective simulations. Neutron source is 14.1 MeV, D-T source with neutron yield of 10^8 neutrons per second which is industry standard specification for pulsed neutron generators. The source is modelled as 5 cm long cylinder with 3 cm diameter. The detailed input files are given in Appendix A4.6.

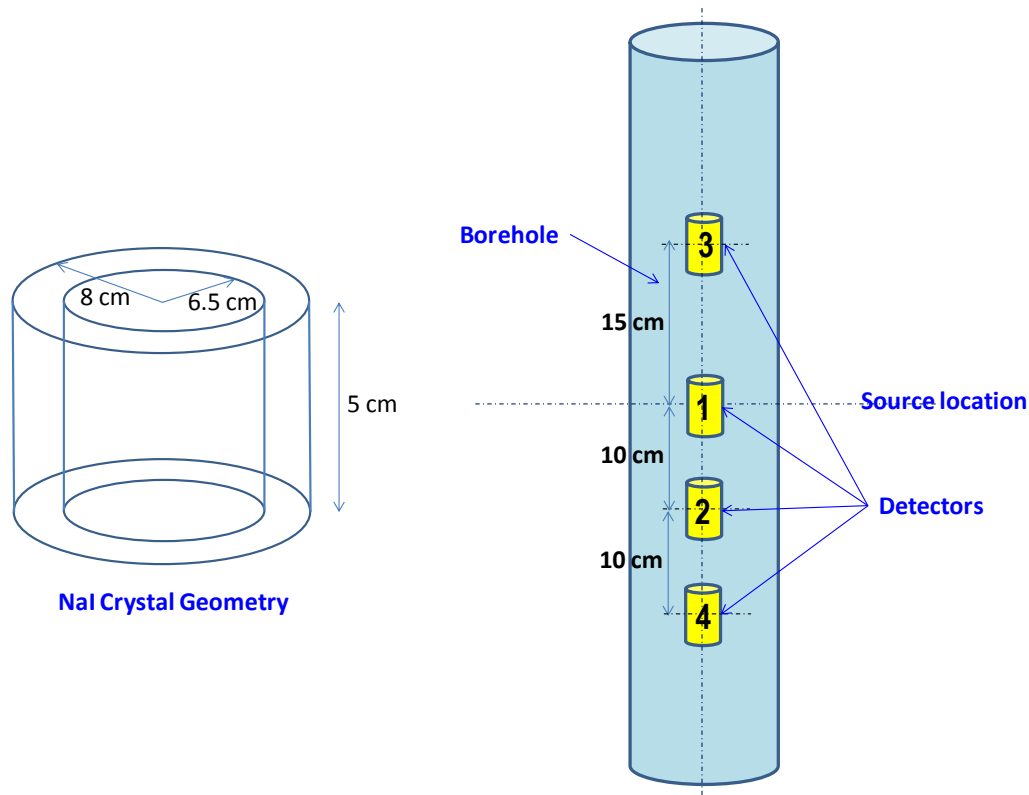


Figure 24: Crystal geometry and location of detectors

In the second simulation, the detector is modelled with a NaI scintillation crystal of well type design with a length of 5 cm and having 6.5 cm inner radius and 8 cm outer radius to give larger capture volume. The detector will be moving with the BHA while drilling ahead. To see the effect of detector position on the signal strength four detectors are modelled as shown in Figure 24. One detector is modelled at the location of source (Detector 1) and other three at 10 cm (Detector 2) and 15 cm (Detector 3) and 20 cm (Detector 4) from the source. The photon flux with its time is calculated in each detector to identify the time window with sufficient signal strength.

3.2.3.2. Results

The neutron transport simulation was carried out for 10^8 neutrons and the location of each activated nuclei is obtained in a so called PTRAC file [36]. On post processing the PTRAC file the number of activated atoms of Na-23, Cl-37 and Si-30 are found to be 14050, 3222 and 5555 respectively. As Monte Carlo simulations use random sampling of a probability distribution, the uncertainty in the results usually reduces with the increase in number of source particles (*nps*) for the run. As demonstrated in Figure 25, on increasing the number of source particles by 10 times, the standard deviation of total flux per source particle over 10^5 seconds (27.8 hrs) in detector 4 get reduced to 31% (from 0.0325 to 0.0100).

Considering the sensitivity of the results on the number of particles, the number of photons for the second simulation was increased artificially to 100 times of the outcome of first simulation.

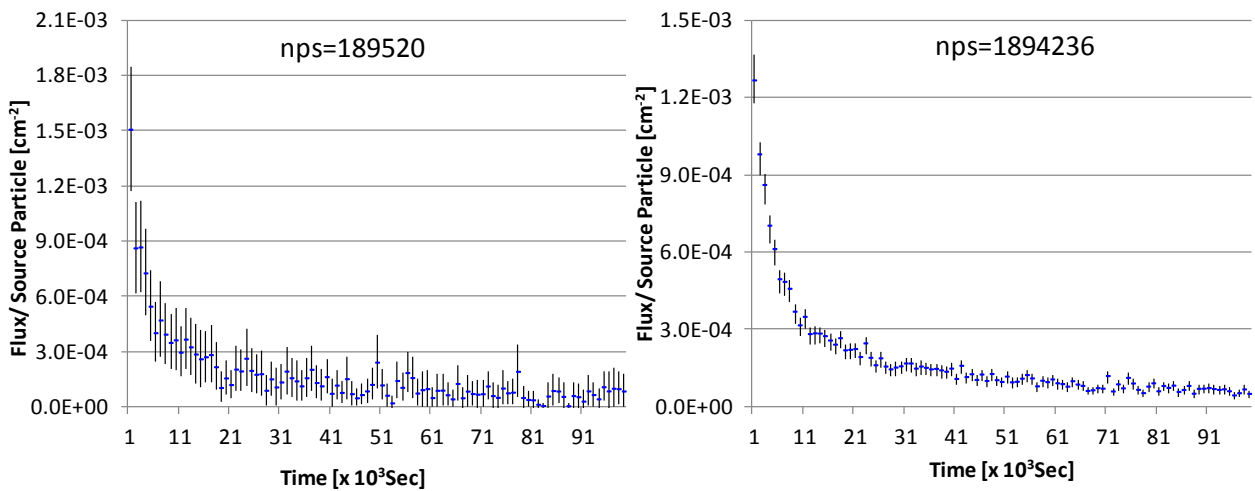


Figure 25: Statistical variation in results for different number of source particles with 95% confidence

The spread of activated nuclei in subsurface both in radial direction (X, Y) and in axial direction (Z) is shown in the Figure 26 given below.

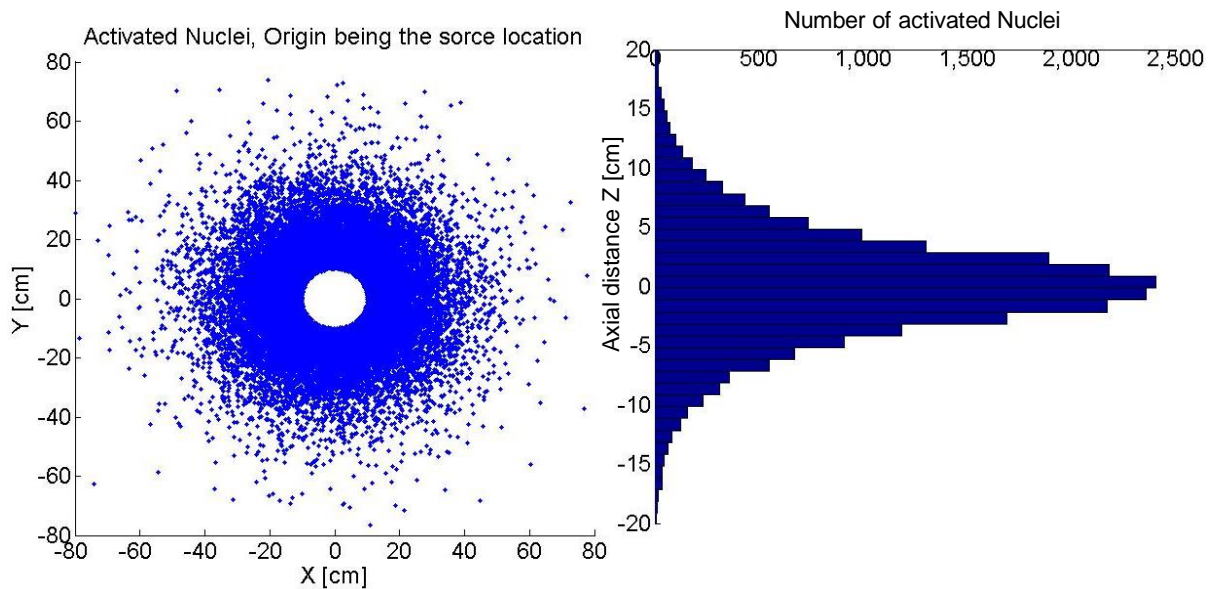


Figure 26: Spread of activated nuclei in subsurface

As the neutrons starts uniformly in all directions from the source it is important to look at the spread of activated nuclei along the axis of the well bore. The histogram showing the number of activated nuclei along the axis of the borehole (Figure 26) suggests that the axial spread of activated nuclei's is limited to 20 cm from the source location. Due to the limited axial spread, the uncertainty associated with locating the source position at the time of activation is reduced to ± 10 cm, which helps in achieving higher accuracy with such a marker-detector system. However, this simulation is carried out for a static source and in practice the source will be moving in the BHA while drilling ahead. The actual spread of activated zone (Z) will increase due to movement of source itself. The increase in axial spread of activated zone will be equal to length drilled while the source was kept on.

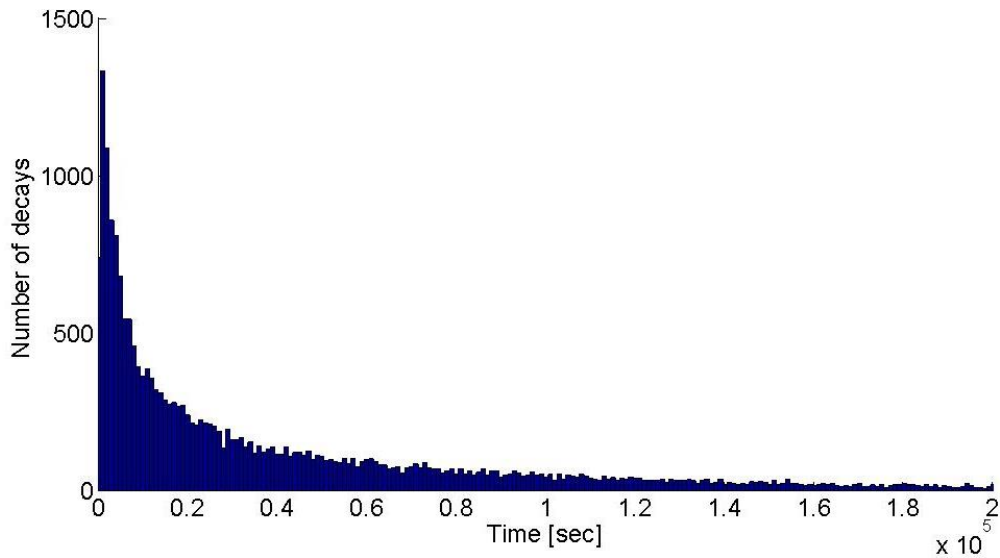


Figure 27: Decay profile of activated nuclei

The signal strength in the detector depends upon

1. Proximity to the activated location
2. The time elapsed after activation.

Radioactive nuclides follow exponential decay as shown in Figure 27. If the number of photons produced per unit time remains constant, the signal in the detector should increase while closing in to the activated location due to increase in concentration of activated nuclei. But due to the exponential decay, the number of photons produced and their associated signal decreases exponentially with time. Hence the actual signal in the detector will be the resultant of a linear increase in signal due to the detector closing in to the source location and exponential decrease of signal itself, which might introduce an uncertainty in locating the activated zone. The variation of photon flux per source particle with time and detector distance from source location is shown in Figure 28

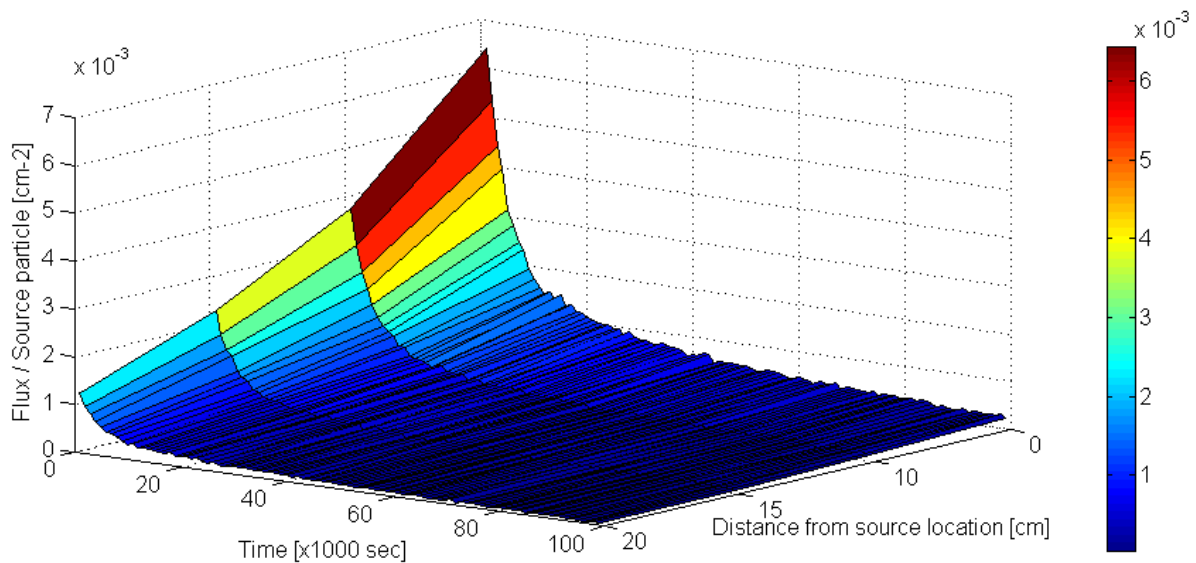


Figure 28: Flux variation in moving detector with space and time

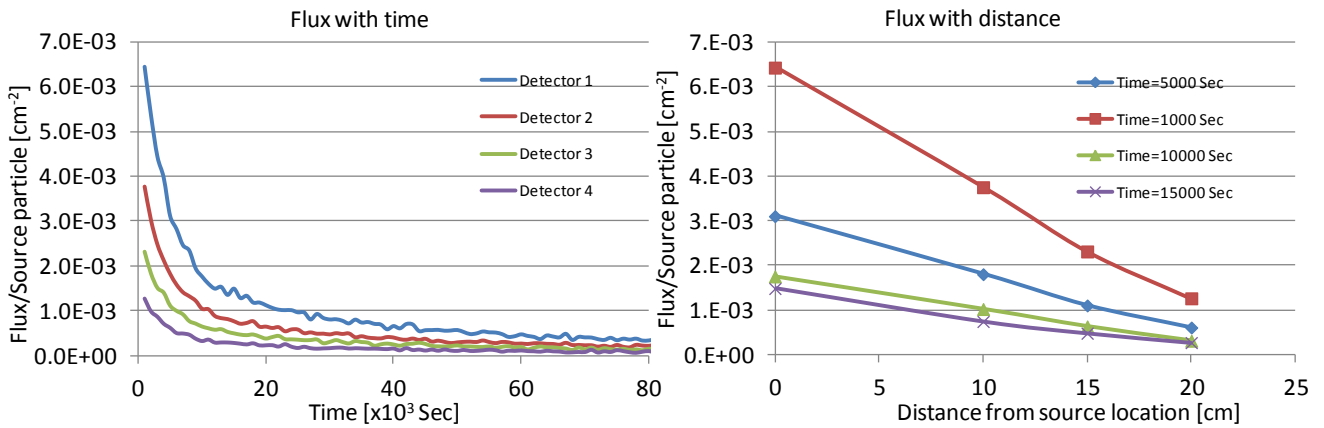


Figure 29: Change in photon flux in detectors with time and distance from source

However on analysing results of the photon transport shown in Figure 29 above, it can be seen that the flux increases five times while closing in to the activated zone from 20 cm to 0 cm. Assuming a modest ROP of 8 m/hr the distance of 20 cm can be drilled within 100 seconds in which the signal strength gets reduced by less than 5 percentage as shown in the Figure 30. It suggests that the effect of closing in to the activated zone is much more significant compared to the exponential decay.

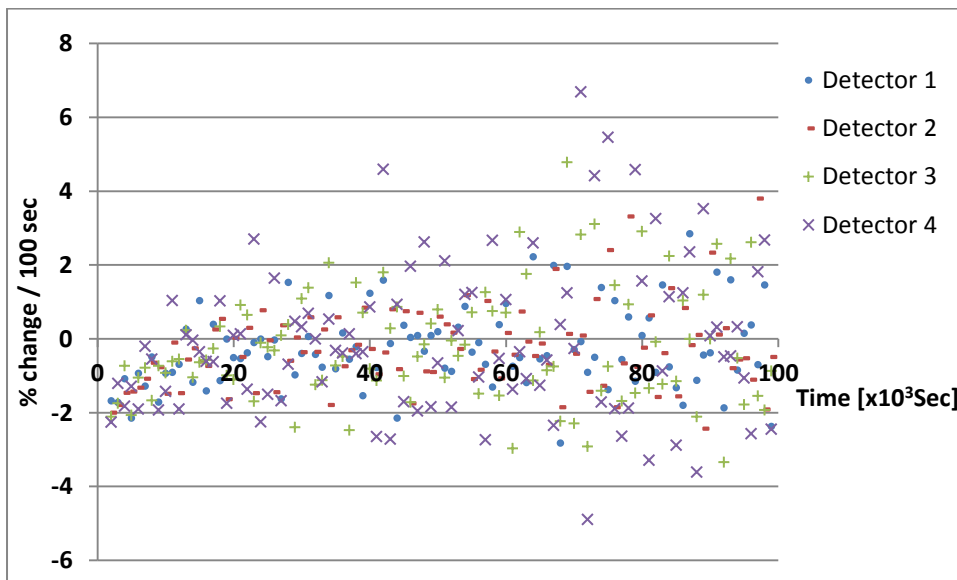


Figure 30: Percentage change in signal strength per 100 sec. at detector locations

The number of light photons generated for the incident gamma ray varies based on the type of scintillation crystal used in detector. However, for every crystal the efficiency of converting the incident gamma ray into a light photon depends on the geometry and the energy of incident radiation.

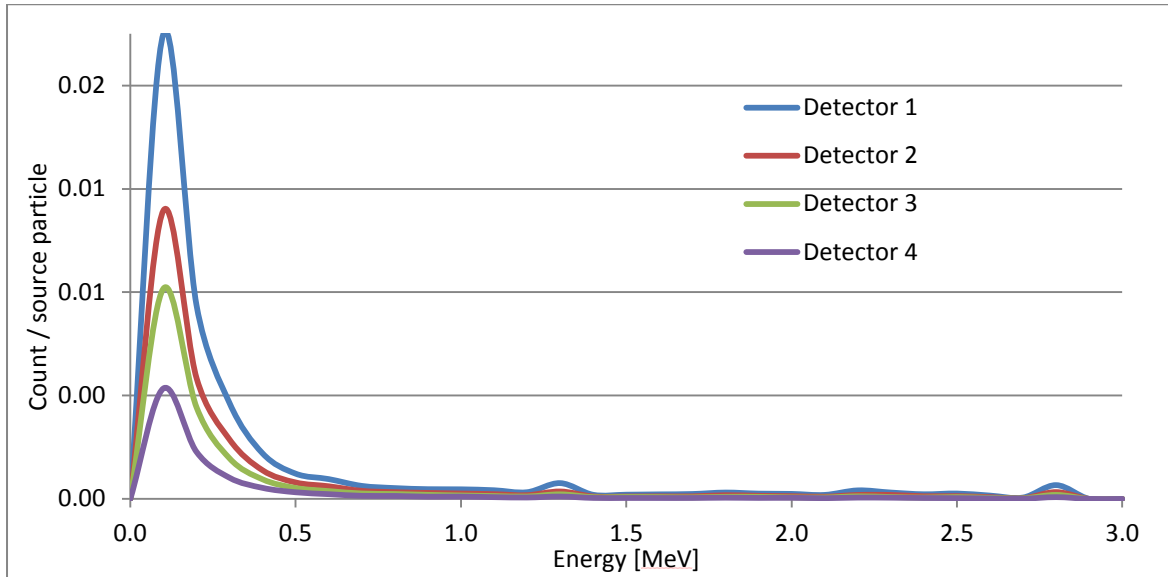


Figure 31: Energy distribution of photons in the detectors

As shown in Figure 31, the energy of most photons crossing the detectors is less than 0.5 MeV and as the efficiency of scintillation crystals increases (eg. NaI Figure 32) with decrease in the photon energy, this will result in a higher signal in the detector. However, the peak related to characteristic energies for Si-31, Cl-38 and Na-24 (1.3, 2.1 and 2.75 MeV, respectively) is very small even for detector 1 and might not be detectable.

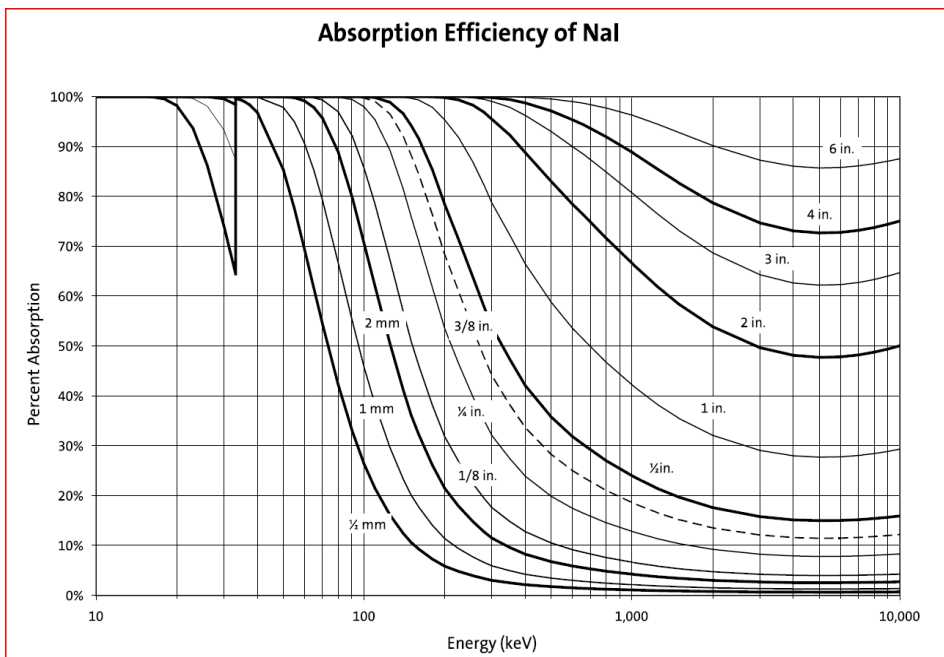


Figure 32: Absorption efficiency of NaI crystals of different thickness

4. Application of downhole depth estimation for automated subsurface navigation

The motivation for downhole depth lies in

1. Facilitation of closed loop subsurface navigation
2. Elimination of errors due to surface based measurements in ROP and depth

In the next subsections a scheme is proposed for automated subsurface navigation and an attempt is made to use downhole depth and survey data to follow a predefined well-plan with help of a simplified RSS performance model.

4.1. System for automated subsurface navigation

The main objectives of subsurface navigation are

1. Reaching the reservoir while maintaining optimal well trajectory
2. Following the reservoir layer while fulfilling geosteering objectives
3. Avoiding the geological hazards on the way to the reservoir

A simplified scheme for reaching the reservoir with automated subsurface navigation is shown with help of the flow chart in Figure 33.

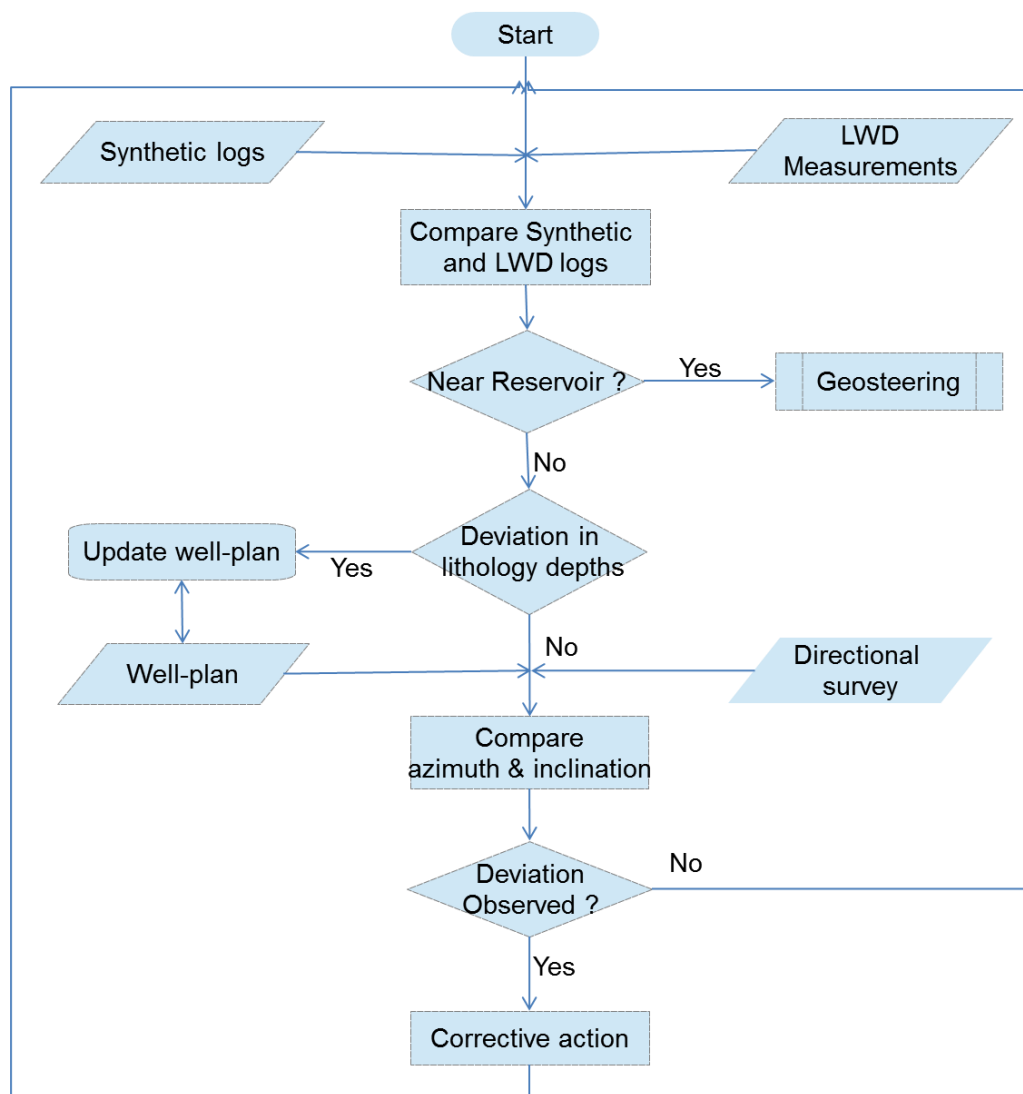


Figure 33: Subsurface navigation flow chart

Well-plans are created by drilling engineers with available seismic measurements, log data and geological information, to avoid a collision with existing wells and achieve an optimum well trajectory to reach the reservoir. These well-plans guide directional driller in well placement. In an automated drilling environment these well-plans can be used to enter the reservoir and later on geosteering algorithm can be deployed for drilling the reservoir section to meet the well objectives.

The well-plan consists of measured depth, inclination and azimuth values. Both inclination and azimuth values are also measured in a directional survey. By continuous monitoring of a planned and measured well path and calculating the deviation, corrective actions can be taken real time for following the planned trajectory. A synthetic log response can be created with the help of log data from the offset wells beforehand to identify approaching the reservoir and correspondingly the entry can be established. Similarly such a synthetic log response can also be used to determine key geological depths for setting of the casing shoe and corrections can be made in the original well-plan accordingly.

4.2. Rotary steerable system (RSS) performance model

Modern RSS systems are programmed from the surface at different tool settings and tool face angles to achieve desired build-up and turn rate. It gives the flexibility and precision in achieving complex three dimensional trajectories. The number of available tool settings varies from tool to tool whereas dogleg severities achievable at any setting depends on many parameters such as rock properties, inclination of hole, BHA design, drilling parameters, etc. Out of these parameters the rock properties such as anisotropy and formation strength have high uncertainty and are responsible for deviation from predicted behaviour. Downhole system of automation gives a unique opportunity of utilizing real time measurement of bit performance and downhole drilling parameters to iteratively correct the bit behaviour model and use it for determining next tool setting.

To achieve automated subsurface navigation, it is important to model the performance of downhole tools in terms of their angle building capability. A simplified mathematical model is used to mimic the tool performance predicted by complex modelling softwares. In a very simplified model it can be assumed that the dogleg severity achievable (β) is proportional to side cutting force (F_s) on a bit.

The same can be expressed as:

$$\beta = k F_s \quad \{14\}$$

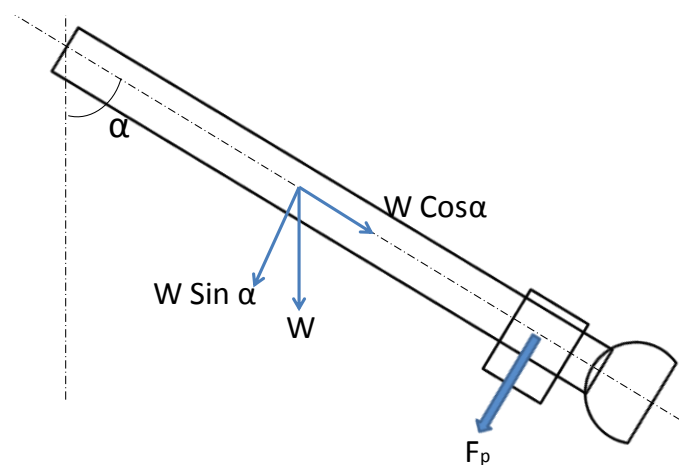


Figure 34: Simplified BHA schematic

The proportionality constant (k deg/Nm) can account for factors such as bit design, rock properties and BHA design. The side force on the bit in case of a ‘push the bit’ design RSS constitute of

- Component of drill string weight (W) due to hole inclination and drill string compression due to drill string bending
- Side force applied by the retractable pads (F_p).

Various arrangements of stabilizers can be used to give a BHA required build, drop or hold tendencies. These arrangements allow the BHA to bend into the desired direction as an elastic beam supported on the borehole wall through stabilizers. RSS uses hydraulically operated pads to create the side force. This side force is controlled by a directional driller from the surface with help of mud pulse telemetry through various tool settings. However other than tool side force, use of stabilizers can also have an additional effect on the angle building capabilities based on their location from the bit. Hence the effect of stabilizers also needs to be considered carefully for better BHA behaviour prediction.

In a simple arrangement we can assume one near bit stabilizer creating a small pendulum effect. This will increase the drop rate and reduce the build-up rate. Based on this assumption build up rate can be simplified to

$$\beta = k (F_p + W \sin \alpha) \quad \{15\}$$

Here, the borehole inclination from the vertical axis is α as shown in Figure 34 . For a given weight of BHA, the DLS depends upon borehole inclination and tool setting.

To validate the model and tune it with realistic values of proportionality constant k , the weight W and the pad side force F_p , we use RSS performance data for a commercial tool used for drilling some well. The tool has 13 settings of tool deflection resulting in different side force from the pad. The data used is shown in the graph below.

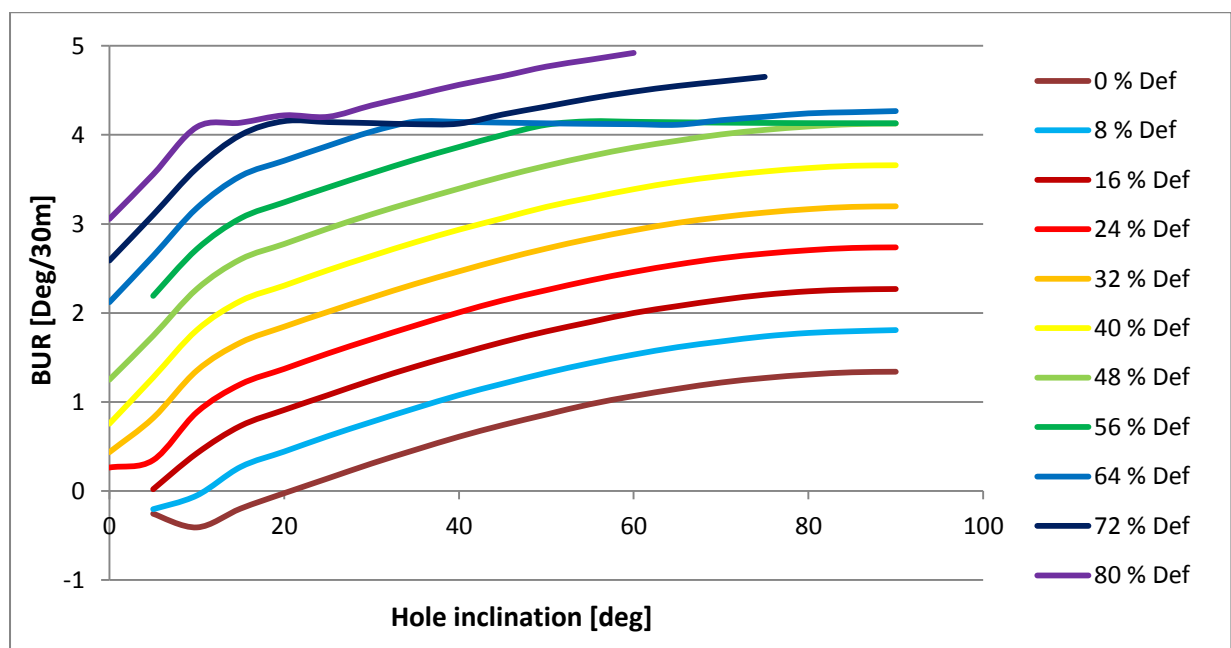


Figure 35: Anticipated BUR at various deflection settings and well bore inclinations

To mimic the same behaviour we can assume that the side force increases linearly with the increasing tool setting neglecting other effects. Using initial values of $k = 1$ deg/kNm, $W = 1.4$ kN and $F_p = 5$ kN the following characteristics can be created, which are close to the computer program predicted BHA behaviour and shown in Figure 36.

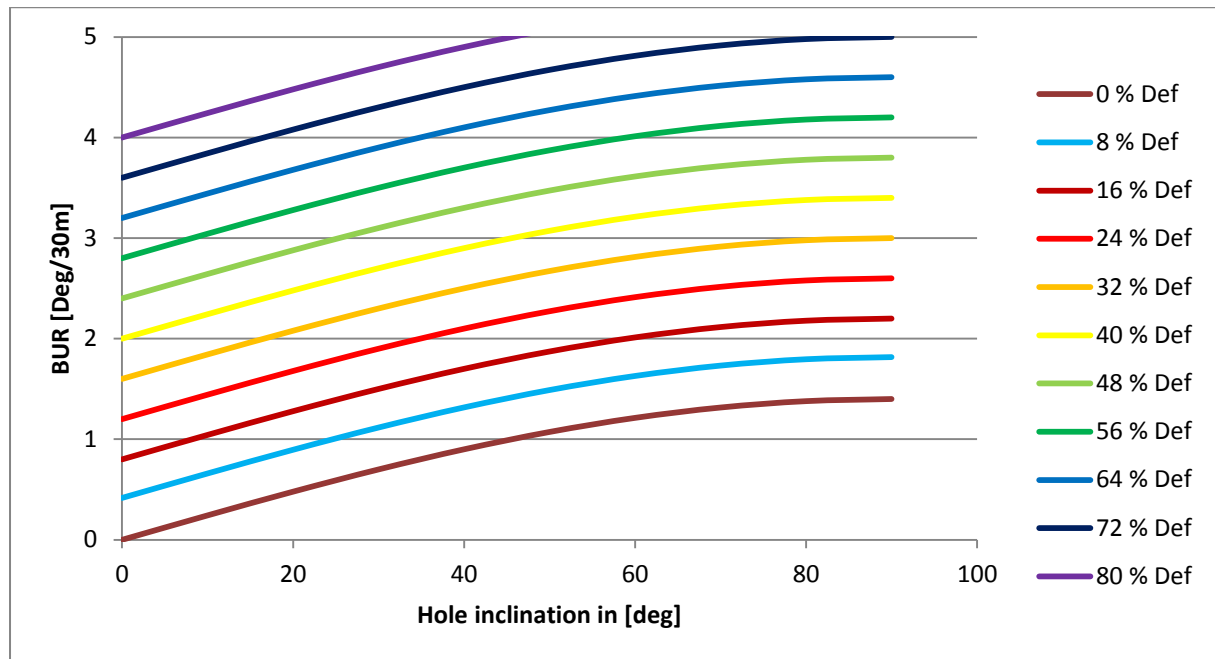


Figure 36: Approximated BUR at various deflection settings and hole inclinations

The same model is used in demonstrating the integration of downhole depth measurement with RSS control to follow a given well path. In practice any deviation between actual performance and model prediction can be accounted for in the proportionality constant k which can be updated on the fly based on real time performance evaluation. The simplicity of the RSS model gives an automated system more robustness and operational ease.

4.3. Automated well-plan execution

The survey instruments give a value for inclination and azimuth at any subsurface point along well trajectory during drilling and with help of surface based depth, adherence to a given well-plan is checked and maintained. Ideally real time comparison of well-plan and well trajectory should result in total confirmation to the well-plan. However, the response of RSS to the subsurface formations and drilling parameters cannot be predicted accurately and hence at any given tool setting the build-up or drop angle can vary and result in deviation from the well-plan. Directional driller on the surface changes the tool setting of the RSS tool in order to minimise the deviation based on experience.

In practice due to the limitation of band width in current mud pulse telemetry systems and associated time lag it is not possible to follow the well-plan accurately. In an automated system the well-plan can be stored in the BHA where downhole depth, inclination and azimuth will be available and by comparing real time measurement of actual trajectory with the well-plan, better drilling performance can be achieved. To simulate the performance of automated well-plan execution, a numerical simulator with varying subsurface response is created. The flow chart for the same is shown in Figure 37.

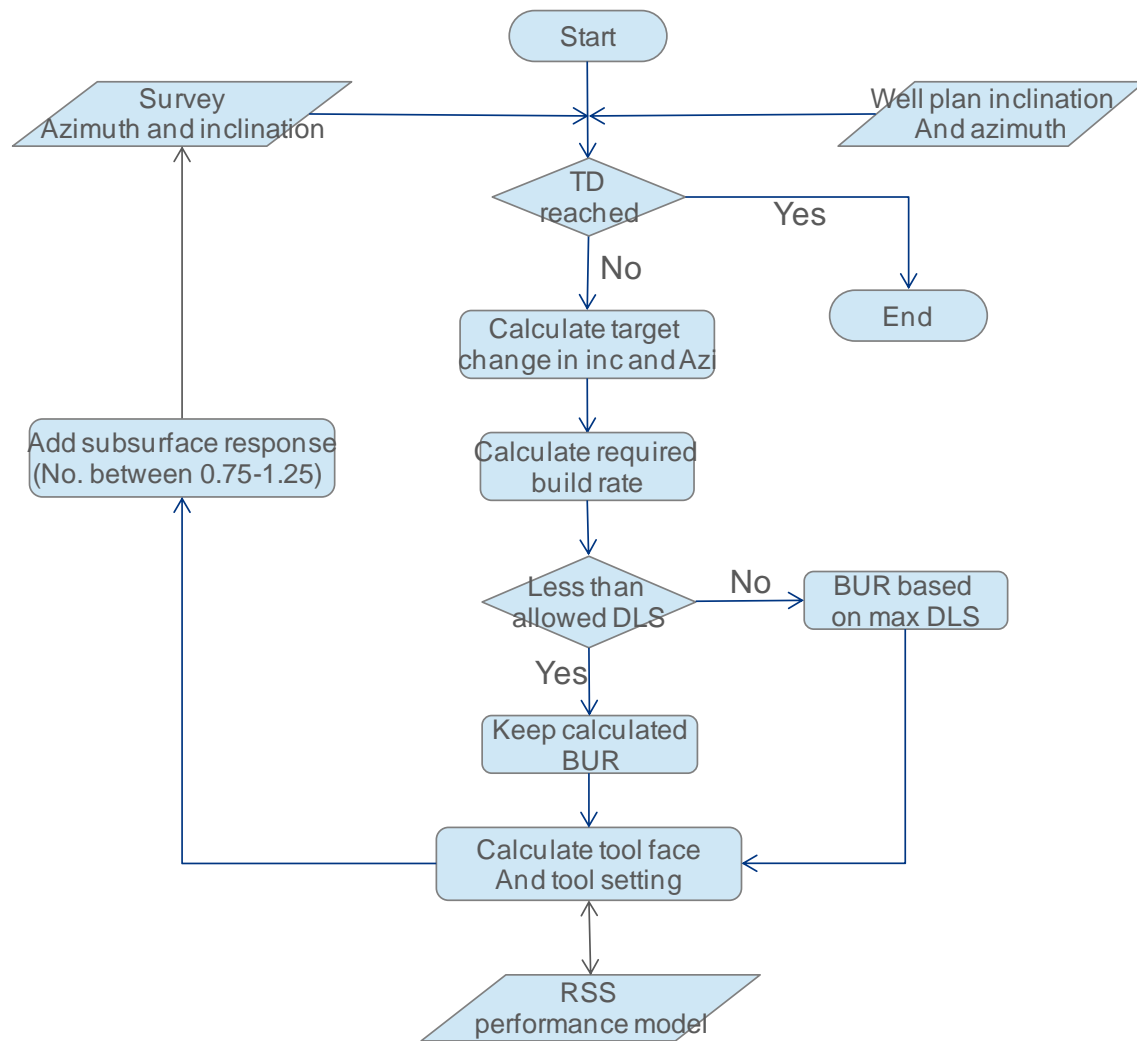


Figure 37: Flow chart for evaluating real time automated well-plan execution

4.4. Simulation results

Two separate simulations were run to benchmark the performance of the real time downhole automation with a surface based automated system for well-plan execution. As surface based system relies on mud pulse telemetry for communication and the number of changes possible in the RSS setting per joint length is limited. On the other hand a downhole based system can make much frequent changes in RSS tool setting to achieve a real time closed loop control. For these simulations it is assumed that a downhole system can make changes in RSS Settings every 0.1 m and the surface based system can make changes only after 2.5 m depth is drilled. Here the RSS performance model was kept the same for the whole simulation and only tool settings are changed based on the deviation from the well-plan caused by random subsurface response. For calculation of downhole depth, the Hybrid pattern matching algorithm is used. The well-plan and gamma ray data are the same as used in section 2.4 for the evaluation of correlation algorithms.

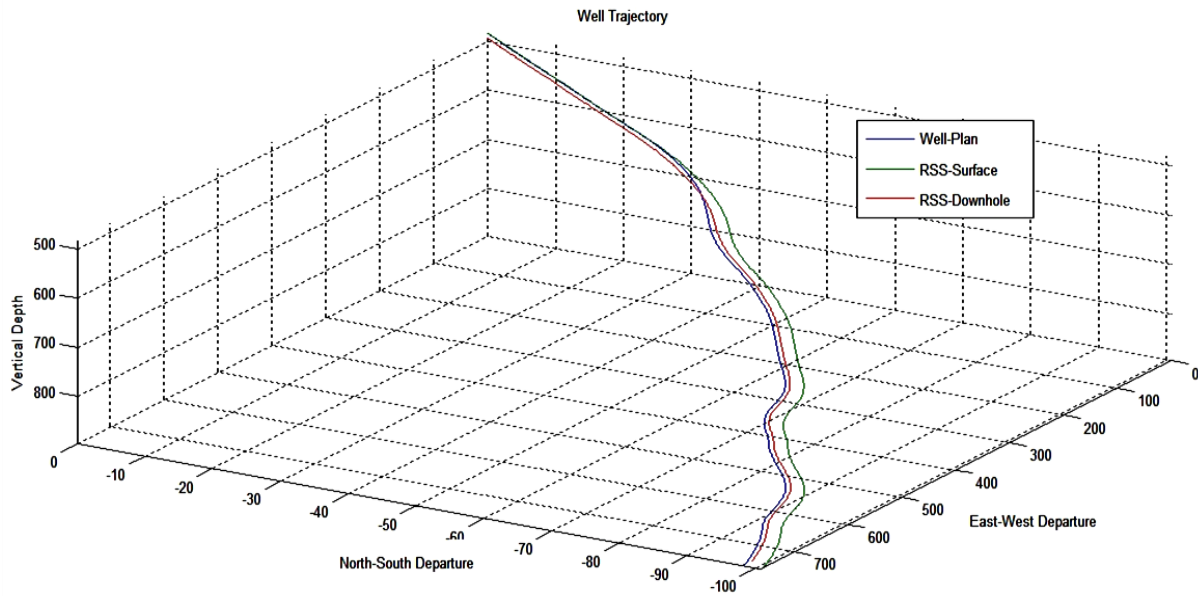


Figure 38: Results of automated well-plan execution from the surface and in downhole

From the results of simulation displayed in Figure 38, it can be seen that due to high tortuosity of the well-plan, both real time downhole control and surface based discrete control deviate from the well-plan. The deviation from well-plan along the depth in east (ΔE), north (ΔN) and vertical (ΔTVD) direction is shown in Figure 39. The error in north direction for surface based system is (2.4 %) greater than error for the downhole system (0.11%) but for the east direction the error of surface based system (0.49%) is lower than downhole system (0.87%). Despite the error in estimated depth for downhole based system, the overall errors in well bore position are comparable for both surface based and downhole automated system. This simulation also establishes the integrability of downhole depth with RSS control for automated drilling.

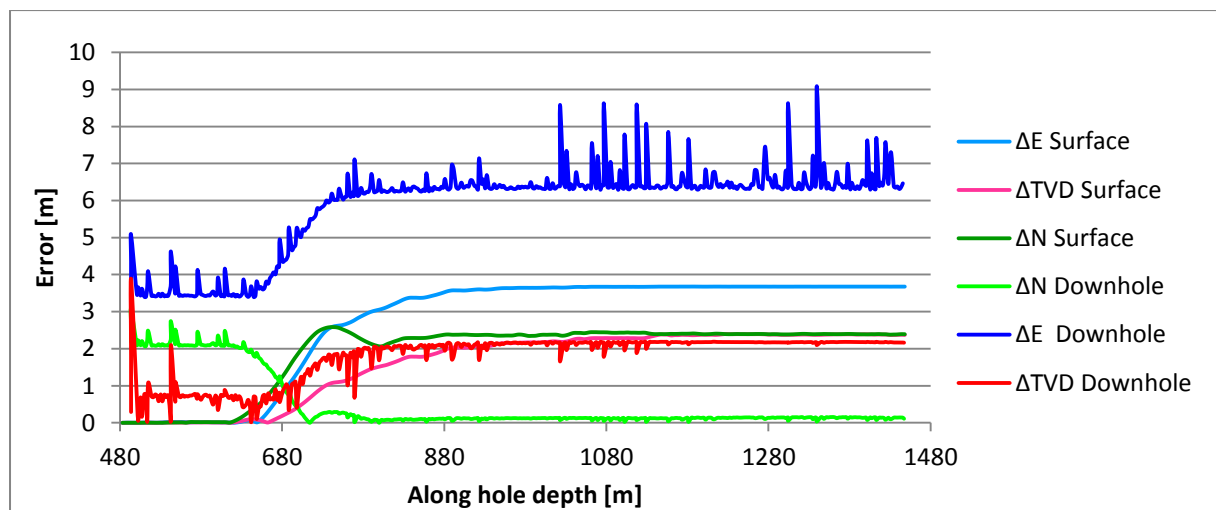


Figure 39: Deviation from well plan in east, north and vertical direction along depth

5. Conclusions and recommendations

The following conclusions are drawn based on the work carried for estimating downhole depth.

1. Correlation of subsurface measurements can be used for estimating downhole depth.
2. Gamma ray and density measurements can be successfully used for correlation.
3. Both cross-correlation and hybrid pattern matching algorithms perform sufficiently well for low noise levels.
4. By optimising on pattern size, algorithm performance can be improved in terms of accuracy and computational efficiency.
5. The cross correlation based method is robust against drift in sensor.
6. ROP variation is a key source of error in correlation of subsurface measurements, and the error can be minimised by minimising ROP variation and sensor separation.
7. The error increases in the horizontal section with smaller gamma ray variation.
8. The error decreases with increase in number of counts associated with each data point
9. The overall error can be reduced with help of secondary system, such as nuclear marker-detector system.
10. The strength of signal from nuclear marker depends on subsurface composition.
11. The error associated with the nuclear marker-detector system is independent of ROP variations.
12. Integration of downhole depth with RSS control can realise downhole automated well-plan execution.

A few recommendations are proposed for future work.

1. Two gamma sensors of the same design should be run to validate the assumptions of statistical behaviour of gamma ray measurements.
2. Gamma ray sensor designs optimised for gathering higher count rates should be used for the exercise.
3. Nuclear detector designs should be evaluated for the estimation of the strength of the signal from the nuclear marker-detector system.
4. More details should be added in the model geometry for nuclear calculations.
5. The efficiency of nuclear calculations can be improved by modifying the MCNP code to directly produce required RSSA file or by combining neutron and photon transport in one calculation using MCNPX or MCNP6
6. Application of average downhole ROP in mechanical specific energy (MSE) calculation and optimization of drilling parameters should be considered.
7. Algorithms for geosteering need to be developed for truly automated drilling.

References

- [1] Chemali, Roland, Advanced geosteering for optimal exploitation of hydrocarbon reserves, Society of petroleum engineers distinguished lecturer program
- [2] Helgesen, Tron B., Geosteering in Norway, Society of petroleum engineers, Stavanger Section – January Meeting, January 11, 2012.
- [3] Hamlin, Kenneth H. , Tait Colin A., TECHNOLOGY There are solutions to LWD depth measurement problems, Oil and gas journal, Volume 94, Issue 24, 1996
- [4] Kirkman, M. And Seim, P., Depth measurements with wireline and MWD logs, SPWLA Houston, 1992.
- [5] Hassan, Gamal A., Kurkoski, phil, Incremental depth measurement for real time calculation of dip and azimuth, US patent no. 7283910, Oct. 16,2007
- [6] Estes, Robert, Cerkovnik et al., Downhole depth computation methods and related system, US patent application no. 2008/0105423 A1, May 8, 2008
- [7] Engler, Thomas W., Lecture notes for PET 370 Spring 2012 (<http://infohost.nmt.edu/~petro/faculty/Engler370/fmev-chap7-GR.pdf>)
- [8] Ekseth, Rogers, Mullin, Stephen Victor et al., System and method for measuring depth and velocity of instrumentation within a wellbore using a bendable tool, US patent application no. US2009/0084546 A1, Apr. 2, 2009
- [9] Dubinsky, Vladimir, Jogi, Pushkar N. et al., Use of axial accelerometer for estimation of instantaneous ROP downhole for LWD and wireline applications, US patent application no. US2002/0195276A1
- [10] Chau, Albert W., Electronic guidance system and method for locating a discrete in-ground boring device, US patent no. 5585726, Dec. 17, 1996
- [11] Witte. Johannes, Downhole measurement of depth, US patent no. 5896939, Apr. 27, 1999
- [12] Fitch, John L., Lyle, W.D. et al., Borehole gravimetry system, US patent no. 4475386, Oct. 9,1984
- [13] DiFoggio, Rocco, Estes, Robert et al., Gravitational method and apparatus for measuring true vertical depth in a borehole, US patent no. US8113041 B2, Feb.14, 2012
- [14] Allen, D.R., Collar and radioactive bullet logging for subsidence monitoring, SPWA tenth annual logging symposium, May 25-28, 1969
- [15] Patton, Bob J., System for controlled drilling of boreholes along planned profile, US patent no. 5341886, Aug. 30, 1994
- [16] Schnitger, Jochen and Macpherson, John, Signal attenuation for electromagnetic telemetry systems, SPE/IADC -118872
- [17] Gao, L., Gardner, W., Robbins, C., Limits on data communication along the drillstring using acoustic waves, SPE reservoir evaluation and engineering, Feb, 2008.
- [18] Drumheller Douglas S., Knudsen Steven D., The propagation of soundwave in drill string, journal of acoustic society of America Vol. 97, No. 4, April 1995
- [19] Squire, William D, Whitehouse, H.J, A new approach to drill string acoustic telemetry, SPE8340, 1979
- [20] Ierubino, J. V. and Ginest, N.H., Use of pulsed neutron logging techniques to prove protection of underground sources of drinking water, SPE 19616, Oct. 1989
- [21] Arps, J.J., Arps, J.L., The subsurface telemetry problem-A practical solution, Journal of petroleum technology, May 1964

- [22] Patton, B.J., Gravley, W. et al., Development and successful testing of a continuous- wave, Logging- while-drilling telemetry system, SPE 6157
- [23] Hutin, R., Tennent, R.W., Kashikar, S.V., New mud pulse telemetry techniques for deepwater applications and improved real-time data capabilities, SPE/IADC 67762
- [24] Carcione, Jos'e M. and Poletto Flavio, Sound velocity of drilling mud saturated with reservoir gas, GEOPHYSICS, VOL. 65, NO. 2 (March-April 2000); P. 646–651
- [25] Cormen, Thomas et al., Section 32.1, Introduction to algorithms, MIT press. 2001
- [26] Karp, Richard M., Rabin, Michael O, Efficient randomized pattern-matching algorithms, IBM journal of research and development, Vol. 31, March 1987
- [27] Knuth, Donald E., Morris, James H., and Pratt, Vaughan R., Fast pattern matching in strings, SIAM journal of computing, Vol. 6, June 1977
- [28] Bird, Richard S., Two dimensional pattern matching, Information processing letters Vol.6, Oct 1977
- [29] Aho, Alfred V., Corasick Margaret J., Efficient string matching: an aid to bibliographic search, The communications of the ACM, Vol. 18 No.6, June 1975.
- [30] Landau, Gad M., Vishkin, Uzi, Efficient string matching in the presence on errors, Foundations of computer science-26th annual symposium, Oct. 1985
- [31] Bush, C.H., Smith, R.C. and Reichard, J.W., Small accelerators as neutron generators for the borehole environment, IEEE transections on neuclear science, Vol. 35, No. 1, Feb 1988.
- [32] Chichester, David L., Simpson, James D., Compact accelerator neutron generator, The industrial physicist, Vol. 9, Issue 6,.
- [33] Stelts, M.L. and Chrien, R.E., Energies and intensities of thermal neutron capture gamma rays from Cl, Al, Fe relative to N, Neuclear instruments and methods, Vol. 155, Issues 1-2, Sept 1978.
- [34] Qualheim, Bern and Hill, Donald G., Modified scintillation detectors to improve slim-hole gamma ray log repeatability in low radioactivity materials, <http://mgls.spwla.org/symposia/95Sym/Papers/Hill/index.html>
- [35] Knoll, Glenn F., Chapter-3, Radiation detection and measurement, ISBN: 9780470131480
- [36] MCNP — A General Monte Carlo N-Particle Transport Code, Version 5, Volume I: Overview and Theory and Volume II: User's guide
- [37] Mughabghab, S.F., Thermal neutron capture cross section resonance integrals and G-factors, IAEA nuclear data section, February 2003
- [38] Azar, Jamal J. and Samuel G. Robello, Drilling Engineering, 2007 Edition, PennWell books.
- [39] Walker, Bruce H., Factors controlling hole angle and direction, Journal of petroleum technology, November 1986.
- [40] Jogi, P.N., Burgess, T.M., Bowling, J.P., Predicting the build/drop tendency of rotary drilling assemblies, SPE Drilling engineering, June 1988
- [41] Aadnoy, Bernt S. and Huusgaard, P., Analytical models for design of wellpath and BHA, IADC/SPE 77220
- [42] J.M. Meese, "The NTD process--a new reactor technology", Proceedings of the Second International Conference on Transmutation Doping in Semiconductors, Plenum Press, NY, 1978, pp. 1-10.

- [43] Wassermann, Ingolf, Hahn, Detlef et.al. Mud-pulse telemetry sees step-change improvement with oscillating shear valves, OIL AND GAS JOURNAL volume-106,issue-24.
- [44] Al-Musharfi, Nedhal M., Bansal, Radhey S. et.al. Real-Time Reservoir Characterization and Geosteering Using Advanced High Resolution LWD Resistivity Imaging, SAUDI ARAMCO JOURNAL OF TECHNOLOGY FALL 2011
- [45] Althoff, Gary, Cornish, Bruce, et.al. New concepts for seismic surveys while drilling, SPE 90751
- [46] Walls, Fred L., Environmental sensitivities of quartz crystal oscillators, , IEEE Transactions on Ultrasonics, Ferroelectrics and Frequency Control(Volume:39 , Issue: 2), March 1992.
- [47] Vig, John R., Quartz Crystal Resonators and Oscillators for Frequency Control and Timing Applications - A TUTORIAL” Rev. 8.5.1.2, July 2001, AD-M001251

Appendix 1. Directional drilling and Geosteering

A1.1. Directional drilling and Geosteering

Geosteering can be understood as an action of steering the bit in the subsurface based on acquired subsurface information from real time measurements. Though directional drilling has been attempted by numerous drillers since late 1930's, the more active form came into existence with the inception of mud-motors and LWD(Logging while drilling)-MWD(Measurement while drilling) systems. With the development of rotary steerable systems, directional drilling has further increased its value by providing smooth and long deviated sections with better hole cleaning and precise real time directional control. In geosteering applications, directional drilling is pushed to its technical limits to maximize reservoir contact area by following strata across the faults and along the folds while avoiding geological hazards.

Geosteering can be classified into two types; namely reactive geosteering and proactive geosteering [1]. As the name suggests reactive geosteering is an action in reaction to the identification of an event which can be entry or exit from the reservoir section with help of resistivity, gamma or density measurements, whereas proactive geosteering involves anticipation of such events before they really occur with help of deep resistivity or sonic measurements.

The objectives of Geo-steering may include

1. Staying in the reservoir rock
2. Maintaining a constant distance from oil-water contact or Gas-oil contact.
3. Keep a constant distance from cap rock or base rock.
4. Follow productive zones and avoid non-productive zones.

Based on geosteering objective specific choice of logging suit can be made, some of the examples of these logging tools are [2].

- Gamma Ray : Basic correlation
- Azimuthal imaging tools : Stratigraphic steering
- NMR : Petrophysical steering
- Resistivity tools : Boundary detection, saturation steering
- Acoustic/VSP-WD : Reduce seismic uncertainty, Look ahead

A1.2. Current state of the art in geosteering

Geosteering is an outcome of advances in two technologies namely direction drilling and real time formation evaluation. Modern day directional drilling assemblies have rotary steerable systems. These systems can be controlled from the service with help of downlink mud pulse telemetry in real time. Any desired change in direction can be conveyed to the RSS with help of commands encoded in pressure pulses, which gives real time control on the borehole trajectory. The change in direction can be made in all three dimensions.

On the other hand, modern sensors on logging while drilling systems can deliver high resolution accurate measurements downhole while drilling. These measurements are conveyed to the service with help of uplink mud pulse telemetry for real time evaluation. With azimuthal measurements, 360° borehole images are created to locate fractures and measure dip angles to decide the borehole trajectory. Deep resistivity and sonic measurements can look deep into the formation to detect nearby changes in lithology or formation fluid saturations, which can be used for making proactive steering decision. Other than LWD data, analysis of cuttings by well site geologist and mud logging data also help in getting information from the bottom of the hole.

To geosteer a well both these technologies are used in combination. For proactive geosteering, data is gathered from previously drilled wells in the area which gives a good estimate of various lithologies and formation fluid present in the subsurface with in associated uncertainties. Based on these data forward models of log response are created for different possible scenarios which can be encountered during drilling. 'These scenarios' can be getting closer to an oil-water contact or a bed boundary etc. The real time measurements are continuously compared with forward models for early detection of any undesirable event and based on that steering decision is taken to avoid reservoir exit or drilling below oil-water contact.

A1.3. Rotary steerable system

With conventional steerable motors change in direction is achieved by stopping the rotary motion from the rig floor and allowing the sliding of mud motor with desired orientation of bend sub. This sliding mode creates higher friction force which reduces the force available at the bit resulting in lower ROP. Also successive sections of sliding and rotating mode create a tortuous borehole profile. Rotary steerable systems were developed in early 1990's to overcome this limit of steerable motors in drilling extended reach complex three dimensional well trajectories [38].

Rotary steerable systems are classified based on two kinds of steering concepts namely point the bit and push the bit system. In push the bit system, a side force is applied to the bit by pushing it against the borehole wall to change the well trajectory while the drill string is rotating. Point the bit system uses principle of bent housing motor and the angle is made by pointing the bit in desired direction. These systems allow continuous rotation of drill string and result in better hole profile, improved hole cleaning, improved ROP and extended reach due to lower friction.

Many factors can affect the angle building quality of a BHA and all these effects cannot be quantified easily. These factors include formation strength and anisotropy, borehole shape and curvature, BHA design, bit design and operating parameters such as weight on bit and RPM [39] [40]. All these factors are studied in detail to predict the behaviour of bit in preparing drilling program and BHA design for each well design. Usually sophisticated computer programs are used for bit behaviour prediction. Out of various factors affecting bit behaviour, hole geometry and BHA design are well known and many authors have used them to create simple analytical models for evaluation for angle building capabilities [41].

A1.4. Wellbore depth measurement system

For the navigation in subsurface, one of the most important measurement is borehole depth at any point in time. Along with directional measurements of azimuth and inclination it gives the location of drill bit with respect to a surface point. There are several uses of this depth measurement such as in locating geological features in subsurface, in following the well-plan in order to achieve optimum trajectory, for the calculation of casing shoe depth and estimating cement quantities etc.

In current system of depth measurement, a surface system records the time and length of the drill string below the rig floor. Kelly busing is generally considered as standard depth measurement reference for land based rigs and mean sea level for offshore rigs. The length of the drill string (combined lengths of the BHA and the drill pipes) to the top drive (or traveling block) and the position of the top drive (or traveling block) in the derrick is used to determine the depth of the drill bit and rate of penetration.

The movement of traveling block is measured by drilling line payout from draw works, which is either calibrated with draw work rotation or measured with help of geograph. In addition to that heave compensator are used to eliminate effect of heave in floating offshore facilities.

Despite all the efforts to make an accurate measurement of depth, current system is prone to errors due to factors related to[3]

- Thermal expansion
- Drill pipe stretch
- Pressure effects
- Error in pipe tally, drill line sensor calibration and heave correction.

The total error due to these factors can be up to 10-12 m over 3000 m depth [4]. There have been efforts to calculate error related to above mentioned phenomenon and use as a correction to determine correct depth but they do not quantify the error accurately and are seldom used in practice. Downhole measurement of depth has a potential to eliminate these errors.

Appendix 2. Downhole depth measurement concepts

A2.1. Concepts of downhole depth measurement

The need for downhole depth measurement is being felt for long time considering the errors in current system as well as for automation. Many systems have been proposed in the literature but their practical applications has not been materialised due to inherent difficulties in development and complexities in implementation.

An overview of relevant literature and challenges underlying each concept are summarized in following subsections.

A2.1.1. Correlation of subsurface markers:

This concept has been proposed separately in Shell internal invention disclosure as well as in patent US 7283910[5]. An application of the concept for calculation of average rate of penetration on surface has also been suggested [44]. The basic idea of the system is to use two or more sensors fixed in the bottom hole assembly with a predetermined distance between the sensors. These sensors measure a characteristic property of the rock formation such as natural Gamma Radiation, resistivity or acoustic properties in time domain.

While drilling ahead these sensors pass through same point in subsurface at different time depending upon their separation and rate of penetration. An algorithm can be used to compare the outputs from these sensors in time to correlate the character of the signals which come from same subsurface formation. As these signals corresponding to same subsurface location will have a corresponding time difference, the progress along the hole as well as rate of penetration can be calculated with the use of known distance between the sensors. For example, a high GR signature passes the first sensor at time t_1 and then the same high GR signature passes the second sensor at t_2 and the sensors are (L) meters apart along the drillstring. It can now be determined that the drill string has progressed a distance of L m along the hole in time difference ($t_2 - t_1$).

Hence rate of penetration (ROP) is $L/(t_2 - t_1)$

By integrating this ROP depth can be calculated.

Some of the key challenges in the application of such a system are

- In horizontal sections, while running in same lithology the characteristic rock property signature might not change significantly to distinguish distinct signature from the noise.
- Logs never repeat exactly. The minor variations in successive gamma ray measurements are usually statistical fluctuations due to the random nature of the radioactive pulses reaching the detector or sensor. For example the accuracy of gamma ray tools is around 5% in general and precision is inversely proportional to square root of logging speed and will be affected by change in instantaneous speed.
- Fluid invasion and change in hole diameter can also change the measured values over time.
- With integration of ROP an integration error gets introduced in the calculated depth which will grow with increase in depth. The size of error depends upon ROP variation, distance between the sensors and frequency of measurements.
- Precision of logging tools decreases with increase in temperature, which might limit high temperature application [7].

A detailed treatment to the system is given in Chapter-2 of this report.

A2.1.2. Use of accelerometers:

This novel method has been suggested in Shell internal invention disclosure along with some patents [8][6][9][10]. In the heart of the system is measurement of instantaneous acceleration in one or more than one direction and then integration of it for velocity and depth computation. Authors have suggested use of single or multi component accelerometers in the BHA to measure the along hole and other components of accelerations. One advantage of this system is that the effect of vibrations will cancel out automatically as it results in an acceleration of same amplitude in opposite directions. Also the success of system does not depend on local geology and the system can be deployed anywhere without any need of customisation, if materialised.

The challenge with this kind of inertial navigation systems is integration drift. During the integration, small errors in the measurement of acceleration and angular velocity are also get integrated resulting into progressively larger errors in velocity, which are compounded into even greater errors in position. Since the new position is calculated from the previously calculated position and the measured acceleration and angular velocity, these errors accumulate roughly proportional to the time since the initial position was the only known input. Therefore the position must be periodically corrected by input from some other types of navigation system to minimise integration drift.

A2.1.3. Use of pipe tally:

As discussed in patent US 5896939[11] and patent US 2008/0105423[6], by means of inputting the pipe tally in BHA memory module and providing it with a signal corresponding to making up of a pipe joint, depth of the bit can be calculated after addition of each pipe stand. In principle it does not eliminate any errors of current system of depth measurement and seems quite simple to implement. But its potential in an automated drilling system is low due to coarse data points which are available at a separation of stand length and dependency on the surface operations. On modern offshore rigs each stand length can be 30-40m to save connection time while drilling, which means that the depth data will only be available after every 30 or 40m of drilling. Never the less this system has a potential to become a secondary measurement to aid primary real time measurement due to its simplicity and robustness. The source of error in such a system can be a faulty signal, error in pipe tally input or even wrong sequence of pipe connections. Hence the designated signal should be distinct and adequate care need to be taken in sequencing of pipe joints both in downhole memory as well as on the surface.

A2.1.4. Use of pressure or gravity measurements

Use of pressure and gravity related measurements for depth calculations are proposed in Patent US - 4475386[12] and Patent US – 8113041[13] respectively. Both these techniques measure change in pressure or gravitational field strength and based on that calculate corresponding change in depth. The limitation of these methods lies in the fact that these properties only change with change in vertical depth and not with along hole depth and in the absence of along hole depth, monitoring of deviated and horizontal sections is not possible. Other possible complications with these systems include quantification of dynamic flow effects and effect of suspended cuttings in case of pressure measurements and mass anomalies in gravitational measurement, which need to be accounted for making correct estimate.

A2.1.5. Use of manmade markers

Manmade markers were initially used in the measurement of subsidence in producing fields[14]. Proposed marking systems in literature include shooting of radioactive bullets, use of casing collars in cased section and magnetization of borehole wall[15]. This method is similar to

correlation of subsurface markers as explained in section 3.1. Here the only difference is that the leading sensor will be replaced by some kind of marking mechanism and the trailing sensor by corresponding detector. If the marking tool and detector are located at a fixed distance (L) from each other and the time difference in making a mark and detecting it is $(t_2 - t_1)$, the average value of ROP for that section will be given by $L/(t_2 - t_1)$ and simultaneously depth can also be computed as a multiple of (L).

Another possible way to make subsurface marker can be with help of pulsed neutron generators (PNG). Pulsed neutron generators have been used in the past to verify casing integrity by detecting water flow behind the casing [20]. The method activates different molecules present in water with help of thermal neutrons and detect the characteristic gamma ray released on deactivation of the those molecules. If a gamma ray tool is installed in BHA following a PNG, in combination it can create a marker-detector arrangement. The principle of method has been discussed in detail under section 3.2

This method also gives relatively coarse measurements based on distance between marker and detector. Also, the success of the system is dependent on robust marking system which should be unaffected from rock types as well as bore hole problems such as caving or differential sticking.

A2.1.6. By means of positive contact with borehole wall

A track wheel can be made a part of the BHA which is pushed towards borehole wall with some kind of spring force to maintain contact with the wellbore surface. With forward motion of BHA, the track wheel will make revolutions which can be picked up with magnetic or electric system to count the wheel rotations and compute the depth travelled by BHA [15]. The wheel should have enough roughness to avoid slippage over the borehole wall.

In the challenging environment of bore hole with annulus filled with cuttings and mud particles, it is a difficult task to design such a wheel assembly which can maintain a positive contact while rotating without slippage over few kilometres. Moreover, in a rotary system the wheel should be on a separate non-rotating sleeve to avoid any damage to formation which might increase complexities of the system.

A2.1.7. Use of acoustic waves in the drill string

Drillstring elastic waves are being considered for a long time as a means for borehole telemetry. Even though the application of drill-string acoustic waves has been limited so far due to problems of signal attenuation in higher frequencies and drilling related noise, this system can be used to determine depth of a borehole. With the help of time synchronized surface based source and downhole receiver, travel time for acoustic wave in the drill-string can be calculated and with wave velocity calculation, corresponding depth can be determined.

The system can be developed based on the studies in the field of acoustic telemetry. A drillstring velocity model needs to be created by taking into account different components of BHA and effects of temperature and loading on wave velocity. A more detailed introduction to acoustic waves in drill-string is given in section **A2.2**.

A2.1.8. Use of pressure pulse in mud

Instead of sending depth measurement data through mud pulse telemetry from the surface, by sending a characteristic pulse from surface to a time synchronised detector in the BHA, travel time of mud pulse can be determined. By computing pressure pulse velocity in mud column corresponding along hole depth can be calculated.

This concept is easily deployable as the mud pulse telemetry systems in existence constitute the necessary hardware for the system. The most challenging part of this concept is to calculate mud pulse velocities which vary with mud density and compressibility. In a dynamic wellbore, mud density and compressibility can vary along the depth due to change in mud type, hole cleaning efficiency and composition due to formation fluid intake. Thus a detailed velocity model and corresponding mud property measurements are needed for this system. Any error in mud property measurements or velocity computations can also cascade into the depth estimation and affect system usability. More detailed information on mud pulse telemetry is given in section **A2.3**

A2.1.9. By means of electromagnetic signals

In parallel to acoustic and mud pulse telemetry, electromagnetic telemetry is also being considered as a potential data carrier for MWD/ LWD systems. But its application has also been limited mainly to the under-balance drilling applications where mud pulse system can't be used due to two phase flow conditions.

EM telemetry is a reliable means of data transmission only when formation and mud properties are supportive and even in those areas the applicability is limited to 9000 feet with a repeater-less system [16]. Signal attenuation increases almost exponentially with depth and becomes even more severe in the presence of conductive bed for higher frequencies. This system can be used to calculate the depth of the drill bit with time synchronised source and detector arrangement as discussed for acoustic waves (**A2.1.7**) and pressure waves (**A2.1.8**). Synchronised time measurement for the system is discussed in section **A2.4**.

A2.2. Acoustic waves in drill-string

The use of telemetry by acoustic waves through the drill string has been suggested since 1940's. Though the system has been used in commercial non drilling application in 2000[17], application in drilling has not seen appreciable progress so far. Acoustic telemetry uses elastic waves in the drill string to code the information. These waves can be axial, lateral or torsional. Axial and torsional waves have been discussed sufficiently in the literature for their velocities and attenuation features and can be used for downhole depth determination system discussed in **A2.1.7**.

A2.2.1. Drill-string channel characteristics

A distinctive feature of the drill string channel is the presence of the passbands and stopbands. The large number of drill pipe joints and different tools in the BHA are the cause of change in acoustic impedance in the drillstring and at every change in acoustic impedance; acoustic waves experience partial transmission and reflection. Consequently these reflected and transmitted waves undergo interference during travel along the drill string. At certain frequencies this interference is destructive which result in complete suppression of those frequencies by the time such waves reach the surface. These frequency bands are known as stopbands. Fortunately, at certain other frequencies, the interference is constructive and signal strength suffers only partial attenuation as it propagates along the string. These frequency bands are known as the passbands.

The loading effect of the tool joints on waves propagating along the drill string can be obtained from the known properties of loaded transmission lines. The location of these bands and their width in frequency is a function of the length of each individual load and its characteristic impedance. The presence of losses also shifts the locations and widths of the bands.

Variations in the actual lengths of individual segments of drill pipe also acts as an imperfection and alter the propagation characteristics of the drill string. Variation in segment length effectively

narrows the range of frequencies which are common in the pass bands of each pipe. It has been observed that length distribution can be a major contributor to signal loss in higher passbands and causes a complete blocking of energy above certain passbands [18].

A2.2.2. Wave velocity

Wave velocity in the solids is given by

$$c = \sqrt{\frac{E}{\rho}} \quad \{16\}$$

Where

c = wave velocity

E = Elastic modulus of material

ρ = Material density

For steel the wave velocity is approximately 5130 m/s.

But due to presence of tool joints, the phase and group velocities of extensional waves are strong function of frequency. The dispersion relation relating frequency ω to wave number k is

$$\cos k(d_1 + d_2) = \cos \frac{\omega d_1}{c} \cdot \cos \frac{\omega d_2}{c} + M \sin \frac{\omega d_1}{c} \cdot \sin \frac{\omega d_2}{c} \quad \{17\}$$

$$\text{Where reflection coefficient } M = \frac{a_1}{a_2} + \frac{a_2}{a_1} \quad \{18\}$$

The parameters a_i and d_i represents cross-sectional area and length of tube and tool joint respectively.

$$\text{The phase velocity is given by } c_p(\omega) = \omega/k \quad \{19\}$$

$$\text{and group velocity is equal to } c_g(\omega) = \frac{d\omega}{dk} \quad \{20\}$$

For frequencies below 100 Hz, this dispersion relation shows that phase and group velocities are approximated by the zero frequency limits.

$$c_p(0) = c_g(0) = \frac{c(d_1+d_2)}{\sqrt{d_1^2 + \left(\frac{a_1+a_2}{a_1}\right)d_1d_2 + d_2^2}} \quad \{21\}$$

The tool joints influence the velocity of the wave even when the wavelength is far greater than the spacing between the tool joints as the tool joints add mass to the system without appreciable increase in stiffness. Thus the velocity in drill-string can be approximated to 4800 m/s for frequencies below 100 Hz. But above 100 Hz, the phase and group velocities in a drill string depends on frequency.

A2.2.3. Signal attenuation

Signal attenuation in acoustic waves generally increases with increasing acoustic frequency and is composed of intrinsic losses in the pipe material (mostly mechanical hysteresis), viscous losses due to the motion of the pipe surfaces in the drilling fluid and Radiation losses [19]. For both extensional and torsional waves, the intrinsic losses are completely negligible in drill-string communication applications. For extensional waves, the radiation loss due to the radial motion coupled to the extensional motion by Poisson's ratio, totally dominates the viscous loss and accounts for the huge attenuation at higher frequencies for this mode.

There is no comparable radiation loss for torsional waves; here the dominant loss is viscous loss. For radiation to occur in torsional waves shear waves must propagate into the fluid but liquids such as circulating drilling fluids do not support appreciable shear stress and hence, do not support appreciable shear wave propagation. However, it is important to note that for many

types of drilling fluids, when circulation of the fluid is terminated the fluid begins to gel, which starts to support shear waves and radiation losses begin to occur for torsional waves.

Dynamic variations in attenuation can also occur due to various phenomena associated with drilling processes and borehole conditions [18]. These conditions include characteristics of the borehole/ casing, deviation of borehole, physical properties of the drilling mud and the extent of contact between drill-string and borehole wall. Any instantaneous variation in one or more of the properties changes the attenuation.

A2.2.4. Noise

Top drive, bit formation interaction and normal rig operations can generate significant noise in an acoustic system. For example, stick-slip phenomenon is a source of noise for torsional waves, whereas bit bouncing is for axial waves. Noise from PDC is generally lower than roller cone bit. To avoid damage to the acoustic receiver due to bit noise and complexities of BHA acoustic properties the sensor should be put on the top of the BHA, near to drill collars which are good conveyers of acoustic energy.

A2.3. Mud pulse telemetry

Mud pulse telemetry was first introduced in year 1964 using a plunger valve to generate discrete mud pulses [21]. Data rates of less than 1 bit/s could be achieved using this type of modulator. As an improvement over current system, in 1977 continuous-wave telemetry using phase shift keying modulation was developed. This system uses rotating valve mechanism (also known as a mud siren) to generate continuous pulses. Data rates of up to 3 bits/s were claimed with the use of such system [22]. Since then mud pulse telemetry has been further developed along with data compression and established as an industry standard for reliable downhole communication.

There are three main types of signal generating systems being used in MWD

I. Positive pulse :

Positive pulses are generated by momentarily increasing the pressure in the mud column. This is done by momentarily partially blocking the flow of mud through the drillstring.

II. Negative pulse:

Negative pulses are generated by momentarily reducing the pressure in the drillstring. This is accomplished by diverting the mud from inside the drillstring to the annulus via a dump valve.

III. Continuous wave:

This signal constitute of continuous wave of positive pulses created with help of a rotary valve. Continuous wave telemetry is capable of operating frequencies as high as 24 Hz[23] .

A2.3.1. Signal attenuation

Signal attenuation in mud column is mainly due to mud viscosity. The power loss in signal transmission is function of distance travelled and mud viscosity.

For 'high frequency telemetry' (>10 Hz) based on Lamb's law of pressure wave attenuation

$$P(x) = P_0 e^{-\frac{x}{L}} \quad \{22\}$$

$$\text{Where } L = \frac{d_i c}{2} \sqrt{\frac{2}{v_w}} \quad \{23\}$$

$P(x)$ = pressure wave amplitude at distance x , Pa (psi)

P_0 = pressure wave amplitude at signal source, Pa (psi)

ν = kinematic viscosity, m^2/s (ft^2/s)

ω = angular frequency, radians/s

d_i = pipe internal diameter, m (ft)

c = wave velocity, m/s (ft/s)

$$c = \sqrt{\frac{B}{\rho}} \quad \{24\}$$

B = bulk modulus of the mud (inverse of compressibility), Pa.

ρ = density, kg/m^3

From the equation above it can be seen as signal attenuation increases with smaller pipe diameter, greater compressibility, higher viscosity and higher frequencies. As mud viscosity and density are temperature dependent, attenuation also depends on temperature.

For 'Low frequency telemetry' (<1 Hz), another model is used [23].

$$P(x) = P_0 \left(1 - e^{-\frac{x}{RC}} \right) \quad \{25\}$$

$$\text{Where } R = \frac{P}{Q} \text{ and } C = \frac{V}{B} \quad \{26\}$$

R = mechanical resistance, Pa/ (m^3/s)

C = mechanical compliance, m^3/Pa

P = mud pressure, Pa

Q = volumetric flow rate, m^3/s

V = mud volume above MWD tool, m^3

B = bulk modulus of the mud, Pa

Both the resistance and compliance of the mud are functions of depth and mud properties. The flow rate can be assumed to be constant, but the pressure is affected by depth.

A2.3.2. Wave velocities:

The velocity of pressure wave in mud depends on its compressibility given by equation 9. There are various models available to compute wave velocities in the oil based and water based mud [24] and these models include effect of hydrocarbons in the mud along with temperature and pressure. Usually the wave velocities range from 1200- 1500 m/s.

Even with all advancements in technology, the data rates of current systems remain significantly low for real time depth data transmission to the downhole tools. Most of the system capability is used to send maximum data to the surface for monitoring. The data transmission also suffers time lag, especially in the extended reach horizontal sections along with noise related to mud pressure fluctuation at pumps.

A2.4. Synchronised time measurement

The idea of synchronized measurement of time at the surface and downhole to measure travel time for drill string acoustic signal, electromagnetic signal or mud pulse pressure signal is analogous to the seismic while drilling applications. Thus search for a potential system can start at commercially available systems in the domain of seismic while drilling.

These kind of system use time synchronized source on the surface and receiver in the BHA to measure travel time of sound waves in the subsurface. Time is measured with help of quartz

crystals oscillating at a known frequency by counting their oscillations with a counter. Some technical features of quartz based time measurement system are

- The time resolution of clock depends upon the frequency of crystal and counter capability [45].
- A crystal's frequency characteristic depends on the shape or 'cut' of the crystal.
- Temperature influences the operating frequency and various forms of compensation can be used for that [47].
- The temperature sensitivity depends primarily on the cut; the temperature compensated cuts are chosen as to minimize frequency/temperature dependence.
- Downhole shocks and vibrations also influence the crustal frequency [46].
- Aging also changes the frequency of the crystal and can cause clock drift. Commercial system from Halliburton claims clock drift as low as 120 μ sec per day and measurements are usually taken in ms.

A2.5. Concept selection for downhole depth measurement system

Out of various concepts for a downhole depth measurement system, few can be identified as concepts with higher potential of success and lower risk in development. This selection is based on strengths and weakness of each concept along with competencies of the author in further development of the concept.

Table 1: Strengths and weaknesses of downhole depth measurement concepts

S.N.	Concept	Strengths	Weakness
1	Correlation of subsurface markers	<ul style="list-style-type: none"> i. Uses existing technology, No hardware development required. ii. Measurements made can further be used for formation evaluation. 	<ul style="list-style-type: none"> i. Different formation might require different measurements which need to be identified in advance. ii. In absence of enough heterogeneity correlation can be erroneous. iii. Small errors due to integration can drift results from true values. iv. Measurement resolution will depend on time for acquiring each data point.
2	Use of accelerometers	<ul style="list-style-type: none"> i. Uses existing technology, No hardware development required. ii. Does not depend upon geology. iii. Measurements can be made on finer scale. 	<ul style="list-style-type: none"> i. Due to repeated integration, errors keep on growing with time. ii. A secondary system is required for correction.
3	Use of pipe tally	<ul style="list-style-type: none"> i. Robust system with no subsurface measurement dependency. ii. An extension to existing systems, hence easy to implement. 	<ul style="list-style-type: none"> i. Require integration with surface operations and require operational discipline. ii. Measurements will suffer from errors due to thermal and material elasticity effects.

			<ul style="list-style-type: none"> iii. Coarse measurement, depending upon stand length. iv. Will require existing mud pulse telemetry for data transmission.
4	Use of pressure or gravity measurements	<ul style="list-style-type: none"> i. Measurements are relatively simple. 	<ul style="list-style-type: none"> i. Can only give vertical depth which is of limited use ii. Resolution highly dependent on measurement accuracy and mathematical models. iii. Subsurface anomalies can severely affect the results.
5	Use of manmade markers	<ul style="list-style-type: none"> i. Dependency on geological features and properties is low. ii. Measurement resolution can be chosen based on application. 	<ul style="list-style-type: none"> i. Need to identify a robust marking system. ii. Associated hardware development. iii. Accuracy will depend on the precision of detector.
6	By means of positive contact with borehole wall	<ul style="list-style-type: none"> i. Robust system for direct measurement. ii. Can take into account temperature and material elasticity effects. 	<ul style="list-style-type: none"> i. Will add severe mechanical complexities to BHA. ii. Needs to be effective in all borehole conditions and in case of washouts etc.
7	Use of acoustic waves in the drill string	<ul style="list-style-type: none"> i. Independent of subsurface geology or hole condition ii. Does not affect existing LWD/ MWD systems. 	<ul style="list-style-type: none"> i. Needs a robust wave velocity model. ii. Resolution depends upon the wave velocity accuracy iii. Drilling noise need to be treated effectively.
8	Use of pressure pulse in mud	<ul style="list-style-type: none"> i. Independent of subsurface geology or hole condition. ii. No hardware development needed. 	<ul style="list-style-type: none"> i. Needs a robust wave velocity model and real time measurements of mud properties. ii. Resolution depends upon the wave velocity iii. Accuracy can be limited due to dynamic nature of mud system. iv. Can't be used in underbalanced drilling.
9	Use of electromagnetic waves	<ul style="list-style-type: none"> i. No mechanical systems involved in the signal generation. ii. Can work with underbalanced drilling applications as well 	<ul style="list-style-type: none"> i. Needs a robust wave velocity model and real time formation property evaluation. ii. Resolution depends upon the wave velocity iii. Attenuation is dependent on the formations which might be unknown and can limit applicability depth.

Appendix 3. Pattern matching and gamma measurement

A short summary of the findings from these domains is presented in the following subsections.

A3.1. String matching

The task of searching a pattern of log response in another log response is analogous to string matching problem in text editors. However, in string matching problem, the match need to be exact whereas in the log response matching exercise to account for measurement precision and tool accuracy, there should be a tolerance value in which both patterns should be considered as a valid match. Never the less the string matching algorithms in the literature gives a good starting point for the development of a more specific solution.

To explain some of the algorithms available in the literature let us assume that there exist a set of n characters or numbers given by

$$Y(t) = \{y_1, y_2, y_3, \dots, y_n\} \text{ and } Y \in \mathbb{R}$$

and a pattern to be matched given by

$$X(t) = \{x_1, x_2, x_3, \dots, x_m\} \text{ and } X \in \mathbb{R} \quad n \geq m$$

Here \mathbb{R} is the set of real numbers & characters and m & n are number of elements in pattern and set respectively.

One of the simplest ways to solve this problem is to compare the first m -characters of the set and the pattern and, after a match or a mismatch, slide the entire pattern by one character in the forward direction of the set. This process is repeated until the pattern is positioned at the $(n-m+1)$ position of the text. This method can be interpreted graphically as sliding a template. This approach is commonly known as a naive brute-force method. This process is not an optimal procedure as it does not use any pre-processing based on information gained from the pattern or set[25].

Rabin and Karp[26] proposed a method which can also be used for two dimensional pattern matching. This method uses a pre-processing step of converting the pattern X to a digit with some hash function and using same hash function to create $(n-m)$ digits out of main set Y for each possible match. Then it tries to match the hash function output digits form pattern to set and if it finds a match, it further match individual character. This method is more efficient in matching of multiple patterns compared to other methods. Method also find application in situation when only a small part of main set Y changes with time and only that part needs the pre-processing reducing the overall execution time.

Knuth-Morris-Pratt algorithm [27] uses the information within the pattern to determine the minimum shift with which match could be found after each mismatch rather than making single character shift each time and thus avoid re-examination of previously matched characters. This is done by pre-processing the pattern and calculating a shift table beforehand.

To match array of more than one linear pattern in the given array of values, there are two approaches, one is to use linear search multiple times or use a multidimensional search algorithm for better efficiency. In literature there have been proposed a lot of multidimensional pattern matching algorithms. The Bird's[28] algorithm is one of the first two dimensional pattern matching algorithm and is a combination of Aho-Corasick's[29] algorithm for search in rows followed by Knuth-Morris-Pratt algorithm[27] for search through columns.

A3.2. Approximate string search

All string matching algorithms explained in section A3.1 search an absolute match of pattern \mathbf{X} in the set \mathbf{Y} but in case of measurements as discussed earlier, there exist some differences between two sets of measurements due to tool precision and accuracy, also there exists a possibility of erroneous data points which might not have a corresponding match in second dataset. To deal with the situation of erroneous data points there are approximate array matching algorithms in the literature, which are used in spell checking or spam filtering. These search algorithms are also called ‘string matching with at most k mismatches’.

A brute force or naive approach to the problem will be to create substrings $\mathbf{Y}_1, \mathbf{Y}_2, \dots, \mathbf{Y}_{n+m+1}$ from the set \mathbf{Y} where $\mathbf{Y}_i = y_i, y_{i+1}, \dots, y_{i+m-1}$ and compute difference between the substrings \mathbf{Y}_i and pattern \mathbf{X} . These numbers of differences are also called as hamming distance. The minimum difference will be choice for match. This technique is computationally very inefficient and can result in large run times. An improvement over this technique was suggested by Landau and Vishkin[30] exploiting the fact that there is no need to calculate hamming distance more than allowed mismatch k. In this method an analysis is done on pattern \mathbf{X} and set \mathbf{Y} to create separate arrays to find least common prefix.

A3.3. Minimum squared distance method for pattern recognition

Similar to cross-correlation coefficients, calculation of minimum squared distance between points within pattern and a potential match can give an idea of degree of match between the two. This method is also being used in signal processing and has its advantages with retaining the mean in the calculation of squared distance compared to cross correlation coefficient which normalises it. Here also squared distance need to be calculated for all potential matches and the minimum value will identify the closest match. The calculation is computationally simpler compared to cross correlation coefficient calculation.

If a set of N data points and pattern of M data points are taken from measurements made by leading sensor 1 and tailing sensor 2 respectively such that

$$\begin{aligned} \mathbf{X}(t_s) &\in \mathbb{R}, & \mathbf{X}(t_s) &= \{x(t_2^j)\}_{j=1}^M \\ \mathbf{Y}(t_s) &\in \mathbb{R}, & \mathbf{Y}(t_s) &= \{y(t_1^k)\}_{k=1}^N \end{aligned}$$

Then the squared distance for any subset $\tilde{\mathbf{Y}}(t_s) \subset \mathbf{Y}(t_s)$

Such that $\tilde{\mathbf{Y}}(t_s) \in \mathbb{R}$,

$$\tilde{\mathbf{Y}}(t_s) = \{y(t_k)\}_{k=a}^{a+M-1}$$

is given by

$$d_i = \left\{ \sum_{l=1}^m (x_l - y_l)^2 \right\}_{l=1}^{N-M+1} \quad \{27\}$$

A3.4. Gamma ray measurement for identifying geological markers

Gamma ray is one of the most common logs run in an LWD system of modern drilling operations due to its low cost, reliability and ability to identify different geological layers based on their radioactivity. Unlike porosity and density measurements gamma ray measurement does not require any neutron source and can be run in cased holes. In comparison with resistivity logs, gamma ray logs shows better repeatability as their response does not get affected by the angle between bed boundary and tool. Gamma ray measuring tools also provide a lot of flexibility in terms of design and operation to choose optimum data acquisition strategy on case to case basis.

Considering all these advantages gamma ray measurements can be considered as most suitable measurement for geological profiling of subsurface in correlation application.

Gamma ray emissions occur during radioactive decay of unstable radioisotopes. Macroscopic observations of radioactive decay involve counting the number of decay emissions from millions of unstable nuclides over finite lengths of time. Because of the large number of events (radioactive decay emissions) and the small probability for a given unstable nucleus to decay (Due to higher half-life), radioactive count rates can be modeled by either Poisson or Gaussian probability distributions [34]. For either of these probability distributions, the distribution standard deviation is equal to the square root of the estimate [35].

If the total count is x then the standard deviation $\sigma_x = \sqrt{x}$

and the relative total count standard deviation is $\sigma_{rel} = \frac{1}{\sqrt{x}}$

i.e. bigger is the total count lesser is the relative error and hence for the better repeatability of the signal. Design of tool and data acquisition scheme should be such that it gives higher total count pertaining to each data point in the signal. Some of possibilities to improve total count include increase in size of the crystal, reduction in attenuation due to tool collar and increase in time window for each measurement.

Appendix 4. MCNP and Nuclear simulation input

In subsections following, a brief description of various simulation parameters and the simulation tool itself is given. Section A4.5 gives an explanation about creating the input for the second simulation from the output of the first simulation.

A4.1. Introduction to MCNP and the Monte-Carlo method

MCNP is a general-purpose, continuous-energy, generalized-geometry, time-dependent, coupled neutron/photon/electron Monte Carlo transport code. It can be used to simulate interaction of nuclear particles in different geometries and materials over time [36]. MCNP is written in ANSI-Standard FORTRAN 90 and is developed and released by Los Alamos National laboratory. In contrast to deterministic methods which solve the transport equation for the average particle behaviour, Monte Carlo obtains answers by simulating individual particles and then averaging the outcome.

The Monte-Carlo method is particularly useful for complex three-dimensional, time-dependent problems. In particle transport, the Monte Carlo technique is pre-eminently realistic (a numerical experiment). It consists of actually following each of many particles from a source throughout its life to its death in some terminal category (absorption, escape, etc.). Probability distributions are sampled with random numbers using transport data to determine the outcome at each step of its life. Extensive data files with nuclear interaction data for neutrons and photons are available with the MCNP code.

MCNP results are normalized to be per starting particle and are printed in the output accompanied by a second number R , which is the estimated relative error defined to be one estimated standard deviation of the mean divided by the estimated mean. For a well-behaved tally, R will be proportional to $1/\sqrt{N}$ where N is the number of histories. Thus, to halve R , we must increase the total number of histories fourfold. The Central Limit Theorem states that as N approaches infinity there is a 68% chance that the true result will be in the range of one standard deviation from the mean value and a 95% chance in the range of two of standard deviation from the mean value. Though these confidence levels refer only to the precision of the Monte Carlo calculation itself and not to the accuracy of the result compared to the true physical value, still as more and more histories are followed, the neutron and photon distributions become better known. For a poorly behaved tally, R may increase as the number of histories increases [36]

A4.2. Neutron Generator

Deuterium-tritium fusion based electronically operated pulsed neutron sources are in application in borehole environments for a long time. These systems can operate in environments up to 150°C and 20,000 psi [31]. Most of these compact devices use deuterium-deuterium and deuterium-tritium reactions which generate neutrons of energy ~2.5 MeV and 14.1 MeV respectively. Corresponding reactions are shown below.



The basic construction of the device consist of a source to generate positively charged ions, an ion accelerator (usually up to 110 kV) and a metal hydride target loaded with either deuterium, tritium or a mixture of the two[31]. The life time of such a tube generator get affected by

1. Internal surface contamination, causing arcing

2. Erosion of the target
3. Buildup of He-3 gas pressure due to decay of tritium.

A4.3. Gamma ray detector

Scintillator based gamma ray detectors are very common in the well logging industry. These detectors use scintillator crystals which on interaction with photons generates light. Small amounts of impurities (called activators) are added to all scintillators to enhance the emission of visible photons. One important consequence of luminescence through activator impurities is that the bulk scintillator crystal is transparent to the scintillation light. On entering the crystal, gamma ray produces fast electrons by three different processes.

1. Photo electric effect
2. Compton effect
3. Pair production (Photon energy > 1.02 MeV)

These fast electrons create scintillations and produce light photons. These light photons then pass through a photomultiplier tube which scales up the signal to be finally detected in the form of electric pulse. The pulse height quantifies the incident gamma ray energy and count of pulses quantifies the amount of gamma ray photons reacting with the crystal. Since the gamma ray energy is usually very high compared to binding energy of electron, when a gamma ray loses its energy due to photoelectric effect almost all the energy associated with it gets transferred to the electron and those electrons create a photo peak in the spectra. On the other hand the spectra related to Compton scattering is almost a flat plateau as the energy distribution of Compton scattered electrons is constant with energies ranging from 0 to maximum energy loss called Compton edge.

A wide variety of organic and inorganic crystals and liquids can be used as a scintillator such as BGO (Bismuth Germanate), $\text{LaCl}_3(\text{Ce})$ (Lanthanum chloride doped with Cerium), Polyethylene naphthalate etc. Thallium doped sodium iodide crystal $[\text{NaI}(\text{Tl})]$ is the most common choice in making the detectors due to its higher light yield among commonly used scintillators and the same has been used in the simulations. To maintain the simplicity in model only the crystal is modeled. To improve the detection efficiency, an annular design with an outer diameter of 8 cm, inner diameter of 6.5 cm and length of 5 cm is considered. Detector schematic is shown in the Figure 40

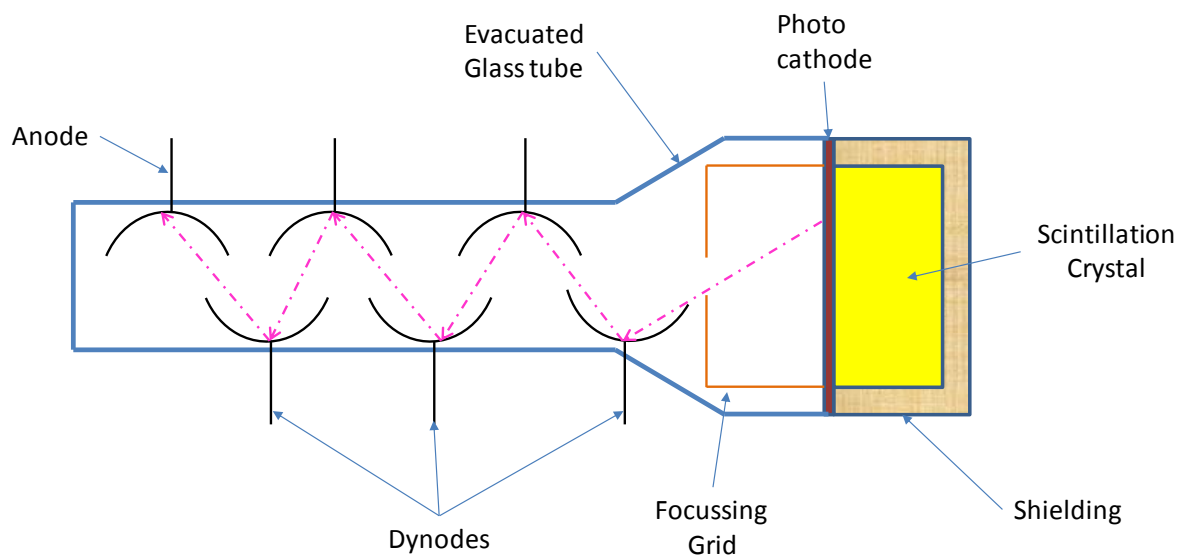


Figure 40: Detector schematic

A4.3.1. Detector counting efficiency

Detector counting efficiency (η) can be defined as the ratio of number of photons counted in detector (n_d) to the number of photons emitted by the source (n_s). Detector counting efficiency depends upon following factors

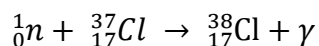
1. Crystal geometry and shielding
2. Optical efficiency of the crystal: It quantifies the photons which can manage to transmit through the crystal out of the total produced photons.
3. Quantum efficiency of the photo cathode: It is the ratio of the number of photoelectron emitted to the number of incident photons
4. Dynode multiplication factor: It is the ratio of number of secondary electrons emitted to the primary incident electrons. The emission of secondary photons is a statistical process, so the multiplication factor is not a constant but varies from event to event around a mean value.
5. Efficiency of anode collection: It is the ratio of number of photo electrons received at the anode to the total photoelectrons generated at the last dynode.

A4.4. Subsurface elements

Among numerous elements present in subsurface the elements of relevance for the simulations were chosen based on their abundance and half-life criteria. The following section gives nuclear properties of three isotopes of special interest for the application in a nuclear marker system.

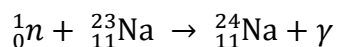
A4.4.1. Chlorine-37

Chlorine is found in saline formation water bounded in pores as chloride ions. It has a 33 barn thermal capture cross-section and it produces many intense gamma rays between 1.5 to 8.6 MeV on decay [33]. Cl-37 is a naturally occurring isotope of chlorine with natural abundance of 24.2%. This naturally occurring Cl-37 can be converted to Cl-38 or Cl-39 (isotopes of chlorine) by neutron capture but for Cl-37 the neutron capture cross section area is only 0.433 barn. The characteristic energies of gamma rays related to the decay of chlorine-38 are 1.6 MeV and 2.1 MeV with the half-life of Cl-38 being 37.24 min, which gives a time window of 0-37.2 minutes (time for 50% depletion) to detect the gamma rays produced from the decay. Corresponding reactions are summarized below.



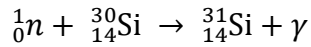
A4.4.2. Sodium-23

Sodium is also present in the saline formation water bounded in pores along with chlorine. Sodium-23 has a nuclear capture cross section of 0.530 barn [37] and Na-24 has a half-life of 14.96 hr. The characteristic gamma rays related to beta decay of Na-24 have energies of 1.369 and 2.754 MeV. The corresponding reactions are given below.



A4.4.3. Silicon-30

Silicon is one of the most abundant elements in the earth. Natural silicon contains Si-28 (92.23%), Si-29 (4.67%) and Si-30(3.1%), out of which Si-30 can be an element of interest for neutron activation. Silicon-30 has neutron capture cross-section of 0.11barn [42] and half-life of 157.3 min. The energy of the characteristic gamma ray from the decay is 1.266 MeV.



A4.5. Creation of photon source for the second simulation

MCNP is capable of accepting a user specified source in the form of a binary RSSA file with the SSR input card. The RSSA file should contain information about starting location, time, energy and direction of each source particle. MCNP can write a surface source file (WSSA) from a simulation capturing events at a surface for use in another simulation. But it cannot write a volume source file which is needed for this problem as the activated nuclei will not be limited to any surface and will be distributed over volume. This requires an unusual approach to define a volume source file containing all the required inputs. This is achieved with help of a separate FORTRAN program.

A brief explanation of the FORTARN program and the process of writing the volume source file are explained in the next sub-section.

5.1.1. Location of activated nuclei

In the first simulation, particle events for each neutron are recorded in a so-called PTRAC file. This file gives information about event type, location of particle, time of event, energy of particle, material involved etc. To limit the file size and improve handling, the events to be written in the PTRAC file can be filtered using keywords based on type of event, number of events, cell, surface, tally, etc. In this problem only the neutron capture events for selected isotopes are of interest and only their location is the information of interest. Unfortunately this is not possible to do this filtering in MCNP itself. Hence the location of selected nuclides undergoing neutron captures was filtered out with help of a separate FORTRAN code. These activated nuclei will be the starting location for gamma ray in the RSSA file. The RSSA file to be produced by the FORTRAN program has a different (binary) format than the PTRAC file.

5.1.2. Energy of gamma ray

Most of the radioactive sources on decay emit gamma rays of a few, precisely defined energies. Energies of these characteristic gamma rays from the decay of each radioactive nuclide are available in the literature and can be substituted for the energy of the corresponding nuclide in RSSA file. However, to retain the simplicity only one energy value is associated with each nuclide. The values of associated energies are given below.

Nuclide	Energy (MeV)
Cl-38	2.167
Na-24	2.754
Si-31	1.266

5.1.3. Time of decay

Radioactive isotopes follow an exponential decay and the decay time of any nuclei is governed by its decay constant. At any time t from the activation, the ratio of remaining active nuclei to the originally activated nuclei is given by

$$\frac{N}{N_0} = e^{-\lambda t}$$

$$\lambda = \frac{\ln 2}{T_{1/2}}$$

Where λ is the activity constant for the decay reaction (s^{-1})

N_0 is the initial population of activated nuclei

N is the population of activated nuclei at time t

$T_{1/2}$ is the half-life of radioactive nuclide

The cumulative distribution in time up to time t of the ratio of remaining active nuclei to the originally activated nuclei $\frac{N}{N_0}$ can attain a value in interval $(0,1]$ with equal probability for each value. A random selection from a uniform distribution of values in interval $(0,1]$ can be used to calculate corresponding time and the same can be used as the decay time in RSSA file.

$$t = -\frac{1}{\lambda} \ln(r)$$

Here, r is a random number form uniform distribution $(0,1]$

5.1.4. Initial direction

The decay creates an isotropic photon source with no preference to any direction. The direction of photon is defined in terms of direction cosines u , v and w the angle it makes with a given direction as in the MCNP RSSA file is defined to create the volume source. As there is no surface to be defined for the source we can conveniently assume the angle with source surface equal to zero. However, the direction cosines u , v should obey following equality

$$u^2 + v^2 + w^2 = 1 \quad \text{here } w \text{ is the third direction cosine.}$$

To define the direction cosines, one of the direction cosine say w can be given a value uniformly distributed in the interval $[-1,1]$.

Similarly we can randomly pick an azimuthal angle φ from uniformly distributed in an interval $[-\pi, \pi]$ which the projection of direction vector on x-y plane makes with x axis.

$$w = 2 * r_1 - 1$$

$$\varphi = 2\pi * (r_2 - 0.5)$$

$$u = \sqrt{1 - w^2} \cos \varphi$$

$$v = \sqrt{1 - w^2} \sin \varphi$$

where r_1 and r_2 are random number form uniform distribution $[0,1]$

A4.6. MCNP input files

In following sections input files for neutron transport and successive photon transports are given with commented description.

A4.6.1. Neutron simulation

Activation around bore hole

```

c *****
c Cell cards for the problem
c *****
c CellNo.  MaterialID  MaterialDensity  CellGeometry  CellParameter
1 100      -0.01      -20                $ neutron source
2 200      -1.0        -10 -30 20        $ bore hole
3 300      -2.6        (-41) #2 #1      $ rock 1
4 300      -2.6        (-42 41) #2 #1   $ rock 2
5 300      -2.6        (-43 42) #2 #1   $ rock 3
6 300      -2.6        (-30 43) #2 #1   $ rock 4
7 0        30
c *****
c Surface card description
c *****
c SurfaceNo.  SurfaceType  EqParameters
10 CZ  10                $ infinite cylinder for bore hole
20 RCC  0 0 -2.5  0 0 5  1.5    $ finite cylinder for n-source
30 RPP -500 500 -500 500 -500 500  $ Large formation
41 RPP -500 500 -500 500 -2.5 2.5  $ Small section of formation
42 RPP -500 500 -500 500 -5.0 5.0  $ Small section of formation
43 RPP -500 500 -500 500 -20 20    $ Small section of formation
c *****
c Data cards      Use partical designator :N- Neutron, :P- Photon
c *****
IMP:N 1 1 1 1 1 1 0
c Mode card
mode n                $ Neutron transport mode
c Cell and surface parameter card
c -----
c Source specification card
c SDEF POS CEL ERG WGT TME PAR
SDEF POS=0 0 0 CEL=1 ERG=14.1 WGT=1 TME=0 PAR=1  $ uniform, isotropic n-
source in cell 1
c Tally specification cards
c Tallytype:Particaltype
F4:N  3 4 5 6          $ Flux in the cells
F14:N  2                $ Flux in cell 2
FM14  -1 200 -2        $ Neutron absorption in water
F1:N  10                $ Current across borehole wall
c Material specification MaterialID - ZZZAAA.nnX  Weightfraction - negative
c mMaterialNo. MaterialID Atomic/WeightFraction
c Formation material
m300  14028.62c  -0.30    $ Si-28
      14029.61c  -0.015   $ Si-29
      14030.62c  -0.01    $ Si-30
      8016.62c   -0.63    $ Oxygen 8016
      1001.70c   -0.032   $ Hydrogen 1H1
      11023.62c  -0.004   $ Sodium
      17035.61c  -0.0046  $ Chlorine-35
      17037.61c  -0.0018  $ Chlorine-37
c Formation water

```

```

m200      1001.70c    2      $ Hydrogen
           8016.62c    1      $ Oxygen
mt200 lwtr.01t      $ Card for water bound hydrogen
c Neutron generator
m100      1002.70c    1      $ Deuterium
           1003.70c    1      $ Tritium
vol 1 1 1 1 1 1 0
nps 100000000      $ Number of particles to be simulated
cut:n 2j 0 0.      $ Analogue neutron capture only
c Writing PTRAC file for collision and termination events
PTRAC FILE=ASC TYPE=N CELL=3 4 5 6 WRITE=ALL TALLY=4 &
      MAX=1000000000 BUFFER=2000 EVENT= col ter
PRINT -85 -86      $ File 85 and 86 will not be printed

```

A4.6.2. Photon simulation

Photon transport to the detector

```

c *****
c Cell cards for the problem
c *****
c CellNo.  MaterialID MaterialDensity CellGeometry CellParameter
1  100    -3.67    -21 20      $ detector1
11 100   -3.67    -23 22      $ detector2
12 100   -3.67    -25 24      $ detector3
13 100   -3.67    -27 26      $ detector4
2  200    -1.0     -10 -30 21 23 25 27      $ bore hole
3  300    -2.6     (-41) #2    #1 #8 #11 #12 #13 $ rock 1
4  300    -2.6     (-42 41) #2 #1 #8 #11 #12 #13 $ rock 2
5  300    -2.6     (-43 42) #2 #1 #8 #11 #12 #13 $ rock 3
6  300    -2.6     (-30 43) #2 #1 #8 #11 #12 #13 $ rock 4
7  0      30
8  200    -1.0     -20 -22 -24 -26      $ Inside detector

c *****
c Surface card description
c *****
c SurfaceNo.  SurfaceType  EqParameters
10 CZ    10      $ infinite cylinder for bore hole
20 RCC   0 0 -2.5   0 0 5 6      $ finite cylinder for detctor1
21 RCC   0 0 -2.5   0 0 5 8.5
22 RCC   0 0 -12.5  0 0 5 6      $ finite cylinder for detctor2
23 RCC   0 0 -12.5  0 0 5 8.5
24 RCC   0 0 12.5   0 0 5 6      $ finite cylinder for detctor3
25 RCC   0 0 12.5   0 0 5 8.5
26 RCC   0 0 -22.5  0 0 5 6      $ finite cylinder for detctor4
27 RCC   0 0 -22.5  0 0 5 8.5
30 RPP   -500 500 -500 500 -500 500 $ Large formation
41 RPP   -500 500 -500 500 -2.5 2.5
42 RPP   -500 500 -500 500 -5.0 5.0
43 RPP   -500 500 -500 500 -7.5 7.5

c *****
c Data cards      Use partical designator :N- Neutron, :P- Photon
c *****
IMP:P 1 1 1 1 1 1 1 1 1 0 1
c Mode card
mode P      $ Photon transport mode
c Cell and surface parameter card
c -----
c Source specification card
SSR      $ (P-source) from deactivation

```

c Tally specification cards

c Tallytype:Particaltype

```

F4:P      1 11 12 13          $ Flux in the detector
T0  0 1.+11 2.+11 3.+11 4.+11 5.+11  $ time grid for decay Cl-38
      6.+11 7.+11 8.+11 9.+11 1.+12
      1.1+12 1.2+12 1.3+12 1.4+12 1.5+12 1.6+12 1.7+12 1.8+12 1.9+12 2.+12
      2.1+12 2.2+12 2.3+12 2.4+12 2.5+12 2.6+12 2.7+12 2.8+12 2.9+12 3.+12
      3.1+12 3.2+12 3.3+12 3.4+12 3.5+12 3.6+12 3.7+12 3.8+12 3.9+12 4.+12
      4.1+12 4.2+12 4.3+12 4.4+12 4.5+12 4.6+12 4.7+12 4.8+12 4.9+12 5.+12
      5.1+12 5.2+12 5.3+12 5.4+12 5.5+12 5.6+12 5.7+12 5.8+12 5.9+12 6.+12
      6.1+12 6.2+12 6.3+12 6.4+12 6.5+12 6.6+12 6.7+12 6.8+12 6.9+12 7.+12
      7.1+12 7.2+12 7.3+12 7.4+12 7.5+12 7.6+12 7.7+12 7.8+12 7.9+12 8.+12
      8.1+12 8.2+12 8.3+12 8.4+12 8.5+12 8.6+12 8.7+12 8.8+12 8.9+12 9.+12
      9.1+12 9.2+12 9.3+12 9.4+12 9.5+12 9.6+12 9.7+12 9.8+12 9.9+12 1.+13

```

```

F14:P      2          $ Flux in cell 2

```

```

FM14      -1 200 -2          $ Photon absorption in water

```

```

F6:P      1 11 12 13          $ Energy per cell

```

```

F8:P      1 11 12      13     $ Photon energy distribution

```

```

E8  0 0.1 0.2 0.3 0.4 0.5 0.6 0.7 0.8 0.9 1.0
      1.1 1.2 1.3 1.4 1.5 1.6 1.7 1.8 1.9 2.0
      2.1 2.2 2.3 2.4 2.5 2.6 2.7 2.8 2.9 3.0          $ Energy bins

```

```

c Material specification MaterialID - ZZZAAA.nnX Weightfraction - negative

```

```

c mMaterialNo. MaterialID Atomic/WeightFraction

```

```

c Formation material

```

```

m300  14000.01g  -0.325          $ Silicon
      8000.01g   -0.63           $ Oxygen 8O16
      1000.01g  -0.032          $ Hydrogen 1H1
      11000.01g -0.004          $ Sodium
      17000.01g -0.0064         $ Chlorine

```

```

c Formation water

```

```

m200  1000.01g   2          $ Hydrogen
      8000.01g   1          $ Oxygen
mt200 lwtr.01t          $ Water bound hydrogen

```

```

c Neutron generator

```

```

m100  11000.01g  0.5          $ Sodium
      53000.01g  0.5          $ Iodine

```

```

vol 1 1 1 1 1 1 1 1 1 0 1

```

```

cut:P 1.+13 0.01 $ -0.2 -0.1          $ Energy and time cutoff

```

```

print -85 -86

```

```

PHYS:P 0.1 1

```

Appendix 5. MATLAB codes

A5.1. MATLAB code for Cross-correlation with surface correction

```

clc;
clear all;
close all;

n=100; % number of values to be compared with
m=25; % number of values to be compared
c1=zeros(n,2); % c1 from sensor1 n rows
c2=zeros(m,2); % c2 from sensor2 m rows
rop=zeros(1000,2); % rop with time
depth=zeros(1000,2); % depth with time
depth(1,1)=0; % initial time
depth(1,2)=483.2; % initial depth of sensor1
L=2.5; % distance between sensors
fid=fopen('resultCCN1_Corr.txt','wt'); %creating an output file
fprintf(fid,'n=%d \t m=%d \t L=%d \n',n,m,L);
fprintf(fid,'\t %s \t %s \t %s \n %f %f %f \n', 'time', 'rop', 'depth', depth(1,1),0,depth(1,2)); % writing headers and
initial values

%% Read data from sensor1 and sensor2
filename1 = fopen('Sensor1N1.txt'); % open data file from sensor 1
filename2 = fopen('Sensor2N1.txt'); % open data file from sensor 2
filename3 = fopen('DepthInTime.txt'); % Measured depth at surface
sensor1 = textscan(filename1,'%f %f %f',1, 'headerlines',1);
sensor2 = textscan(filename2, '%f %f %f',1, 'headerlines',1);
SurfaceDepth = textscan(filename3, '%f %f', 1, 'headerlines',1);

%% Dynamically update and compare data
a=2; % main indexing variable
while ~feof(filename1)
% Make vectors of n and m rows from loaded files respectively n>m

for i=1:1:n-1
    c1(i,1)=c1(i+1,1);
    c1(i,2)=c1(i+1,2);
end
c1(n,1)=sensor1{2};
c1(n,2)=sensor1{3};

for i=1:1:m-1
    c2(i,1)=c2(i+1,1);
    c2(i,2)=c2(i+1,2);
end
c2(m,1)=sensor2{2};
c2(m,2)=sensor2{3};

%% Cross Correlation
fit=zeros(1,n-m); % CrossCorrelation vector %
i=1;
while i<=n-m+1
    for j=1:m
        c1set(j)=c1(i+j-1,2);
    end
    mc1set=mean(c1set); % mean of set 1
    mc2=mean(c2); % mean of set 2

```

```

num=0; % Numerator
deno1=0; % Denominator term 1
deno2=0; % Denominator term 2
    for k=1:m
        num=num+(c1set(k)-mc1set)*(c2(k,2)-mc2(2));
        deno1=deno1+(c1set(k)-mc1set)^2;
        deno2=deno2+(c2(k,2)-mc2(2))^2;
    end
    fit(i)= num/(sqrt(deno1)*sqrt(deno2));
    i=i+1;
end

%% Calculate ROP
rop(a,1)=sensor1{2};
[R,r]=max(fit);
if R<1
    dt=c2(m,1)-c1(r+m-1,1);
    rop(a,2)=L*60/dt;
    if rop(a,2)>150 || rop(a,2)<0
        rop(a,2)=0;
    else
        end
else
    rop(a,2)=0;
end

%% Calculate depth and update with redundant measurement
dt=0;
for i=a-1:-1:1
    if rop(i,2)==0 && i>1 && depth(a-1,2)-depth(i-1,2)==0;
    else
        dt=rop(a,1)-rop(i,1);
        break
    end
end
depth(a,1)=sensor1{2};

if SurfaceDepth{1}-sensor1{2}< 0.001 % If surface correction is available
    depth(a,2)= SurfaceDepth{2};
    SurfaceDepth = textscan(filename3,'%f %f',1);
else
    depth(a,2)=depth(a-1,2)+rop(a,2)*dt/60;
end
fprintf(fid,'%f %f %f \n',rop(a,1),rop(a,2),depth(a,2)); % write in output
file

sensor1 = textscan(filename1,'%f %f %f',1);
sensor2 = textscan(filename2,'%f %f %f',1);
end

%% Plot the results
hold on
[haxes,hline1,hline2]=plotyy(depth(:,1),depth(:,2),rop(:,1),rop(:,2));
axes(haxes(1));
ylabel('Depth(m)')
axes(haxes(2));
ylabel('ROP(m/hr)')
xlabel('Time (min)')
title('Calculated ROP and Depth')
hold off
fclose all;

```

A5.2. MATLAB code for Hybrid pattern matching with RSS integration

```

clc;
clear all;
close all;

n=100; % number of values to be compared with (Set size)
m=25; % number of values to be compared (Pattern size)
c1=zeros(n,2); % Initialize variable c1 from sensor1 n rows
c2=zeros(m,2); % Initialize variable c2 from sensor2 m rows
rop=zeros(1000,2); % Initialize variable rop with time
depth=zeros(1000,2); % Initialize variable depth with time
depth(1,1)=0; % initial time
depth(1,2)=483.2; % initial depth of sensor1
match=0.68; % 68 Percent match
L=2.5; % Distance between sensors in meters
fid=fopen('resultPM1N.txt','wt'); %creating an output file
fprintf(fid,'n=%d \t m=%d \t L=%d \t match=%d \n',n,m,L,match);
fprintf(fid,'%s \t %s \t %s \n %f %f %f \n','time','rop','depth',depth(1,1),0,depth(1,2)); % writing headers and
initial values

%% Read data from sensor1 and sensor2
filename1 = fopen('Sensor1N.txt'); % open data file from sensor 1
filename2 = fopen('Sensor2N.txt'); % open data file from sensor 2
sensor1 = textscan(filename1, '%f %f %f', 1, 'headerlines',1);
sensor2 = textscan(filename2, '%f %f %f', 1, 'headerlines',1);

%% load Survey and initialize navigation variables
fsurvey=fopen('MeasuredSurvey.txt','wt'); % Measured survey
fprintf(fsurvey,'%s \t %s \t %s \n','Depth','Inclination','Azimuth');
frss=fopen('RSSToolSetting.txt','wt'); % Record RSS tool settings
fprintf(frss,'%s \t %s \t %s \t %s \n','Depth','Toolsetting','Toolface','DLS');
wellplan = importdata('SurveyInterp.txt');
dogleg_distance = 30; % for dogleg expression, (e.g. deg/30m) (m)
TF= 122.8; % Degree
TS= 2; % Position of tool 1-13
DLS=1.6; % Angle build up rate (deg/30m)
dep=depth(1,2); % initial well plan depth (m)
fprintf(frss,'%f %f %f %f \n',dep,TS,TF,DLS); % write initial Tool settings
abd=dep; % initial measured depth (m)
inc=22.2; % initial well plan inclination (deg)
abi=inc; % at bit inclination (deg)
azi=120.9; % initial well plan azimuth (deg)
aba=azi; % at bit azimuth (deg)

%% Dynamically update and compare data
a=2; % main indexing variable
while ~feof(filename1)

% Make vectors of n and m rows from loaded files respectively n>m

for i=1:1:n-1
    c1(i,1)=c1(i+1,1);
    c1(i,2)=c1(i+1,2);
end
c1(n,1)=sensor1{2};
c1(n,2)=sensor1{3};

for i=1:1:m-1

```

```

        c2(i,1)=c2(i+1,1);
        c2(i,2)=c2(i+1,2);
    end
    c2(m,1)=sensor2{2};
    c2(m,2)=sensor2{3};

%% Calculation of tolerance
    for p=1:m
        tol(p)=sqrt(2*c2(p,2));
    end

%% Pattern Matching
    fit=zeros(1,m);           % Test vector to check the match
    i=n;
    Sum=zeros(n-m+1,1);
    SqDist=zeros(n-m+1,1);
    while i>=m
        if abs(c1(i,2)-c2(m,2))<= tol(m)
            for k=1:m
                fit(k)=~(abs(c1(i+k-m,2)-c2(k,2))<=tol(k));
            end
            SqDist(i)=sum( (c1(i-m+1:i,2)-c2(:,2)).^2);
            Sum(i)=sum(fit);
        else
            end
            i=i-1;
        end
    end

%% Calculate ROP
    rop(a,1)=sensor1{2};
    R=max(Sum);
    indices=find(Sum==R);
    [D,d]=min(SqDist(indices));
    r=indices(d);
    if R>= match*m
        dt=c2(m,1)-c1(r,1);
        rop(a,2)=L*60/dt;
        if rop(a,2)>150 || rop(a,2)<0
            rop(a,2)=0;
        else
            end
    else
        rop(a,2)=0;
    end

%% Calculate depth and update with redundant measurement
    dt=0;
    for i=a-1:-1:1
        if rop(i,2)==0 && i>1;
            else
                dt=rop(a,1)-rop(i,1);
                break
            end
    end
    depth(a,1)=sensor1{2};

fprintf(fid,'%f %f %f \n',rop(a,1),rop(a,2),depth(a,2)); % write data in
output file
sensor1 = textscan(filename1,'%f %f %f',1);
sensor2 = textscan(filename2,'%f %f %f',1);

```

```

%% Navigation
if depth(a,2)==depth(a-1,2)
else
    dmd=depth(a,2)-depth(a-1,2);    % Progress from last measured depth
    rra=0.75+(rand(1)*0.5);        % random response
    rri=0.75+(rand(1)*0.5);        % random response
    quadrant = ceil(TF/90);        % TF quadrant
    if quadrant == 2
        angle = (180 - TF)*pi/180;
        aba=aba+(DLS*dmd*rra*sin(angle)/dogleg_distance);
        abi=abi-(DLS*dmd*rri*cos(angle)/dogleg_distance);
    elseif quadrant == 3
        angle = (TF - 180)*pi/180;
        aba=aba-(DLS*dmd*rra*sin(angle)/dogleg_distance);
        abi=abi-(DLS*dmd*rri*cos(angle)/dogleg_distance);
    elseif quadrant == 4
        angle = (360 - TF)*pi/180;
        aba=aba-(DLS*dmd*rra*sin(angle)/dogleg_distance);
        abi=abi+(DLS*dmd*rri*cos(angle)/dogleg_distance);
    else
        angle = TF*pi/180;
        aba=aba+(DLS*dmd*rra*sin(angle)/dogleg_distance);
        abi=abi+(DLS*dmd*rri*cos(angle)/dogleg_distance);
    end

abd=depth(a,2);
fprintf(fsurvey,'%f %f %f \n',abd,abi,aba); % write data in output file
g=find (wellplan.data(:,1)<=depth(a,2)); % find last closet point on
well plan
G=length(g)+03; % target well plan point
dep=wellplan.data(G,1); % well plan depth (m)
inc=wellplan.data(G,2); % well plan inclination (deg)
azi=wellplan.data(G,3); % well plan azimuth (deg)
[TS,TF,DLS]=rss(dep, abd, inc, abi, aba, azi); % RSS performance model
fprintf(frss,'%f %f %f %f \n',abd,TS,TF,DLS); % Print tool setting
end
a=a+1;
end

%% Plot the results
figure(1);
hold on
[haxes,hline1,hline2]=plotyy(depth(:,1),depth(:,2),rop(:,1),rop(:,2));
axes(haxes(1));
ylabel('Depth(m)')
axes(haxes(2));
ylabel('ROP(m/hr)')
xlabel('Time (min)')
title('Calculated ROP and Depth')
hold off
fclose all;

```

```

function [TS,TF,DLS] = rss(dep, abd, inc, abi, aba, azi)

%% DEFINE MAIN VARIABLES
% abi = deg, at bit inclination calculated
% abd = m, current depth/ last survey depth
% TS = New tool setting (determined)
% TF = deg, new toolface (determined)
%% SET CONDITIONS AND LIMITS
survey_length = dep-abd;    % Target and current/ survey depth difference m
dogleg_distance = 30;      % m, for dogleg expression, (e.g. deg/30m)
DLS_limit = 7;            % deg/dogleg_distance (Maximum allowed
tortuosity )

%% CALCULATE DLS REQUIRED TO DRILL PLANNED TRAJECTORY
dls_req=(sqrt((azi-aba)^2+(inc-abi)^2))*dogleg_distance/survey_length;
if dls_req<=DLS_limit
else
    dls_req=DLS_limit;
end

%% ANGLE BUILD RATE CALCULATION
% DEFINE THE R.S.S. CHARACTERISTICS
k=1;    % Formation factor
Fp=5;   % Maximum tool sideforce
w=1.4;  % Maximum weight on bit
% DEFINE THE R.S.S. AVAILABLE DEFLECTION SETTINGS, percent
home=0; pos2=0.08; pos3=0.16; pos4=0.24; pos5=0.32; pos6=0.40; pos7=0.48;
pos8=0.56; pos9=0.64; pos10=0.72; pos11=0.80; pos12=0.90; pos13=1.0;
def_pos=[home pos2 pos3 pos4 pos5 pos6 pos7 pos8 pos9 pos10 pos11 pos12
pos13];

%% Calculate the tool face
if abs(azi-aba)<0.001 && abs(abi-inc)<0.001
    TF=0;
elseif abs(inc-abi)<0.001
    TF=90;
else
    theta=atan(abs(azi-aba)/abs(inc-abi))*180/pi;
    if azi>aba && inc>abi
        TF= theta;
    elseif azi>aba && inc<abi
        TF= 180-theta;
    elseif azi<aba && inc<abi
        TF= 180+theta;
    else
        TF= 360-theta;
    end
end

%% calculate the build rates
for i=1:13
    dls(i) = k*(Fp*def_pos(i)+ w*sind(inc));
end
pos=length(find(dls<=dls_req));
if pos>0
else
    pos=1;
end
TS = def_pos(pos);    % required tool setting
DLS = dls(pos);      % Required build rate

```